TECHNISCHE UNIVERSITÄT MÜNCHEN

TUM School of Natural Sciences

The beneficial effect of mass transport limitation on catalytic performance of LaX zeolite in isobutane/2-butene alkylation

Verena Brigitte Helga Höpfl

Vollständiger Abdruck der von der TUM School of Natural Sciences der Technischen Universität München zur Erlangung des akademischen Grades einer

Doktorin der Naturwissenschaften (Dr. rer. nat.)

genehmigten Dissertation.

Vorsitz:		Prof. Dr.-Ing. Kai-Olaf M. Hinrichsen
Prüfer der Dissertation:	1.	Prof. Dr. Johannes A. Lercher
	2.	Hon.-Prof. Dr. Richard W. Fischer

Die Dissertation wurde am 12.09.2022 bei der Technischen Universität München eingereicht und durch die TUM School of Natural Sciences am 01.02.2023 angenommen.

Ich habe gelernt, dass der Weg des Fortschritts weder kurz noch unbeschwerlich ist.

Marie Curie

Für meine Familie

Acknowledgement

Vielen Dank, Prof. Johannes A. Lercher, für die Möglichkeit an deinem Lehrstuhl zu promovieren. Dein Vertrauen und die gegebenen Freiheiten haben mir ermöglicht mich frei zu entfalten und mich sowohl wissenschaftlich als auch persönlich weiterzuentwickeln.

Thanks, Prof. Yue Liu, for your permanent support, your creativity, your patience. Thanks for providing your scientific knowledge as well as practical help in the lab. It was a pleasure to be part of your flock of sheep at TCII.

Thanks to my industry partners, FHR and INVISTA, for the financial support and in person Will Cross and Keith Whiston for many fruitful discussions and the professional input. Special thanks to Keith for giving the opportunity to join the RSC Conference in London.

Vielen Dank, Uli, Bettina, Steffi, und Katja für die administrative Betreuung und ein herzliches Dankeschön an Xaver und Andreas für die technische Unterstützung.

Vielen lieben Dank, Tessi, für die entspannte und problemlose Zusammenarbeit im Projekt. Danke, dass du die letzten Jahre gemeinsam mit mir erlebt, durchgestanden, überstanden hast.

Vielen Dank, liebe TCII-Kollegen, jung wie alt, ehemalig und aktuell, ohne Hilfe geht es nicht. Vielen Dank, Ehrmi, Ferdi, Melzer, Steib, Felix, Weber, Wagenhofer, Martl, Roli, Martina, Laura, Insu, Lara, Ruixue, Lingli, und viele mehr für die tägliche Unterstützung im Labor, lustige Mittagspausen, abenteuerliche Konferenzausflüge und süffige Grillabende. Es war eine Ehre.

Ein besonderer Dank geht an meine zahlreichen Studenten, allen voran meine Masteranten Philipp und Simon, die mich mit fleißigen Händen an den Reaktoren tatkräftig unterstützt haben.

Vielen Dank liebe Familie, dass ihr meinen gelegentlichen Frust ertragen, mich immer ermutigt und jederzeit unterstützt habt.

Zu guter Letzt, Niklas, ein unendliches Dankeschön für deine bedingungslose Unterstützung. Du hast meine Promotion leichter, machbarer, schöner gemacht.

Abstract

The catalytic performance of LaX zeolite in 2-butene/isobutane alkylation is drastically improved by using the beneficial effect of mass transport limitation induced by pellet size. Due to intra-pellet diffusion a butene gradient is formed over catalyst pellet, markedly reducing the local olefin concentration at active sites. Side reactions are suppressed and deactivation is slowed down. The integral alkylate yield is raised by a factor of 6 with simultaneous increase of high-octane fraction.

Kurzzusammenfassung

Die katalytische Aktivität von LaX Zeolithen bei der 2-Buten/Isobutan-Alkylierung wird durch den positiven Effekt der korngrößen-induzierten Stofftransportlimitierung drastisch verbessert. Diffusionsbedingt bildet sich ein Butengradient über das Korn, der die lokale Olefinkonzentration an den aktiven Zentren deutlich reduziert. Nebenreaktionen werden unterdrückt und die Deaktivierung verlangsamt. Die Alkylatausbeute wird versechsfacht bei gleichzeitiger Steigerung der hochoktanigen Fraktion.

Table of content

Abbreviations

A	Area
ASO	Acid soluble oils
BAS	Brønsted acid site
BET	Brunnauer, Emmet, Teller
BPD	Barrels per day
c	Concentration
C	Celsius
cm^{-1}	Wavenumber
CSTR	Continuous stirred tank reactor
d	Diameter
D	Diffusion coefficient
DMH	Dimethylhexane
EFAL	Extra-framework aluminum
FAU	Framework type code for Faujasite
FCC	Fluid catalytic cracking
FID	Flame ionization detector
Fig	Figure
g	Gramm
h	Hour
IR	Infrared
k	Rate constant
l	Liter
LAS	Lewis acid site
LaX	Lanthanum exchanged X type zeolite

m	Meter
mol	Mol
PFR	Plug-flow reactor
P/O	Paraffin to olefin
r	Rate / Radius
R	Universal gas constant
RVP	Reid vapor pressure
s	Second
SBAS	Strong Brønsted acid site
SI	Supporting information
SLAS	Strong Lewis acid site
TMP	Trimethylpentane
TOS	Time on stream
T	Temperature
V	Volume
wt%	Weight percent
x	Distance
°	Degree
ρ	Density
µ	Mikro

Chapter 1

1. General Introduction

1.1. History of alkylation

In March 1935, Ipatieff and co-workers from the Universal Oil Products Company (UOP) reported the discovery of "a new catalytic reaction consisting in the direct addition of olefins to paraffins under very mild conditions" forming higher weight paraffins. Metallic halides (of Al, B, Be, Ti, Zr, Hf, TH, Cb and Ta) where found to be active as catalysts for alkylation of isoparaffins with light olefins, whereas main focus was placed on aluminum chloride ($AlCl_3$) and boron trifluoride (BF_3) combined with nickel powder and water. The reaction was carried out in a high-pressure Ipatieff rotating autoclave connected to a high vacuum apparatus in order to collect and separate the obtained product mixture (see Figure 1.1). Regarding the alkylation of isobutane with isobutene at 25°C mostly octanes and dodecanes had been generated.[1]

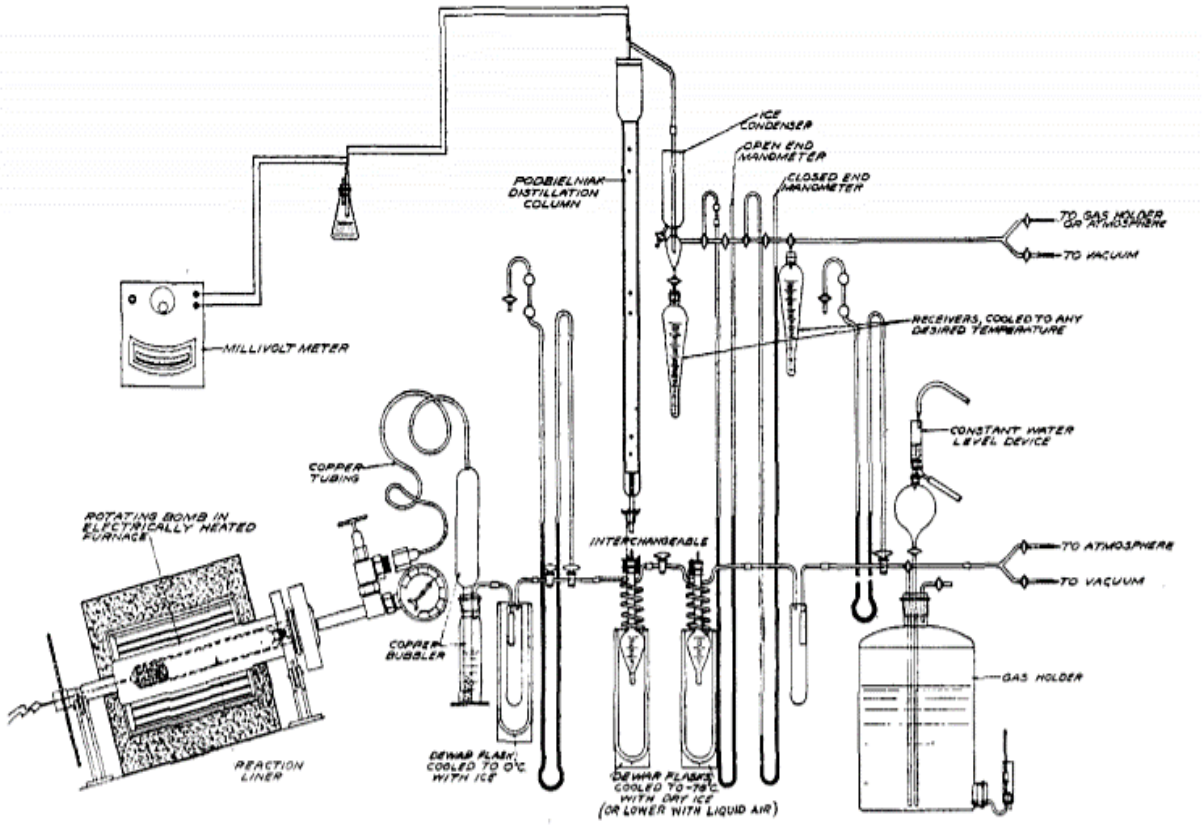

Figure 1.1. Drawing of experimental setup used for alkylation reactions including high pressure Ipatieff rotating autoclave and Podbielniak low and high temperature fractionation columns. Reprinted with permission from Vladimir N. Ipatieff and Aristid V. Grosse; "Reaction of Paraffins with Olefins" *Journal of the American Chemical Society* 1935, 57 (9), 1616-1621. Copyright 1935 American Chemical Society.

The inventors' motivation originated from the research on more profitable use of by-products from already widely established thermal and catalytic cracking processes. The substantial quantities of light hydrocarbons generated in refineries, such as ethylene, propylene, butylene and isobutane had limited use in gasoline due to their high vapor pressure and therefore required an efficient upgrading process. Based on the discovery of the reaction by Ipatieff several petroleum companies experimented simultaneously on commercialization of isobutane alkylation, all using sulfuric acid (H_2SO_4) as catalyst. Finally, Humble Oil and Refining Co. launched in cooperation with Anglo Iranian in 1938 the first industrial alkylation unit at Baytown, Texas. With other companies participating in early development work on alkylation process six commercial sulfuric acid alkylation units were on stream by the end of 1939 producing 3526 BPD of aviation alkylate. Three years later, on Christmas Day 1942, the first hydrofluoric acid (HF) alkylation unit by Philips at Philips's Borger in Texas started up. While other HF and H_2SO_4 units followed quickly, the thermal and $AlCl_3$ catalyzed alkylation processes did not catch on.[2]

Alkylate turned out to be extremely well-suited for aviation fuel due to its research octane number of about 93-97 and slightly smaller motor octane numbers. The cooperative effort of American companies to produce the high-quality gasoline played an important role in the outcome of World War II as Allied warplanes showed surpassing performance.[3] The high demand by military forces during war years increased the number of alkylation units up to 40 in 1945, whereas 31 used sulfuric acid and 9 hydrofluoric acid as catalyst. The total capacity had reached 169 000 BPD.[4] After World War II ended worldwide demand for aviation fuel dropped, however, since late 1950's the tightening of motor gasoline regulations and the increasing demand for alkylate as blending feedstock for automotive motor fuels provided an alternate use. Reaching the end of 1970's about twice as many sulfuric acid units as hydrofluoric acid units had been installed before construction of HF units became dominant for the following 30 years and about 50% of the alkylate was produced by HF.[2,3] However, since early 2000's alkylate production by HF catalysis is almost stagnating due to multiple accidents, whereas the most infamous happened on 30th of October in 1987 at the Marathon Oil Company refinery in Texas. After a crane dropped its load onto an anhydrous hydrogen fluoride tank within the HF alkylation unit 6548 gallons of HF were released causing the evacuation of approximately 4000 people and medical treatment for over 1000 of them.[6]

1.2. Alkylation in refining industry

The alkylation unit of a refinery is located down-stream of fluid catalytic cracking (FCC), catalytic reforming and isomerization units as you can see in Figure 1.2 showing a simplified flowsheet of a modern high-conversion refinery where vacuum gas oil and lighter cuts with boiling points below 560°C are processed. As isobutane is alkylated with light olefins such as propylene or butylene to branched hydrocarbons in gasoline range, low-value gases are upgraded to high-octane liquid products during this process.[6]

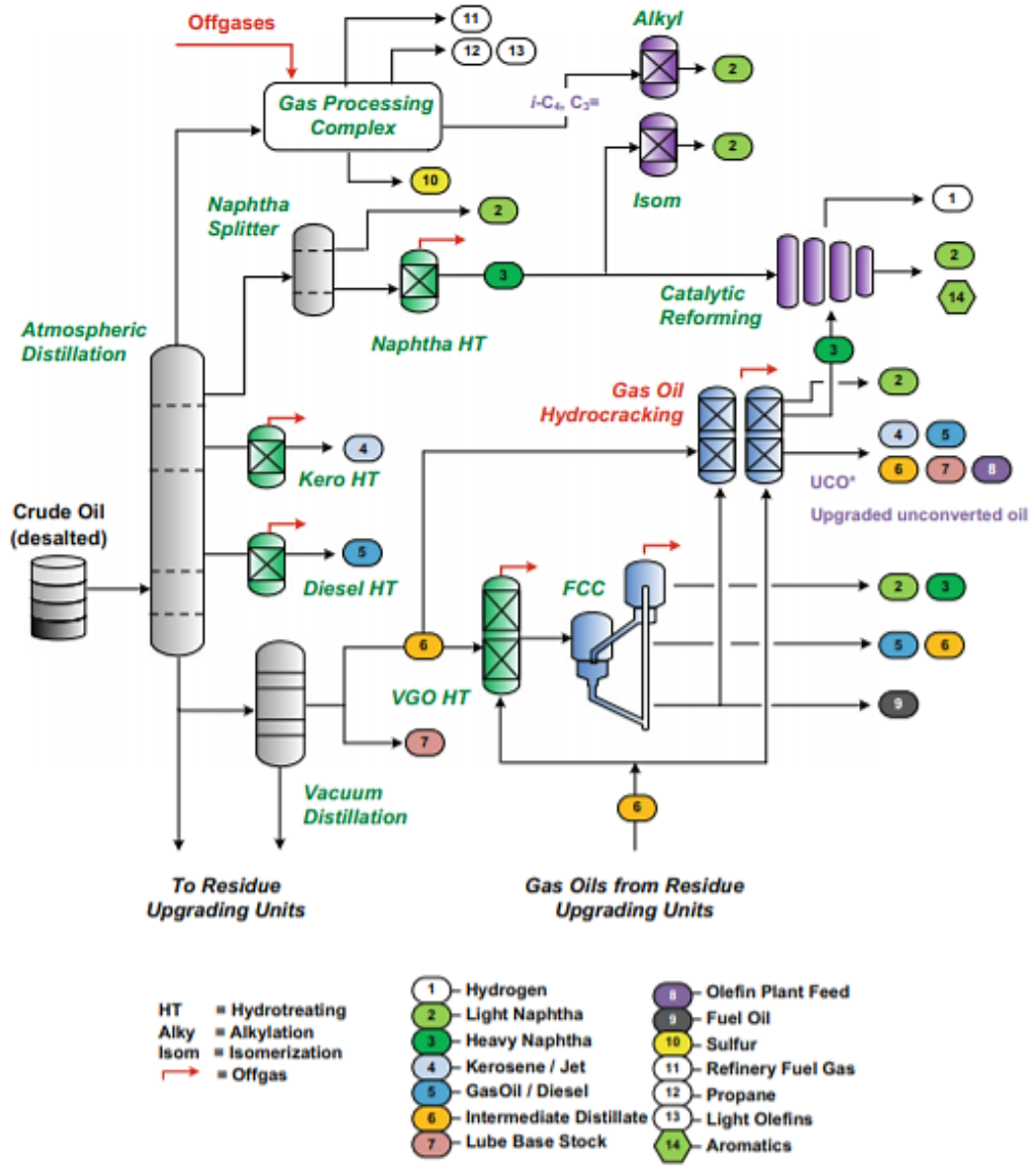

Figure 1.2. Schematic flowsheet of oil refinery process units for upgrading processes for top-of-the-barrel cuts (vacuum gas oil and lighter) adopted from [6].

Due to its excellent anti-knock properties and low Reid vapor pressure (RVP) alkylate is still highly demanded as blending feedstock for gasoline pool.[7] The reaction of isobutane and olefin is catalyzed by strong acids like H_2SO_4 or HF at moderate temperatures below 50°C and a pressure lower than 30 bar. In the absence of catalysts severe conditions such as 500°C and 200-400 bars are required to form alkylate products.[7]

Since early development work in 1930's and 1940's five processes have been established as commercial alkylation technologies using liquid acid catalysts. Sulfuric acid processes were designed by DuPont, ExxonMobil and Kellogg, whereas the last two have similar reactor designs.[3] In case of HF, Conoco-Phillips and UOP successfully launched processes. While liquid acid processes have proven themselves for over 80 years, commercial alkylation technologies using solid acids are still in their infancy.[3] Several licensors try to establish their processes, whereas quite different designs were developed. Main competitors are UOP, Akzo Nobel/CBI, LURGI and Haldor Topsøe. However, most recently commissioned alkylation units are based on DuPont's STRATCO sulfuric acid alkylation technology both installed by China Petroleum & Chemical Corp. (Sinopec) each having a alkylate capacity around 10 000 BPD.[8]

Both liquid acid alkylation processes share the same basic structure consisting of three main components: reactor, acid settler and product separator. Liquefied isobutane and olefin feed is mixed with liquid acid in the reactor, where alkylation reaction takes place. After acid recycling in the settler excess isobutane is recovered and product is fractionated.[7]

1.3. Commercial sulfuric acid processes

Sulfuric acid alkylation technology is well-established and licensed by four companies with processes by DuPont (STRATCO process) and ExxonMobil (ExxonMobil process) dominating the market. While Kellogg no longer offers their sulfuric acid alkylation technology, the Lummus' CD Alky technology first commercialized from CB&I in 2013 is gaining reputation,[9] e.g. Mc Dermott launched 2019 a CD Alky reactor with a capacity of 9000 BPD in China.[10] Comparing these individual technologies the major difference can be found in their reactor designs.[7] The following describes the two most important processes.

The process schemes in section 1.3, 1.4 and 1.5 are drawn using Microsoft Powerpoint, whereas reactor illustrations are combined with overall simplified flowsheets based on related sources.

1.3.1. STRATCO® Alkylation Technology by DuPont

The general scheme of the effluent refrigeration alkylation process STRATCO® by DuPont is shown in Figure 1.3. Cooled isobutane and olefin feed are mixed and dehydrated in the coalescer before entering the Contactor™ reactor. The Stratco reactor is a horizontal pressure vessel with an inner tube bundle consisting of either 613 tubes with 1” diameter or 1093 tubes with ¾” diameter enabling an efficient removal of reaction heat by an extremely large surface area of around 1000 m². The two phases are kept liquid by operating at a pressure of about 3.5 to 5.0 bar at reaction temperatures of 5-10°C. The vigorous stirring of the mixing impeller leads to the formation of an emulsion of hydrocarbons and acid instantly initiating alkylation reaction at the boundary layer of droplets, meanwhile high recirculation rates ensure efficient control of the reaction temperature and acid concentration uniformity. The product mixture is obtained by removing part of the emulsion and separate sulfuric acid in the settler before returning it to the suction side of the impeller. Additionally, part of the acid is replaced continuously to maintain the acid strength as high as possible. The hydrocarbon phase is sent to the suction trap/flash drum to separate vapor and liquid phase. While liquid product is washed to eliminate sulfates before entering the effluent fractionation section, vapor phase is compressed, cooled and directed to the depropanizer. Recovered isobutane from isobutanizer is sent back to the reactor.[11,12,18]

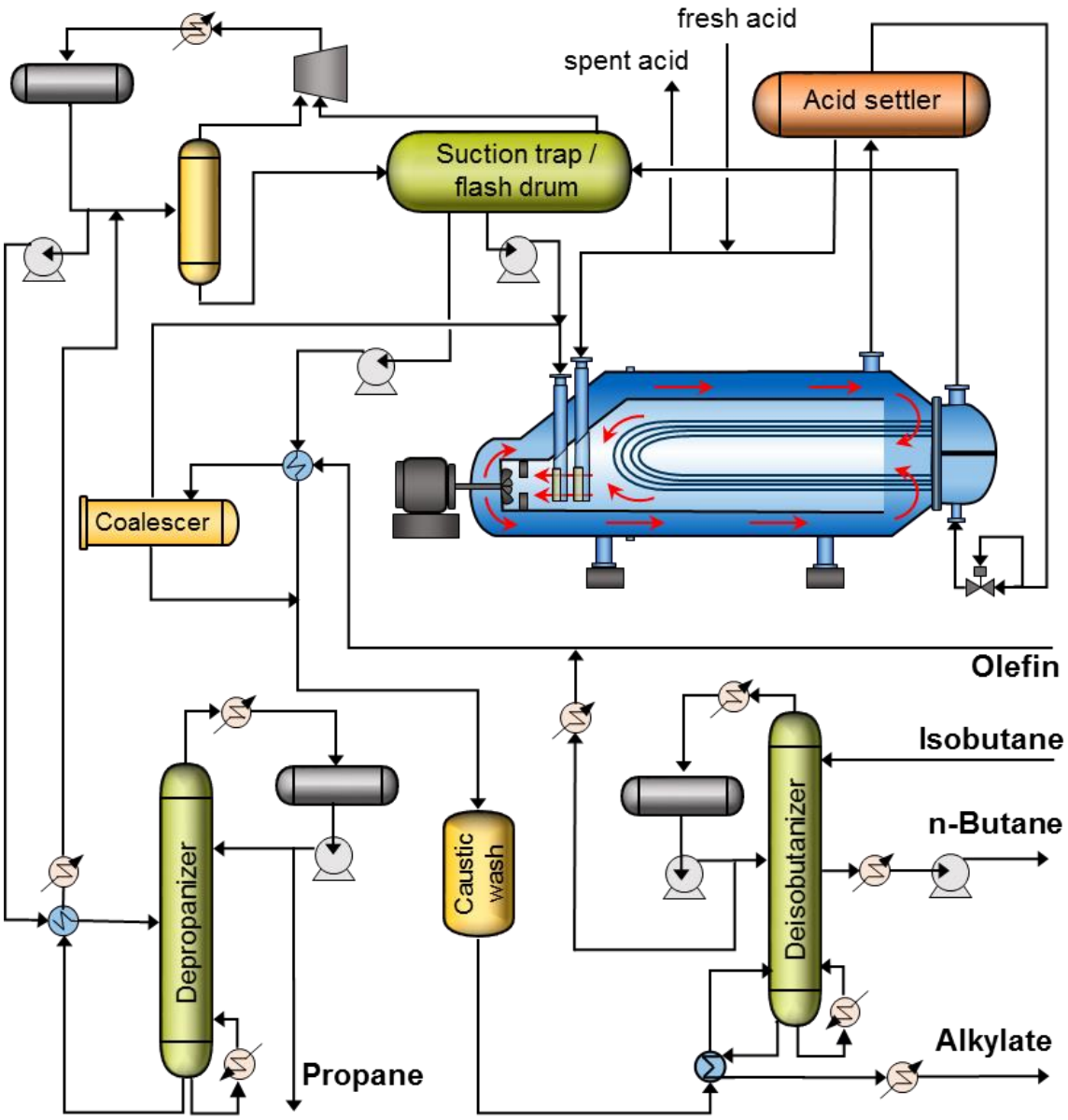

Figure 1.3. Simplified process scheme of STRATCO® Alkylation Technology by DuPont drawn based on [11].

1.3.2. ALKEMAX™ Sulfuric Acid Alkylation by ExxonMobil

The ExxonMobil cascade process (Figure 1.4) is based on auto-refrigeration by direct vaporization of isobutane to maintain the reaction temperature at 4-5°C. The olefin/isobutane mix is cooled and dehydrated in the coalescer before entering the reactor, which is a horizontal vessel containing several compartments with individual impellers to form an emulsion of hydrocarbon and acid. While olefin feed containing feed is added to each section, recycled isobutane and sulfuric acid are fed at the first compartment moving through the cascade by overflowing from one compartment to the other. The heat of reaction is removed by the evaporating of isobutane. As pressure decreases from about 1.5 to 0.5 bar from first to last section, there is usually a settling zone at the end. Vapor phase is sent from the reactor to the refrigeration section before being caustic and water washed and directed to the depropanizer. While propane is removed from the process, isobutane-rich streams are recycled back to the reactor. The liquid products have to be separated from sulfuric acid in the settler before also being washed and fractionated into isobutane, n-butane and alkylate product. The accumulation of feed impurities and acid soluble oils (ASO) built-up by olefin polymerization requires the replacement of spent acid by fresh make-up acid. [11,13,14,18]

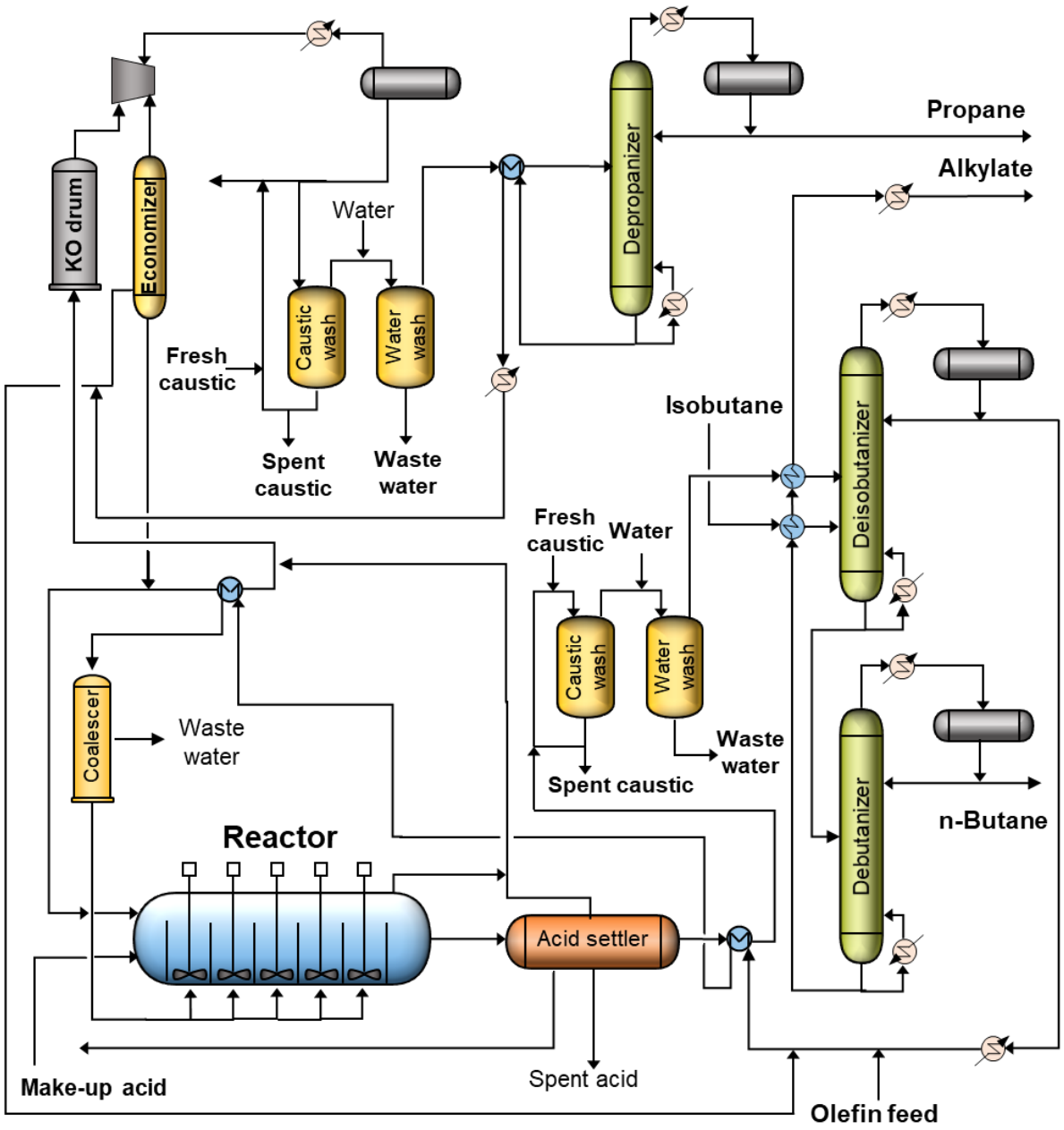

Figure 1.4. Simplified flowsheet of ExxonMobil sulfuric acid alkylation process drawn based on [12].

1.4. Commercial hydrofluoric acid processes

Due to the lower viscosity of HF and better solubility of isobutane in this acid, reactors for fluoric acid alkylation processes do not need mechanical stirring in order to form an emulsion of hydrocarbons and acid phase. Moreover, reaction temperatures are normally choosen in the range of 30-40°C as HF is not oxidative in contrast to sulfuric acid. This enables simplier cooling systems using water as coolant. However, a higher isobutane to olefin ratio is required making a larger fractionation section necessary for recycling.[15]

While some chemical properties of hydrofluoric acid simplify it's application as catalyst for industrial production of alkylate, other properties definitely entail certain disadvantages, which have to be considered and organised responsibly.

Hydrofluoric acid is extremely hazardous causing severe chemical burns if contacted to human skin or lungs. Therefore, exposure to HF can be lethal, if not immediately treated. Unfortunately, its low boiling point of 19.5°C enables vapor formation already at room temperature and the ability to form aerosol clouds further increases its dangerous nature. Moreover, hydrofluoric acid is extremely corrosive, especially, if dissolved in water, which increases the demands for applied equipment as glass, quarz and metals are not applicable.[16]

1.4.1. Conoco-Philipps HF alkylation process

The simplified flow scheme of a typical Phillips process including an illustration of the riser reactor is shown in Figure 1.5. To minimize corrosion of process equipment by HF the olefin and isobutane feeds have to be dehydrated very carefully before being mixed with the acid. Entering the riser reactor the alkylation reaction takes place at 20-27°C, whereas the residence time in the tubular reactor is about 30s. The reaction mixture is then separated in the settler, where acid is accumulated at the bottom and recycled back to the reactor after cooling. In order to maintain the activity of the hydrofluoric acid catalyst, water and polymerized hydrocarbons are removed from slipsteams in the acid rerun column. Remaining ASO and HF-water azeotrope are further proccessed. The hydrocarbon phase at the top of the settler contains alkylate, propane, isobutane, n-butane as well as traces of HF. It is separated by the large fractionation unit, whereas isobutane is reused as reactant.[11,17]

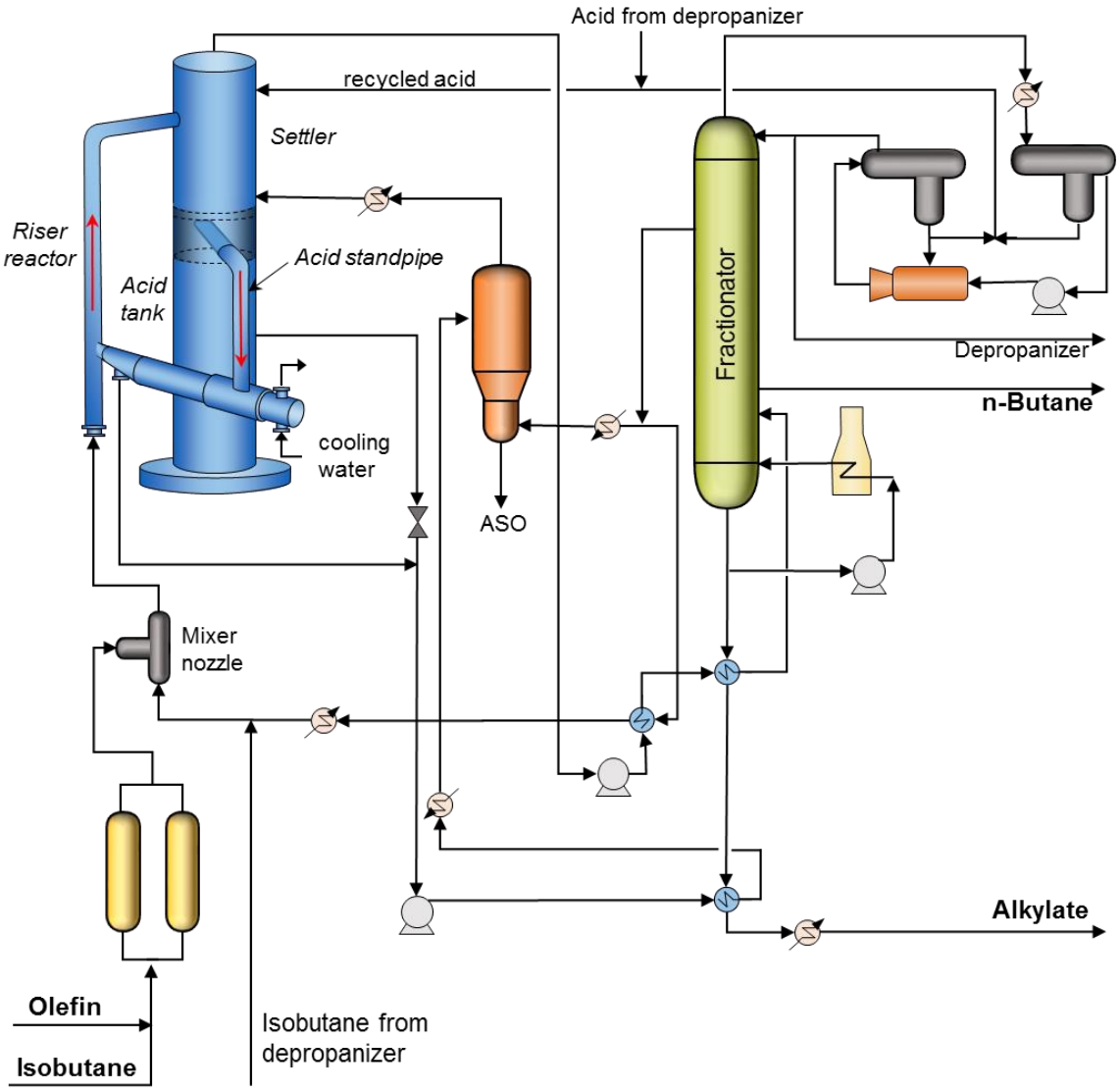

Figure 1.5. Simplified flowsheet of Conoco-Philipps HF alkylation process drawn based on [11].

1.4.2. UOP's AlkyPlus

The hydrofluoric alkylation process by UOP uses reactor nozzles to introduce dried reactants at different reactor heights, while HF is fed from the bottom. The flow scheme of this process can be seen in Figure 1.6. The continuous pumping of acid phase upwards improves mixing between hydrocarbons and catalyst, while cooling water removes reaction heat. The effluent is sent to the acid settler, where most of the HF is separated and recycled. The products alkylate and n-butane are isolated from the hydrocarbon phase in the isostripper and neutralized with KOH. As the remaining effluent contains isobutane, propane and acid residues, it is sent to the HF stripper and afterwards to the depropanizer. Isobutane and acid are recycled back to the reactor.[11,18]

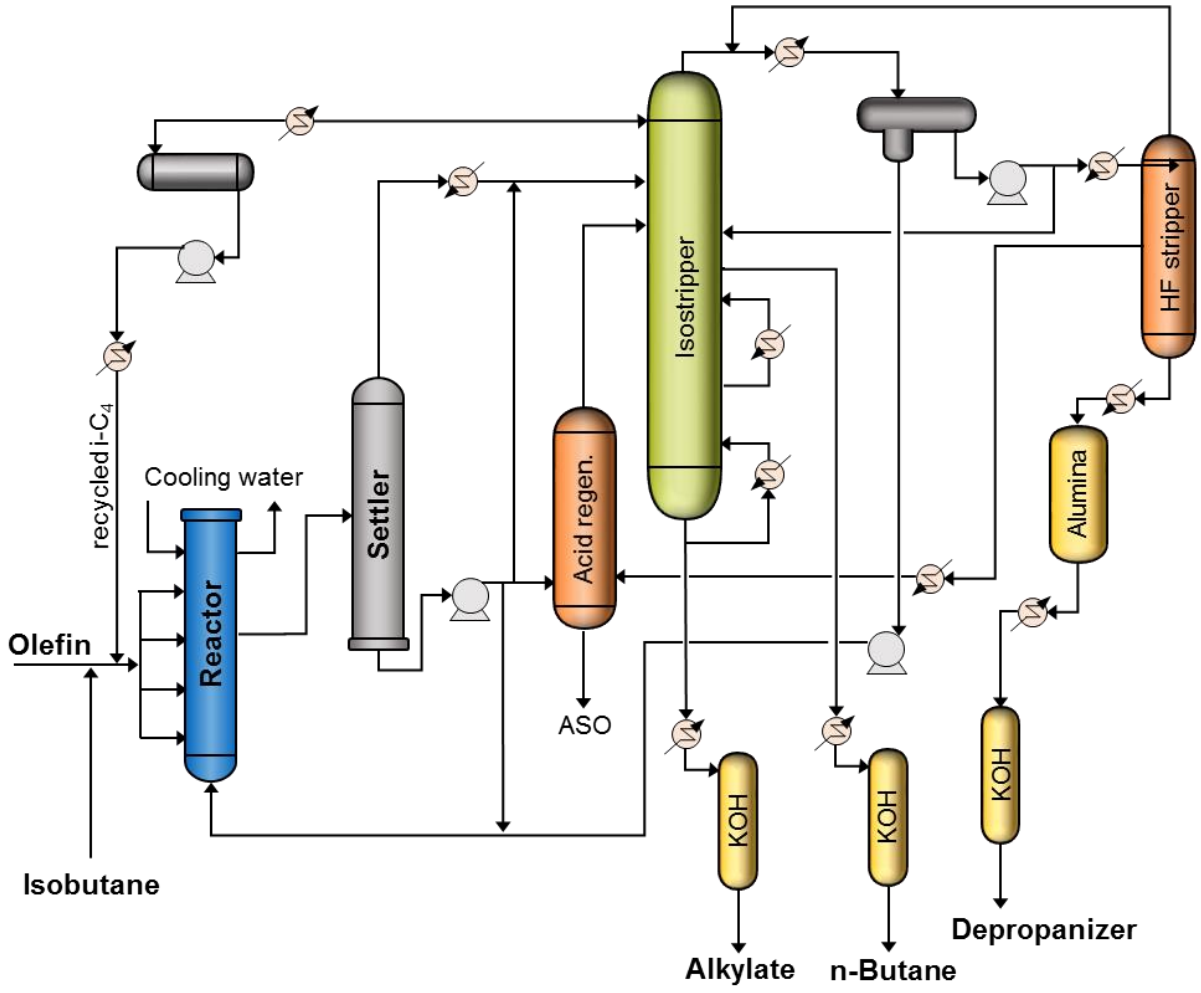

Figure 1.6. Simplified flowsheet of UOP's hydrofluoric alkylation process *AlkyPlus* drawn based on [11].

1.5. Commercial solid acid and ionic liquid acid processes

1.5.1. CB&I / Albemarle AlkyClean process

The solid acid catalyzed AlkyClean process from CB&I was the first commercial alkylation unit not using liquid acid starting in December 2015. A simplified flowsheet is shown in Figure 1.7. It uses three to five vertical fixed bed reactors operating in cyclic batch-wise manner, whereas the olefin feed (imported MTBE raffinate) is mixed with recycled isobutane before entering the reactor. The pretreatment section removes oxygenates, sulfur, nitriles and basic nitrogen components to reach the impurities specification for the applied AlkyStar^{TM} catalyst, which is zeolite based and noble metal functionalized. Moreover, the technology involves a two-step catalyst regeneration process comprising a mild regeneration applied a few times a day as well as a full regeneration once every one to two weeks. The alkylation reaction is carried out between 50 and 90°C at 20 bar in liquid phase using a feeding P/O ratio of 8-15:1. After reaction the product is separated by distillation into light ends, n-butane and alkylate. For mild regeneration the feedstock is switched to isobutane with dissolved hydrogen without changing other operating parameters. This leads to partial cleaning of the deactivating catalyst and returns the reactor back to alkylation mode in a short time interval. The full regeneration step completely restores catalyst activity by isolating the reactor from feedstock and introducing hydrogen at 250°C. Due to the installation of multiple reactors at least one reactor is online processing feedstock while other reactors are in different regeneration steps.[9,19]

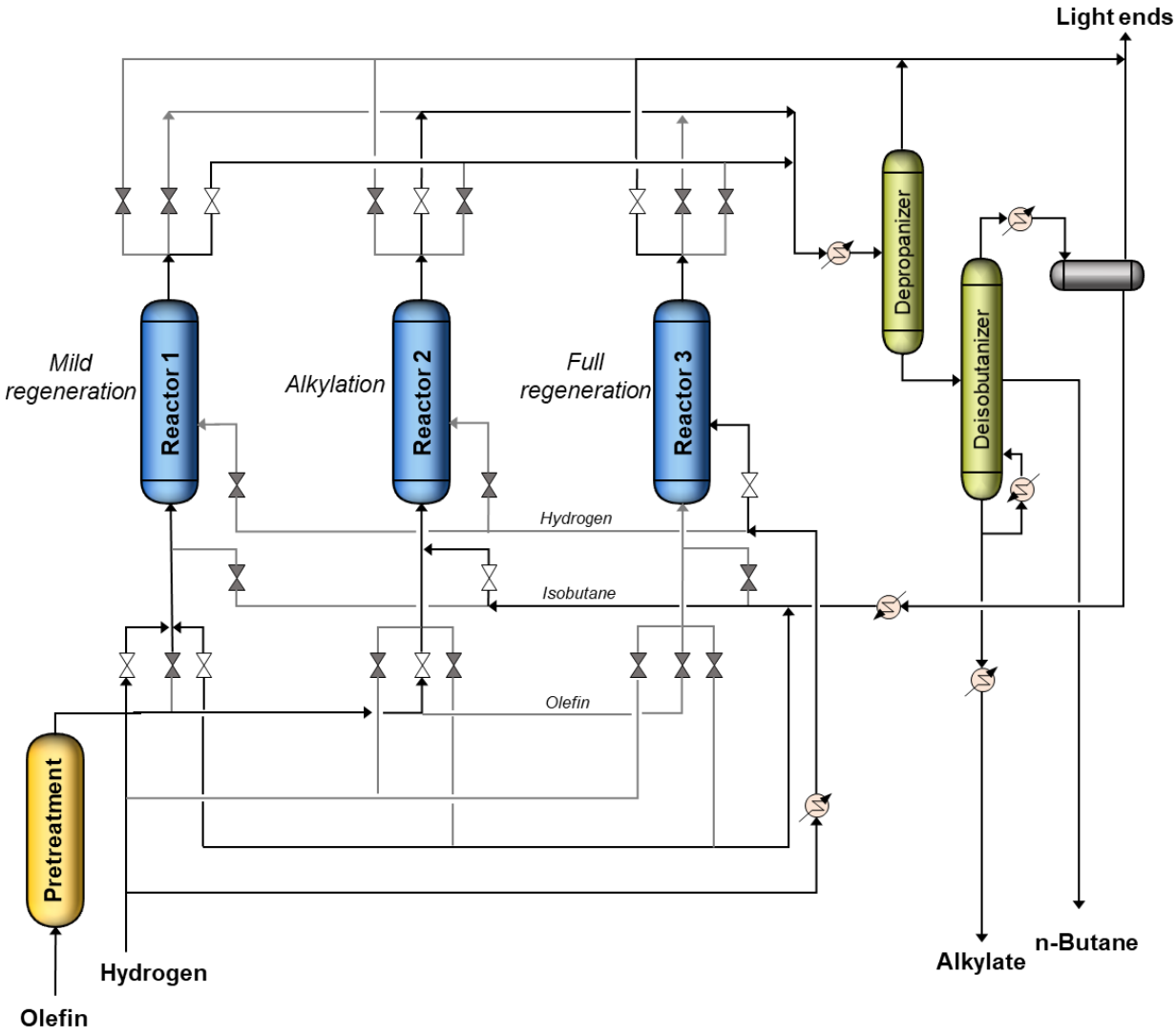

Figure 1.7. Simplified flowsheet of AlkyClean process by CB&I / Albemarle drawn based on [9].

1.5.2. K-SAAT from KBR

The solid acid alkylation process ExSact developed by Exelcus is licensed by KBR as the K-SAAT process (flowsheet in Figure 1.8). It uses two multistage fixed bed reactors and alkylation is carried out in liquid phase at 60-70°C. The applied catalyst ExSact™ is zeolite based and regeneration is performed after alkylation as full regeneration step at 250°C in hydrogen without mild regeneration occurring in-between like in AlkyClean process. This configuration leads to the two-reactor-concept of K-SAAT, where one reactor is in alkylation mode while the other reactor undergoes full regeneration.[9] In January 2019, KBR announced the contract conclusion with Wynnewood Refining Company providing engineering and design services of K-SAA process for their refinery in Oklahoma.[20]

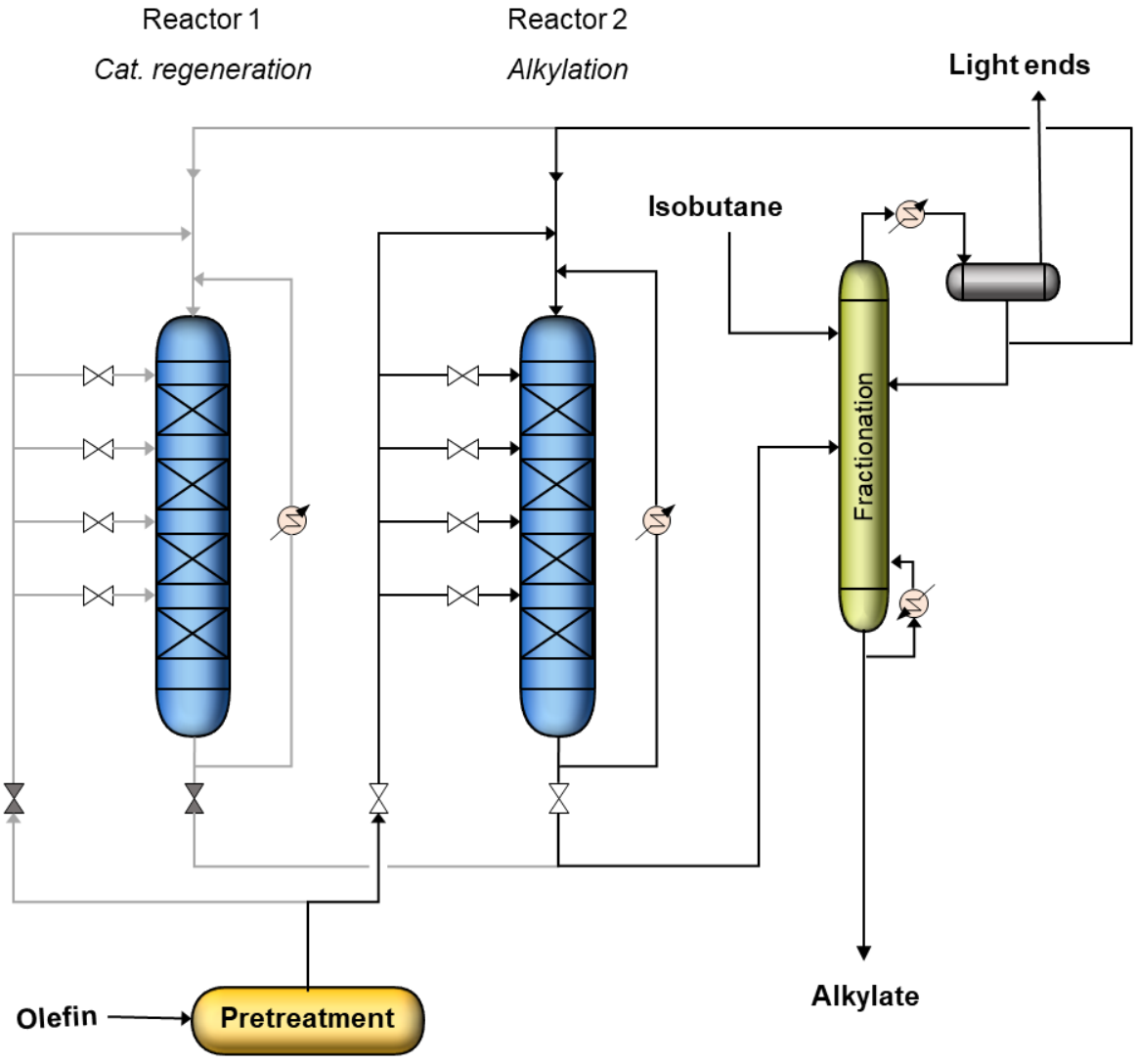

Figure 1.8. Simplified flowsheet of K-SAAT process licensed by KBR based on [9].

1.5.3. UOP's Alkylene process

The UOP Alkylene process (Figure 1.9) is based on a liquid riser reactor together with a hot reactivation vessel for *in situ* regeneration of the solid catalyst being $AlCl_3/Al_2O_3$ with small amounts of Pt.[21] Olefin and isobutane feeds together with the catalyst are pumped upwards the riser reactor with a rate of about one foot per second whereas alkylation reaction is initiated. At the top of the reactor the solid catalyst is separated and directed by gravity to the reactivation zone, where cold isobutane saturated with hydrogen removes heavy hydrocarbons by hydrogenation and desorption. Reaching the bottom of the reactor the catalyst is regenerated and reenters the rising stream. In addition to mild regeneration in the reactivation zone, a catalyst slipstream is regenerated at a higher temperature in a separate vessel in order to remove residual heavy hydrocarbon deposits. The product mixture at the top of the riser is sent to the fractionation section containing deisobutanizer, debutanizer and depropanizer similar to liquid acid catalyzed processes.[11,22]

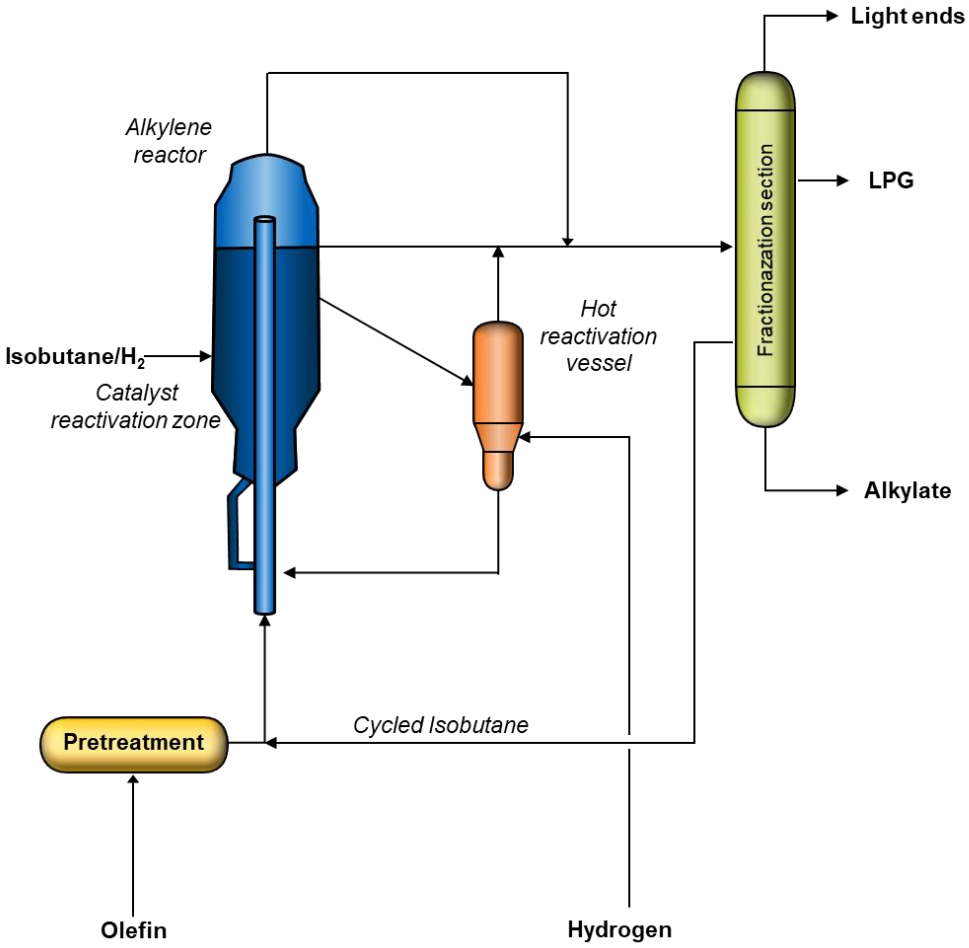

Figure 1.9. Simplified flowsheet of UOP's alkylene process drawn based on [11].

1.5.4. ISOALKY by Chevron / Honeywell UOP

The ISOALKY technology developed by Chevron and Honeywell UOP uses a non-volatile ionic liquid catalyst called ISOALKY^{TM} consisting of chloroaluminate ionic liquid with a trace HCl co-catalyst, whereas HCl is generated in-situ by organic chloride promoter addition. The usage of this catalyst leads toa biphasic reaction system, where reaction takes place at the interface, The simplified schematic flowsheet of this process is given in Figure 1.10.[9,23,24] In April 2019 Honeywell UOP announced that Sinochem Hongrun Petrochemical Co., Ltd. is the first manufacturer to license ISOALKY technology after the ionic liquid process was successfully operating for five years in a demonstration unit of Chevron located in Salt Lake City.[25]

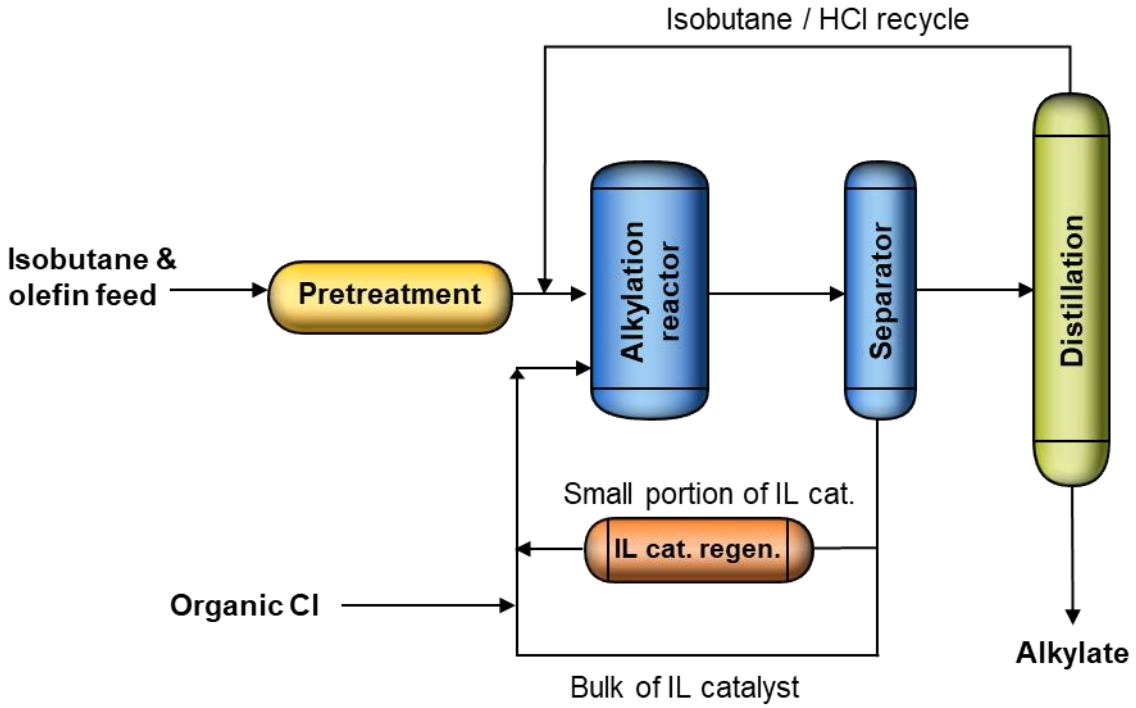

Figure 1.10. Simplified flowsheet of ISOALKY process by Chevron / Honeywell UOP based on [9].

1.5.5. Other processes

Besides mentioned commercialized processes other technologies are under development, however, not yet beyond startup phase or already rejected. For example, Haldor Topsøe invented a fixed-bed alkylation process (FBA^{TM}), which combines liquid and solid acid processes by using liquid trifluoromethanesulfonic acid supported on porous support material. The process was claimed to be robust against feed impurities, but yet abandoned. Another attempt is done by UOP as there are various indices to realize a slurry catalyst alkylation process similar to former EUROFUEL® process developed by LURGI and Süd-Chemie AG. The reaction is performed in a distillation tower with feed slurry including catalyst and liquid isobutane, a olefin feed and a circulating reactor vapor stream. However, no reference for commercialization of this technology could be found.[9,11,26,27]

1.6. Zeolites

1.6.1. General

Aluminosilicate zeolites are minerals first described in 1756 by Axel Fredrik Cronstedt. When collecting minerals in a copper mine in Lappmark, Sweden, he observed the formation of water steam during heating the material. This characteristic gave the inspiration to the term 'zeolite' derived from two Greek roots 'zéō' = 'to boil' and 'líthos' = 'a stone'.[28] Until 19th century numerous minerologists discovered new zeolite types and their basic properties like adsorption or (de)hydration finally resulting in the first definition of zeolite proposed by J. V. Smith in 1963: "an aluminosilicate with a framework structure enclosing cavities occupied by large ions and water molecules, both of which have considerable freedom of movement, permitting ion-exchange and reversible dehydration".[29,30]

Nowadays, they are often described based on their structural composition as crystalline solids consisting of a three-dimensional and regular framework generated by primary building units (PBU) being SiO_4 and AlO_4 tetrahedra, which are linked at their corners via a common oxygen atom. Based on this building principle the net formulae of PBUs are SiO_2 and AlO_2^- resulting in one negative charge per framework aluminum. The chemical composition of an aluminosilicate zeolite is represented with the general formula

$$A_{y/m}^{m+}\left[(SiO_2)_x \cdot (AlO_2)_y\right] \cdot z\, H_2O \qquad (1.1)$$

where A is a cation with the charge m, (x+y) is the number of tetrahedra per crystallographic unit cell and x/y is the framework silicon/aluminum ratio n_{Si}/n_{Al} or Si/Al.[31] As Al-O-Al linkages are forbidden due to Löwenstein's rule, Si/Al ratio has to be greater or equal 1.[32]

So far, 67 natural hydrothermal zeolites have been found since Cronstedt's initial discovery, e.g. faujasite, mordenite, offretite, ferrierite and chabazite, resulting mostly from the conversion of silicate of volcanic origin. In addition to naturally formed zeolites, there are uncounted opportunities to synthesize and post-modify new frameworks giving a large number of zeolites due to the great variety of different arrangements of primary tetrahedra combined to secondary building units (SBUs) or even tertiary ones.[29] Scheme 1.1 shows a selection of three-dimensional zeolite structures formed by primary, secondary and tertiary building units. For

example, a faujasite-type zeolite consists of two different SBUs being double six-membered rings and sodalite cages combined to supercages, which are further connected forming the final 3-D structure.

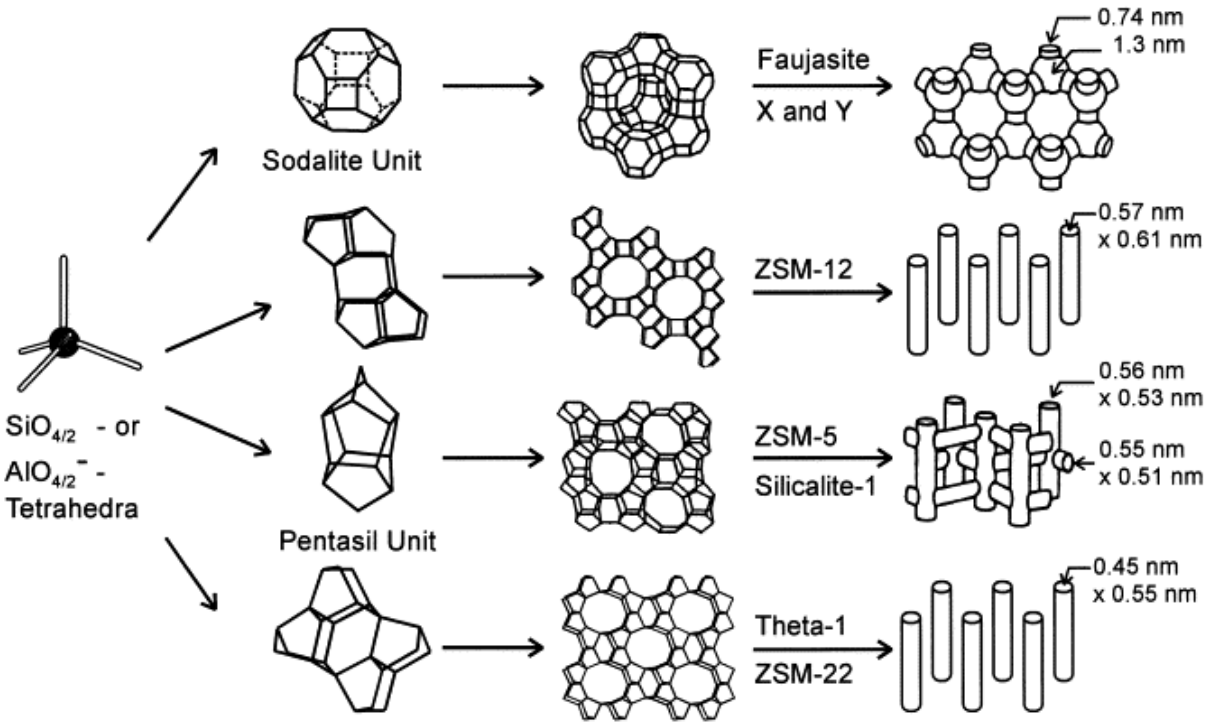

Scheme 1.1. Composition and dimensions of four selected zeolite structures (faujasite, ZSM-12, silicalite-1/ZSM-5 and Theta-1/ZSM-22). Adapted from [31].

Due to its hierarchical structure the framework of a zeolite contains channels, channel intersections and/or cages with dimensions from 2 to 10 Å. Inside these voids water molecules and small cations are stored, which compensate the negative framework charge resulting from AlO_2^- units. Owing to usual chemicals used for synthesis the most common cations are the alkali metals Na^+ and K^+, which are located in the microporous zeolite channel system. Since these ions are easily movable in the framework they can be exchanged by other ions, which enables tuning characteristic properties like pore size, adsorption behavior and catalytic activity.[33]

1.6.2. Acid sites

The application of synthetic zeolites as catalysts was introduced in 1950's with their acidity being one of the most important properties. It has to be differentiated between the nature of acid site, the concentration of sites, their strength as well as their location within the zeolite framework structure. As already mentioned, replacing a silicon atom by aluminum leads to the generation of a negative charge, which can be compensated by protons, metal cations or positive charged molecules like ammonium. In case of protons, Brønsted acid sites are formed (Scheme 1.2A) making the zeolite suitable for proton catalyzed reactions e.g. alkylation or cracking. A popular possibility to generate BAS is the thermal decomposition of ammonium cations as they split into ammonia leaving the catalyst and a proton stick to the framework.[31]

$$NH_4^+ + Na^+Z^- \xrightarrow{-Na^+} NH_4^+Z^- \xrightarrow{-NH_3} H^+Z^- \qquad (1.2)$$

If the negative charge is compensated by metal cations on the other hand, Lewis acid sites are generated (Scheme 1.2b). For example, selective methane oxidation is catalyzed by redox activity of LAS resulting from modification of zeolites with transition metal ions, e. g. with Cu^{2+}, $Fe^{2+/3+}$, Co^{2+} or Mn^{2+}.[34,35]

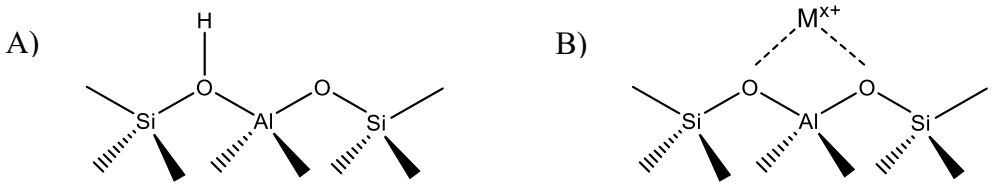

Scheme 1.2 A) Brønsted acid site,[36] B) Lewis acid site in zeolites.[37]

Furthermore, extra-framework Lewis sites can be generated by partial hydrolysis of zeolite framework Al-O und Si-O bonds forming extra-framework aluminum (EFAl) and extra-framework silicon (EFSi) as well as silanol nests surrounding the created voids. This steam treatment is often used to create mesopores as microporosity of zeolites comes along with diffusion limitation for reactants, intermediates and products.[38] The formed species are located in cavities leading to possible confinement effects. Especially EFAl can influence the catalytic activity of the zeolite by interacting with BAS and/or reacting as Lewis acid site, which can be both, beneficial like seen in pentane cracking[39] as well as disadvantages like observed in isobutane/2-butene alkylation[40].

1.6.3. Zeolite modification by lanthanum ions

Due to the very low Si/Al ratio of 1-3 in zeolite X, the concentration of Brønsted acid sites is extremely high leading to significant charge delocalization, which makes the pure HX form unstable. Therefore, other cations have to be introduced to stabilize the zeolite lattice. Lanthanum cations are introduced by exchanging sodium X zeolite with hydrated La^{3+} ions, which can only enter the supercage of faujasite due to their size of 0.79 nm. The decomposition of its hydrate shell enables lanthanum ions further moving into the sodalite cages having six-membered ring-openings of 0.25 nm diameter, whereas water molecules dissociate into an OH group bound to the metal as well as a proton, which forms a Brønsted acid site with the zeolite framework.[41,42] The corresponding reaction is called Hirschler-Plank-mechanism[43]:

$$[La(H_2O)_n]^{3+} \rightleftharpoons [La(OH)(H_2O)_{n-1}]^{2+} + H^+ \qquad (1.2)$$

The resulting LaX zeolite has various $La(OH)_x$ species in different locations within the framework, predominately in the center of 6-rings of sodalite cages as can be seen in Figure 1.11. By interacting with up to three Si-O-Al bridges the framework is stabilized and generated protons can act as Brønsted acid sites.[44]

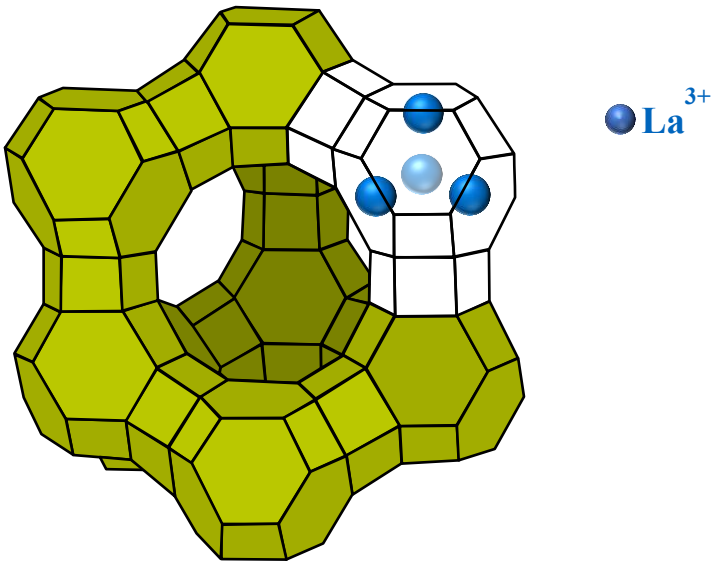

Figure 1.11. Framework of faujasite type zeolite with lanthanum ions located in sodalite cages. Image drawn based on zeolite database.[45]

In addition, the rare-earth metal helps to polarize hydrocarbon molecules, which is displayed in Scheme 1.3. Hydride transfer is enhanced by interaction of the positively charged lanthanum cation with the proton going to be abstracted, while simultaneously the hydrocarbon chain is directed to the negatively charged framework.[44]

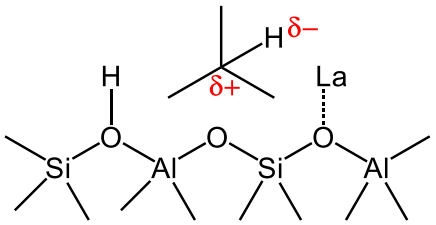

Scheme 1.3. Polarization of hydrocarbons in LaX zeolite.[44]

1.7. Alkylation reaction mechanism

The alkylation reaction (Scheme 1.4) is initialized by the protonation of a 2-butene molecule forming a secondary carbenium ion. In case of zeolite catalysts, the proton originates from bridging Brønsted acid sites (BAS). As tertiary carbenium ions are more stable, hydride transfer occurs from isobutane to the initially formed secondary carbenium ions producing n-butane as byproduct. The herein formed isobutyl carbenium ion is considered to be the dominating species on the catalytic surface during alkylation reaction. The catalytic cycle starts with olefin addition to the tertiary carbenium ion forming the primary alkylation product 2,2,3-trimethylpentyl carbenium ion, which can further isomerize to other octyl carbenium ions. The alkylation cycle is closed by another hydride transfer from isobutane to C_8 carbenium ions, which recovers the isobutyl carbenium ion, while saturated TMP products are desorbed.[46-48]

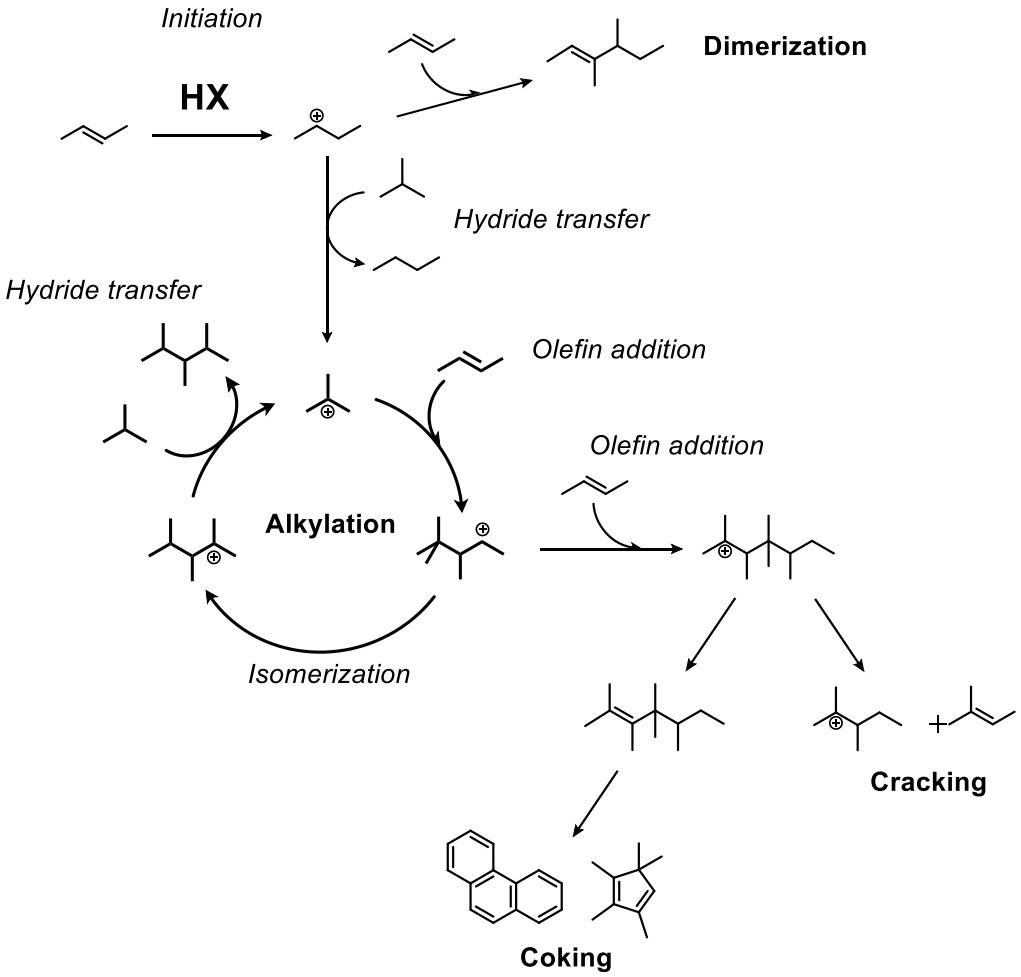

Scheme 1.4. Reaction mechanism of alkylation of isobutane with 2-butene including initiation step, propagation of catalytic cycle and side-reactions dimerization, cracking and coking.

Dimerization and multiple alkylation are undesired side-reactions both occurring if olefin addition is dominating over hydride transfer. When initially formed secondary carbenium ions react with another 2-butene molecule before a hydride is transferred from isobutane, the primary product 3,4-dimethylhexyl carbenium ion is formed. This intermediate can undergo either isomerization to other DMH isomers or hydride transfer to 3,4-DMH. In case of olefin addition to octyl carbenium ions C_{12}^+ intermediates are generated. These undesired intermediates can further react to heavy, unsaturated hydrocarbons or crack to small components in C_5 to C_7 range.

In addition to olefin addition and hydride transfer routes, every formed carbenium ion can desorb from catalytic surface by deprotonation, which leads to the formation of corresponding olefin as well as a free BAS. Deprotonation of secondary carbenium ions result in isomerization of reactant cis-2-butene to trans-2-butene and 1-butene. The desorption of C_8^+ isomers generates unsaturated octenes, while deprotonation of isobutyl carbenium ions forms isobutene. Last one enables another catalytic cycle called self-alkylation, where isobutene alkylates isobutyl carbenium ions resulting in the primary product 2,2,4-TMP^+. The reaction network of tertiary carbenium ions is shown in Scheme 1.5. [46-48]

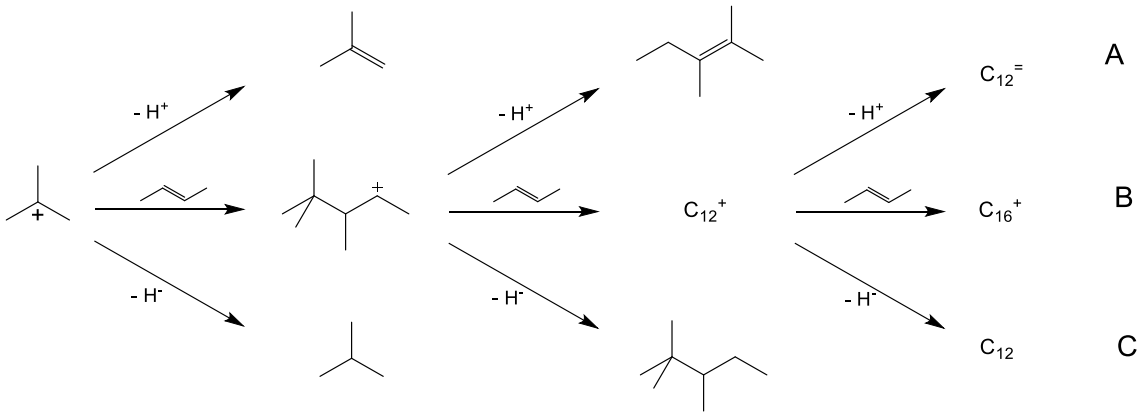

Scheme 1.5. Reaction network of tertiary carbenium ions with A) deprotonation route, B) olefin addition route and C) hydride transfer route.

The selectivity of trimethylpentane isomers is also controlled by the ratio of hydride transfer to alkene addition, as longer residence time on catalytic surface favors the more thermodynamically stable isomers 2,3,3- and 2,3,4-TMP. The isomerization of primary 2,2,3-TMP occurs via hydride and methyl shifts, whereas intermediates with tertiary carbenium ions are favored. The isomerization network of trimethylpentanes originating from standard 2-butene alkylation as well as self-alkylation is shown in Scheme 1.6. [46-48]

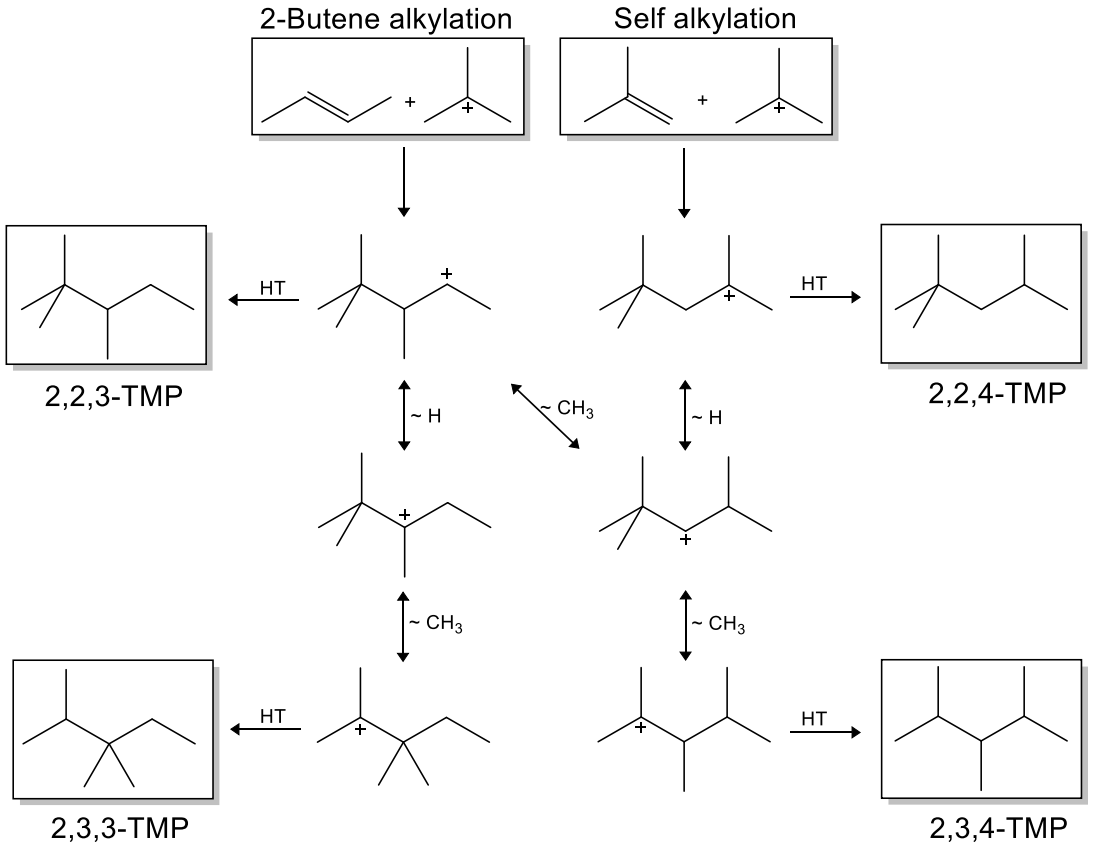

Scheme 1.6. Isomerization network of TMPs generated by 2-butene alkylation and self-alkylation.

Deactivation is assumed to be caused by heavy hydrocarbons formed by multiple alkylation as they block micropores of solid acid catalysts and therefore lead to inaccessible acid sites. Furthermore, olefinic side-products from deprotonation route can adsorb strongly on acid sites, which is also deactivating the catalyst. It is reported that Lewis acid sites interact stronger with unsaturated products than Brønsted acid sites pointing to a negative impact of LAS. [46-48]

1.8. Experimental procedure of alkylation reactions

The catalyst synthesis was done by Teresa Schachtl according to the preparation procedure given in each section. The final powder was stored under constant water vapor pressure over saturated $CaCl_2$ solution for at least 24 h to ensure comparable water content before further processing the material. All weight-based numbers are related to wet weight of catalyst directly measured after removing material from the saturator.

1.8.1. Catalyst pellet formation

In order to prepare pellets in ranges of 0.15-0.25, 0.25-0.35, 0.35-0.5, and 0.5-0.7 mm the catalyst powder was pressed to wafers by using a hydraulic press applying a pressure of approximately 4 tons. The formed wafers were crushed and resulting pellets were sieved into desired ranges. Examples for sieve fractions are shown in Figure 1.12. Pellets larger than 0.8 mm were formed in the shape of cubes by pressing zeolite wafers in the thickness of the desired edge length and cutting them with a scalpel (see Figure 1.13). The maximum pellet size prepared and tested was 3 mm. Shaped catalyst pellets were stored in the saturator for further 24 hours as water content might have been affected by pellet formation procedure.

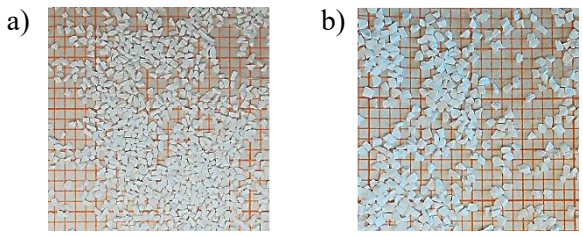

Figure 1.12. Images of pellet size fractions formed by crushing and sieving. a) 0.35-0.5 b) 0.5-0.7 mm. Background: 1x1 mm.

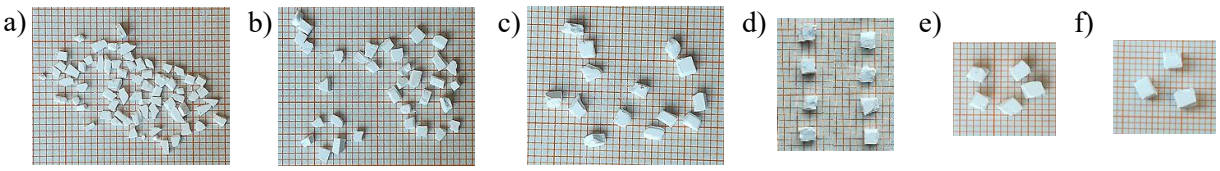

Figure 1.13. Pellets formed by wafer pressing and cutting. a) 0.8 b) 1.0 c) 1.5 d) 2.0 e) 2.5 f) 3.0 mm. Background: 1x1 mm.

1.8.2. Alkylation reaction in continuous stirred-tank reactor (CSTR)

The alkylation of isobutane with cis-2-butene in semi-batch mode was carried out in a 50 ml catalytic packless reactor with a micro-Robinson-Mahoney basket (see Figure 1.14) supplied by Autoclave Engineers. The flowsheet of the alkylation setup with CSTR reactor is shown in Figure 1.16. The required gases H_2, N_2 and syn. Air supplied by Westfalen GmbH were controlled by Bronkhorst mass flow controllers, while liquefied reactants isobutane (3.5, Westfalen) and cis-2-butene (2.0, Rießner-Gase) were fed by Teledyne ISCO syringe pumps. The process pressure was controlled by a TESCOM back pressure regulator (BPR) heated to 150°C. All lines after BPR were heated to 290°C in order to achieve complete evaporation of the product mixture before entering the Agilent 6890 gas chromatograph equipped with a 60 m DP-1 column and a flame ionization detector.

Figure 1.14. Image of catalyst basket with flow markers.

The pressed catalyst pellets were filled in the double-walled catalyst basket (Figure 1.14), which was then installed in the reactor. In order to remove physisorbed water the zeolite was activated in 100 ml/min N_2 flow at 150°C for 12 h. After reaching the reaction temperature of 75°C, the CSTR was filled completely with pure isobutane at 25 bar by closing the valve at lower outlet and enabling N_2 to leave at the upper outlet. The filled CSTR was kept closed during bypass flow was set to a paraffin-to-olefin ratio of 10. At constant butene concentration detected by GC the stirrer was set to 1600 rpm and alkylation reaction was started by switching from bypass to reactor.

The alkylation setup including continuous stirred tank reactor was built within a mobile frame with inlets of different gases being connected to lab gas supply. Individual mass flow controller are protected against solid impurities by 0.5 µm inline particle filters. A picture of the CSTR setup is shown in Figure 1.15.

Figure 1.15. Picture of CSTR alkylation setup.

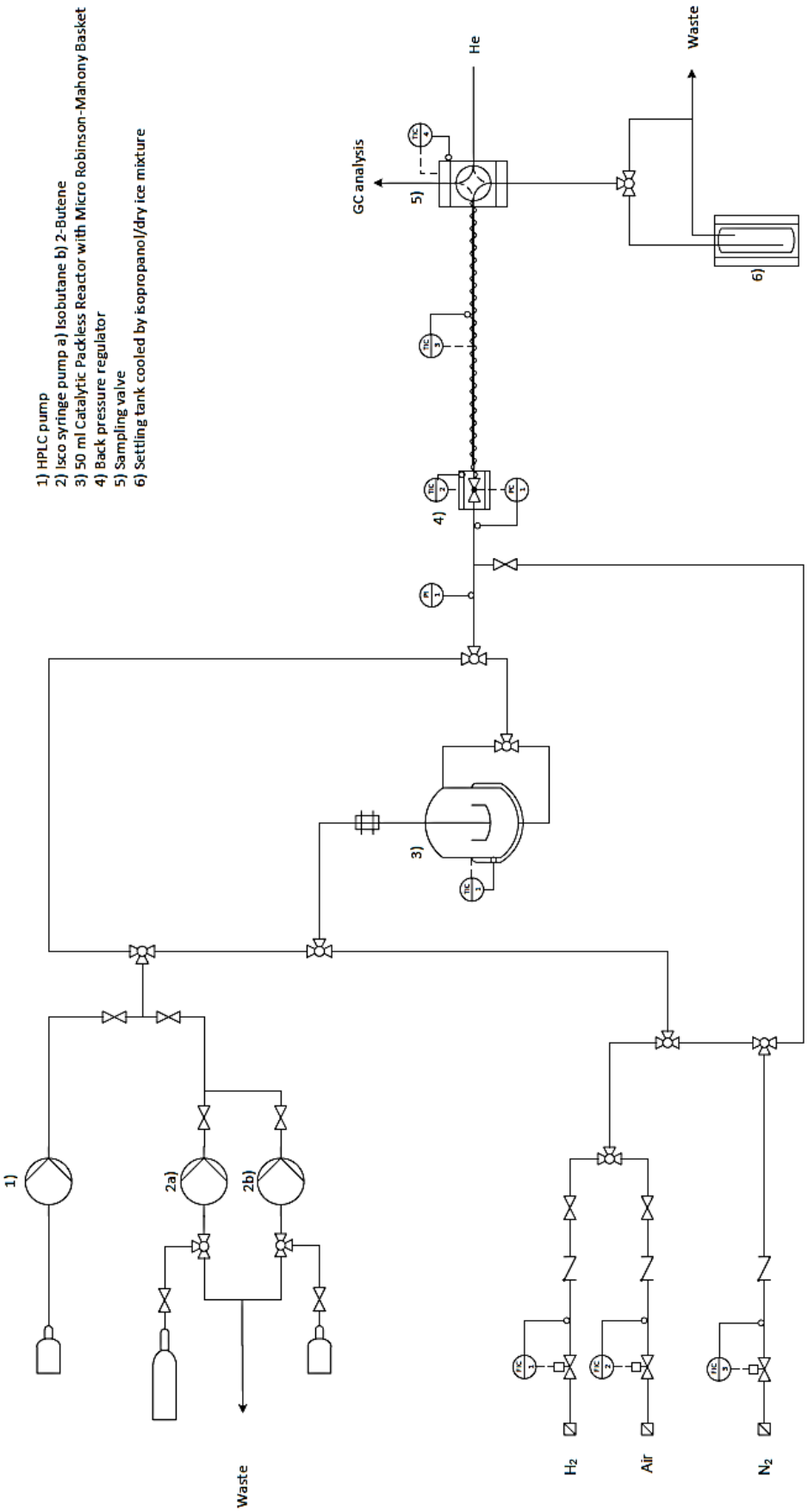

Figure 1.16. Flowsheet of CSTR alkylation setup.

1.8.3. Alkylation reaction in plug flow reactor (PFR)

For carrying out fixed-bed alkylation reaction a setup with two parallel plug flow reactors was built. A picture of the setup is given in Figure 1. 17, the flowsheet is shown in Figure 1.18. The surroundings like reactant and gas supply, back pressure regulator as well as product evaporation is similar to CSTR setup. For product analysis an Agilent 7890 gas chromatograph also equipped with a 60 m DP-1 column and a flame ionization detector is used. Additionally, this setup has a second feed option using a liquid mass flow controller connected to a lecture bottle containing pressurized reactant.

Figure 1. 17. Picture of PFR alkylation setup.

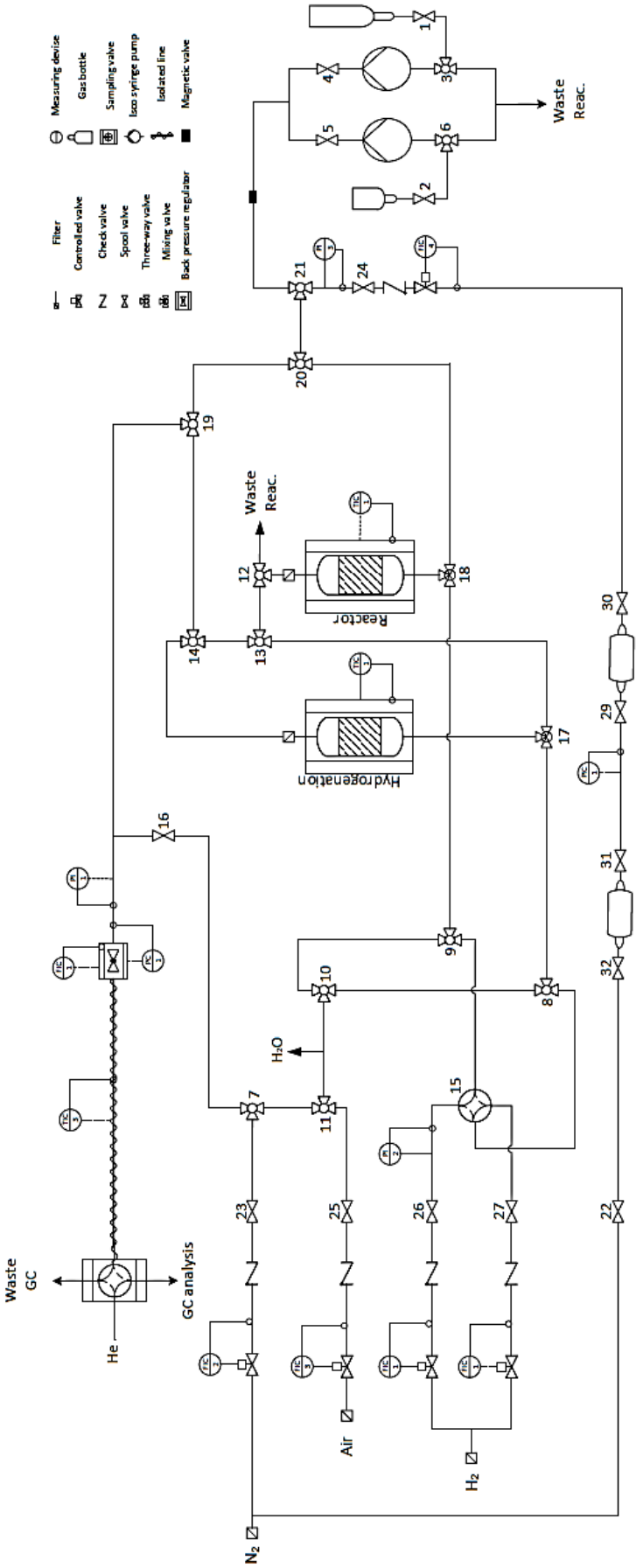

Figure 1.18. Flowsheet of PFR alkylation setup.

1.9. Scope of the thesis

In this work, the catalytic stability and selectivity of LaX exchanged zeolite used for isobutane/2-butene alkylation forming high-octane paraffins shall be improved by using the beneficial effect of intrapellet diffusion on solid acid catalyst. The main focus is put on pretreatment of synthesized catalyst powder, especially pellet formation and *in situ* activation of formed pellets in the reactor to optimize catalytic performance of these catalysts. Crucial parameters to improve are catalyst lifetime and selectivity towards tribranched octane isomers. Furthermore, the consequences of intrapellet diffusion as well as deactivation of catalyst bed in different reactor types are investigated to find the most favorable pretreatment and reaction conditions for isobutane/2-butene alkylation using zeolitic catalysts. To be able to run catalytic tests at constant conditions two setups are built, one setup with a continuous stirred tank reactor and one setup up with two parallel plug-flow reactors. Each alkylation setup has independent reactant feeding and product analysis.

1.10. References

[1] V. N. Ipatieff, A. V. Grosse, *Journal of the American Chemical Society* **1935**, *57*, 1616-1621.

[2] W. L. Lafferty, R. W. Stokeld, in *Origin and Refining of Petroleum, Vol. 103*, AMERICAN CHEMICAL SOCIETY, **1971**, pp. 130-149.

[3] L. F. Albright, *Industrial & Engineering Chemistry Research* **2009**, *48*, 1409-1413.

[4] N. P. Council, *Impact of New Technology on the U.S. Petroleum Industry 1964-1965*, **1967**.

[5] https://www.hse.gov.uk/comah/sragtech/casemarathon87.htm latest access: 04/28/2022.

[6] J. A. Kent, T. V. Bommaraju, S. D. Barnicki, *Handbook of Industrial Chemistry and Biotechnology*, 13 ed., Springer US, **2012**.

[7] M. A. Fahim, T. A. Alsahhaf, A. Elkilani, in *Fundamentals of Petroleum Refining*, Elsevier, Amsterdam, **2010**, pp. 263-283.

[8] R. Brelsford, in *Oil&Gas Journal*, "Sinopec refineries add fresh alkylation capacity", **6/16/2021**.

[9] S. Zhang, L. Wilkinson, L. Ogunde, R. Todd, C. Steves, S. Haydel, Alyklation Technology Study, Final Report, Norton Engineering, **9/9/2016**.

[10] A. Rais, in *Process worldwide*, "Mc Dermott Launches Largest Ever CD Alky Reactor in China", **3/18/2019**.

[11] M. Beccari, U. Romano, *Encyclopaedia of hydrocarbons. , Vol. II*, ENI : Istituto della Enciclopedia italiana, [Rome], **2006**.

[12] DuPont, in *STRATCO® ALKYLATION INNOVATIONS FOR GRASSROOTS APPLICATIONS (2015)*, www.cleantechnologies.dupont.com lastest access: 04/28/2022.

[13] ExxonMobil, in *ALKEMAX ™ Sulfuric Acid Alkylation Technology - fact sheet*, https://www.exxonmobilchemical.com latest access: 04/28/2022.

[14] H. Lerner, V. A. Citarella, *Exxon Research and Engineering Sulfuric Acid Alkylation Technology*, National Petroleum Refiners Association, **1991**.

[15] A. Corma, A. Martínez, *Catalysis Reviews* **1993**, *35*, 483-570.

[16] Fluorwasserstoffsäure, in *GESTIS-Stoffdatenbank*, https://gestis.dguv.de/data?name=520038 latest access: 04/28/2022.

[17] J. Gary, G. Handwerk, *Petroleum refining. Technology and economics. Volume 5*, **1975**.

[18] D. A. Nafis, K. A. Detrick, R. L. Mehlberg, in *Handbook of Petroleum Processing* (Eds.: S. A. Treese, D. S. Jones, P. R. Pujado), Springer International Publishing, Cham, **2015**, pp. 1-17.

[19] CB&I, in *Successful Operation of the First AlkyClean®Solid Acid Alkylation Unit*, http://www.aiche.nl/images/presentations/2017-6-29-ldm.pdf latest access: 28/04/2022.

[20] KBR, in *press release "KBR Secures Contract for Its Solid Acid Alkylation Technology (K-SAAT™)"*, https://www.kbr.com/en/insights-news/press-release/kbr-secures-contract-its-solid-acid-alkylation-technology-k-saattm latest access: 28/04/2022.

[21] M. Bajus, *Petrochemistry: Petrochemical Processing, Hydrocarbon Technology and Green Engineering*, Wiley, **2020**.

[22] C. Roeseler, in *Handbook of Petroleum Refining Processes*, Mc Graw Hill New York, **2004**, pp. 1025-1031.

[23] H. K. Timken, H. Luo, B.-K. Chang, E. Carter, M. Cole, in *Commercial Applications of Ionic Liquids* (Ed.: M. B. Shiflett), Springer International Publishing, Cham, **2020**, pp. 33-47.

[24] Chevron, in *TECHNOLOGY PRESENTATION TO SCAQMDPR 1410 WORKING GROUP MEETING #4 (08/02/2017)*.

[25] Honeywell, in *"Sinochem Hongrun Petrochemicals To Produce Cleaner-Burning Fuels With Honeywell's Groundbreaking Alkylation Technology" (04/25/2019)*, https://www.honeywell.com/ latest access: 04/28/2022.

[26] R. Galiasso Tailleur, S. Rodríguez, C. Farina, S. Derjani-Bayeh, *Energy & Fuels* **2018**, *32*, 2527-2548.

[27] H. Buchold, H. Dropsch, J. Eberhardt, "LURGI EUROFUEL - A NEW ALKYLATION PROCESS" Paper presented at the 17th World Petroleum Congress, Rio de Janeiro, Brazil., **September 2002**.

[28] A. Cronstedt, *Svenska Vetenskaps Akademiens Handlingar Stockholm* **1756**, *17*, 120.

[29] R. Millini, G. Bellussi, in *Zeolites in Catalysis: Properties and Applications*, The Royal Society of Chemistry, **2017**, pp. 1-36.

[30] J. V. Smith, *Mineralogical Society of America Special Papers* **1963**, *1*, 281.

[31] J. Weitkamp, *Solid State Ionics* **2000**, *131*, 175-188.

[32] W. Loewenstein, *American Mineralogist* **1954**, *39*, 92-96.

[33] F. Schwochow, L. Puppe, *Angewandte Chemie* **1975**, *87*, 659-667.

[34] P. Tomkins, M. Ranocchiari, J. A. van Bokhoven, *Accounts of Chemical Research* **2017**, *50*, 418-425.

[35] B. E. R. Snyder, M. L. Bols, R. A. Schoonheydt, B. F. Sels, E. I. Solomon, *Chem Rev* **2018**, *118*, 2718-2768.

[36] J. A. Rabo, G. J. Gajda, *Catalysis Reviews* **1989**, *31*, 385-430.

[37] G. Li, E. A. Pidko, *ChemCatChem* **2019**, *11*, 134-156.

[38] M.-C. Silaghi, C. Chizallet, J. Sauer, P. Raybaud, *Journal of Catalysis* **2016**, *339*, 242-255.

[39] S. Schallmoser, T. Ikuno, M. F. Wagenhofer, R. Kolvenbach, G. L. Haller, M. Sanchez-Sanchez, J. A. Lercher, *Journal of Catalysis* **2014**, *316*, 93-102.

[40] A. Guzman, I. Zuazo, A. Feller, R. Olindo, C. Sievers, J. A. Lercher, *Microporous and Mesoporous Materials* **2005**, *83*, 309-318.

[41] E. F. T. Lee, L. V. C. Rees, *Zeolites* **1987**, *7*, 143-147.

[42] H. Klein, H. Fuess, M. Hunger, *Journal of the Chemical Society, Faraday Transactions* **1995**, *91*, 1813-1824.

[43] M. Hunger, D. Freude, H. Pfeifer, D. Prager, W. Reschetilowski, *Chemical Physics Letters* **1989**, *163*, 221-224.

[44] F. Schüßler, E. A. Pidko, R. Kolvenbach, C. Sievers, E. J. M. Hensen, R. A. van Santen, J. A. Lercher, *The Journal of Physical Chemistry C* **2011**, *115*, 21763-21776.

[45] C. Baerlocher, L. B. McCusker, *Database of Zeolite Structures: http://www.iza-structure.org/databases/* latest access: 28/04/2022.

[46] A. Feller, I. Zuazo, A. Guzman, J. O. Barth, J. A. Lercher, *Journal of Catalysis* **2003**, *216*, 313-323.

[47] A. Feller, J.-O. Barth, A. Guzman, I. Zuazo, J. A. Lercher, *Journal of Catalysis* **2003**, *220*, 192-206.

[48] A. Feller, A. Guzman, I. Zuazo, J. A. Lercher, *Journal of Catalysis* **2004**, *224*, 80-93.

Chapter 2

2. Pellet size-induced increase in catalyst stability and yield in zeolite-catalyzed 2-butene/isobutane alkylation

Abstract

Zeolite-catalyzed alkylation of isobutane is a promising alternative of conventional H_2SO_4 or HF catalyzed processes to produce high octane fuels. Fast catalyst deactivation by deposits of heavy hydrocarbons, blocking pores and acid sites limits industrial applications. Increasing the catalyst pellet size is reported here to be able to reduce catalyst deactivation and to increase the total yield during its lifetime. On nearly fully La-exchanged X zeolite (LaX), catalyst lifetime was increased by more than threefold, while the product yield increased by 6 times when the catalyst pellet diameter was increased from 0.15-0.25 mm to 1.6 mm. This positive effect is caused by limiting mass transport of butene in large pellets, decreasing its concentration at the acid sites in the inner of the particle. The lower butene concentration suppressed multiple alkylation and so also the formation of high molecular weight hydrocarbons blocking active sites. Characterization of used LaX pellets by microscopy of cross sections and IR spectroscopy showed a core-shell structure of carbon deposits. This demonstrates unequivocally that only the outer zone of the particle is deactivated by the heavy hydrocarbons, while the core remained nearly unaffected.

2.1. Introduction

Alkylation of isobutane with light alkenes such as propene and butene to produce highly branched heptanes and octanes is an important refining process upgrading low-value light products to high-octane gasoline. Due to the excellent anti-knock properties, low Reid vapor pressure as well as the low sulfur content, the product is highly demanded as gasoline blending feedstock.[1, 2] Commercial alkylation technologies are based on HF and H_2SO_4. The well-proven technology is, however, either progressively restricted because of safety problems (HF) or suffers from high acid consumption of up to 100 kg/t and costly regeneration (H_2SO_4).[3, 4]

Significant efforts have been made in the last decades to replace existing processes by more environmentally friendly solid catalysts. Zeolites emerged as the most promising candidates that could replace the liquid acids. Large-pore zeolites such as zeolites Y, X, and BEA have been demonstrated to be active and highly selective for isobutane/butene alkylation.[5-7] Ion exchange with rare-earth metals cations improved the catalytic performance, induced by high and stable concentrations of Brønsted acid sites.[8-10] Zeolites suffer, however, from fast deactivation caused by side reactions, leading to heavy hydrocarbons deposited that block zeolite pores and acid sites.[11-14]

Two competing reaction pathways are involved in the 2-butene/isobutane alkylation, i.e., alkene addition and hydride transfer, which is illustrated in the simplified reaction network in Scheme 2.1 Alkylation is initiated by protonation of 2-butene into a butyl carbenium ion. In the next step, it may dimerize with a second butene into an octyl carbenium ion (r_{A1}) or react with isobutane into n-butane and an isobutyl carbenium ion (iso-C_4^+) via hydride transfer (r_{H1}). The iso-C_4^+ reacts with 2-butene to an octyl carbenium ion (C_8^+). In turn, the C_8^+ reacts with 2-butene to higher oligomers (r_{A2}), blocking the active site and deactivating the catalyst, or accepting a hydride from isobutane to yield branched octanes and to form an iso-C_4^+ (r_{H2}), hence, completing the catalytic cycle. Thus, a low relative rate of olefin addition (r_A) to hydride transfer (r_H) helps enhancing the production of octanes and reducing catalyst deactivation. Using strong Brønsted acid catalysts and Lewis acid sites that catalyze high hydride transfer rates, is the key strategy to achieve this.[9, 15, 16]

Decreasing the butene concentration is an effective approach to lower the rate of olefin addition (r_A), thus, reducing deactivation.[11] Low concentrations of butene can be realized by either using a high ratio of isobutane to butene (> 100) in the reaction feed, [17] or to minimize the butene concentration in a continuously operated stirred-tank reactor (CSTR) at high conversions.[4, 18-20] While both approaches lead to a low butene concentration in the liquid reactant mixture, we show here that it is also feasible to reduce the operating butene concentration locally at the active sites by increasing the catalyst pellet size, regulating so the transport of butene.

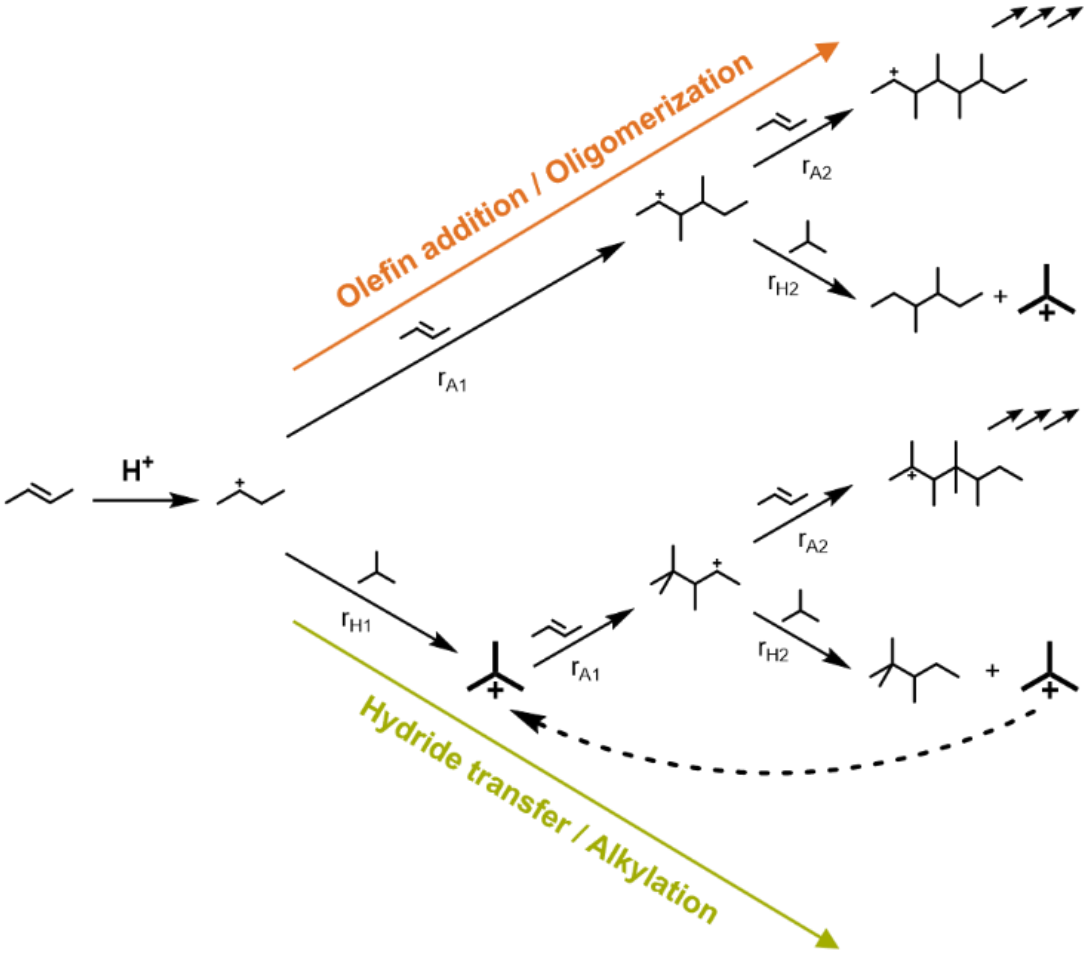

Scheme 2.1. Simplified reaction network in the 2-butene/isobutane alkylation. The r_{Hi} (i = 1, 2) represents the rate of hydride transfer from isobutane to carbenium ions and r_{Ai} (i = 1, 2) represents the nucleophilic addition of olefin (2-butene) to carbenium ion.

The original hypothesis has been based on the expected butene concentration gradient in a catalyst pellet predicted by the Thiele modulus (Figure 2.1). The induced mass transport limitation results in a concentration gradient of butene. In particular, the drop of butene concentration becomes steeper when pellet radius is larger, leading to a lower concentration of butene locally inside the pellet.

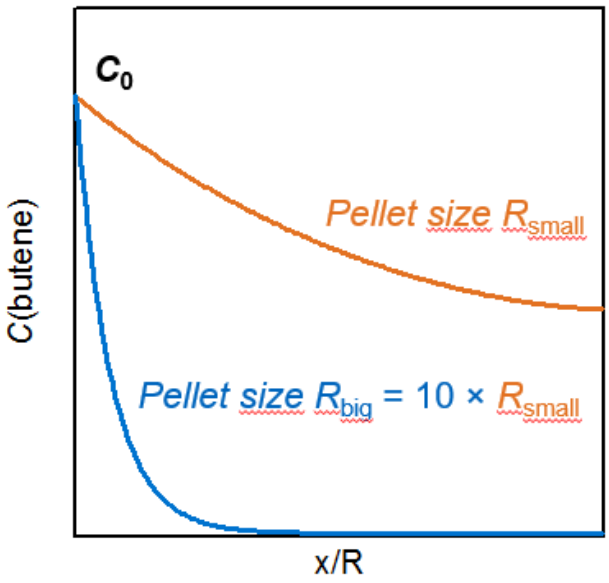

Figure 2.1. Simulated concentration profile of butene in a spherical catalyst pellet dependent on radius R exemplified by small radius (R_{small}) and big radius (R_{big} = 10 R_{small}); x is the distance from spherical pellet surface towards inside; c_0 is the butene concentration outside the pellet. (Detailed derivations see in Supplemetary Informations).

It may appear intuitive at first sight that a large catalyst pellet size is detrimental for catalyst lifetime and selectivity[21] because of the reduced total number of simultaneously accessible sites. This draw-back, however, has been shown to be compensated already in preliminary experiments by a markedly suppressed deactivation. To quantify this effect, we explore here the impact of catalyst pellet diameter on alkylation of isobutane with butene in a fixed bed reactor with high excess of isobutane, mimicking the low butene concentration in a CSTR.

2.2. Experimental section

2.2.1. Preparation of catalysts

La-exchanged zeolite X (LaX) was prepared from NaX (Si/Al = 1.2) provided by Chemische Werke, Bad Köstritz. The parent material was ion exchanged four times with 0.2 M $La(NO_3)_3$ solution at 70°C for 2 h with a liquid-to-solid ratio of 10 $ml \cdot g^{-1}$. The material was washed subsequently with double distilled water and was dried at room temperature. After the second and the fourth ion exchange the sample was calcined in 100 $ml \cdot min^{-1}$ synthetic air with a heating ramp of 0.5 $°C \cdot min^{-1}$ and a maximum temperature of 450°C. The prepared catalyst was stored under constant water vapor pressure over saturated $CaCl_2$ solution.

In order to prepare pellets in the range of 0.15-0.25, 0.25-0.35, 0.35-0.5 and 0.5-0.7 mm the catalyst powder was pressed into wafers, crushed and sieved. Pellet sizes 0.8, 1.1 and 1.6 mm were formed in the shape of cubes by pressing zeolite wafers in the thickness of the desired edge length and cutting them manually.

2.2.2. Catalytic tests

The alkylation of isobutane with 2-butene was performed in a fixed-bed reactor with ¼ inch diameter at 75°C and 25 bar. Prior to reaction, 0.1 g catalyst was activated in situ in H2 at a maximum temperature of 250°C for 1 h using an increment of 2 $°C \cdot min^{-1}$. The reaction was started by feeding a mixture of isobutane and cis-2-butene (Rießner Gase GmbH) with a molar ratio of 200:1 using a high-pressure Teledyne ISCO 500D syringe pump. The alkene space velocity was 0.2 g butene·gcatalyst-1·h-1. The reaction mixture was expanded after the reactor via a backpressure regulator and passed through a six-port valve with a 0.1 ml sample loop. The product distribution was measured using a 60 m DB-1 column (ID = 0.32 mm, film thickness = 1.00 µm) in an Agilent 7890B gas chromatograph equipped with an FID detector.

2.2.3. Characterization of used catalyst pellets

IR spectroscopy was used to characterize the hydrocarbon species on used catalyst pellets. For identification, different parts of the pellets, i.e. outer shell and inner core were mechanically separated based on their coloration. Each fraction was pressed into a thin and self-supporting wafer that was loaded into a reaction cell. There wafer was first activated for 1h at 450°C (temperature increment of 5 $K \cdot min^{-1}$) in 20 mL/min N_2 flow. The IR spectra were collected at 150°C with a resolution of 4 cm^{-1} and an average of 120 scans per spectrum on a Nicolet iS50AEM spectrometer.

The Brønsted (BAS) and Lewis acid site (LAS) concentrations of fresh samples were determined by IR-spectra of adsorbed pyridine using a Thermo Nicolet 5700 in the range of 400-4000 cm^{-1} with a resolution of 4 cm^{-1}. The samples were pressed into thin, self-supported wafers and activated at 450°C for 1 h in vacuum (10^{-6} mbar) with a heating rate of 10 $K \cdot min^{-1}$. Subsequently, pyridine was adsorbed at 0.5 mbar at 150°C for 1 h. After outgassing in high vacuum for 1 h to remove physisorbed pyridine, a spectrum was taken to determine the concentration of adsorbed pyridine. To obtain the concentration of strong acid sites, the sample was heated to 450°C for 1 h (heating rate = 10 $°C \cdot min^{-1}$). For quantification, molar integral extinction coefficients of 0.73 $cm \cdot \mu mol^{-1}$ and 0.96 $cm \cdot \mu mol^{-1}$ were used for pyridine adsorbed on Brønsted and Lewis acid sites, respectively.[22]

Images of cross-sections of used cubes were collected using a Leica MZ 8 Stereomicroscope (magnification 2.0x). The shell thickness was measured by using the software ImageJ. The growth of the shell was investigated by analyzing images of catalysts being exposed to different TOS in the reaction.

For the analysis of carbonaceous deposits, the separated pellet parts were dissolved in 10% HF solution. Excess HF was evaporated and the residue was extracted with CH_2Cl_2. Carbonaceous deposits have been claimed to be completely soluble in organic solvents and to remain unaltered after the treatment with hydrofluoric acid. An Agilent 7890B GC-MS with a nonpolar HP-5 (5%-phenyl) methylpolysiloxane column was used for the measurements. The detector was a MSD of the 5977A series from Agilent with an energy of 70 eV. A 1-µl portion of the extracted sample was injected into the column. The temperature was first increased to 333 K for 3 min and then to 598 K (heating rate, 10 K/min).

2.3. Results and discussion

2.3.1. Effect of pellet size on butene conversion and catalyst deactivation

Figure 2.2 shows the conversion of butene in isobutane/butene alkylation catalyzed by LaX with different pellet sizes. With LaX pellets having the smallest diameter (0.15-0.25 mm), full conversion of butene was reached at the beginning of the reaction until approximately 8 h time on stream (TOS), followed by a sharp drop to 20-30% conversion and a slower drop afterwards. The sharp decrease of butene conversion after the full conversion period is attributed to the deactivation by pore and acid site blockage of catalysts caused by the heavy hydrocarbon byproducts.[11] Increasing the pellet size stepwise to 0.8 mm led to a gradual prolongation of the full conversion period to 20 hours. The rate of conversion decrease became less steep with increasing particle diameter, indicating a slower rate of deactivation. Further increase of the pellet size to 1.6 mm resulted in the reduction of the length of the full conversion period, while the deactivation was, however, further reduced.

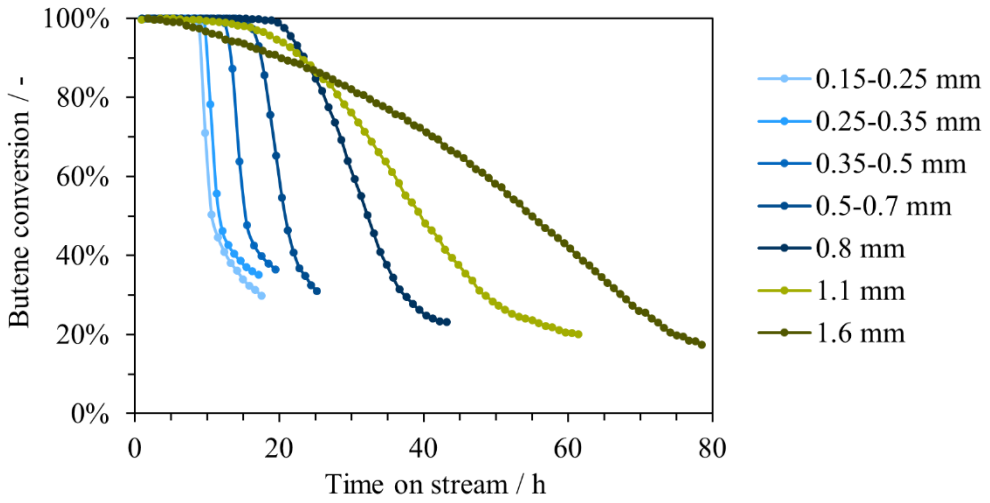

Figure 2.2. Butene conversion with time on stream for different pellet sizes of LaX zeolite (Reaction condition: 0.1 g catalyst, 75°C, 25 bar, Isobutane to cis-2-butene with a molar ratio of 200:1, olefin space velocity 0.2 $g_{butene} \cdot g_{catalyst}^{-1} \cdot h^{-1}$.)

In order to quantify this observation, we define the deactivation rate as the loss of conversion per TOS (d*conv*/d*TOS*) over complete time on stream. Figure 2.3a shows the changes of

deactivation rate with TOS on LaX catalyst with different pellet sizes. The deactivation rate changed with TOS in the shape of a volcano curve. The maximum deactivation rate occurred at the conversions between 60 and 80% for all pellet sizes (see section 2.6 supporting information Figure S2.1). With increasing pellet size the deactivation rate maxima decreased and the span of TOS during the deactivation broadened. The smallest pellet size (0.15-0.25 mm) showed a maximum deactivation rate of $7.6 \cdot 10^{-5}$ s^{-1}, and that for largest pellets (1.6 mm) was $0.43 \cdot 10^{-5}$ s^{-1}. Comparing the deactivation rates at similar butene conversions (Figure 2.3b) illustrates the slower deactivation of larger pellets.

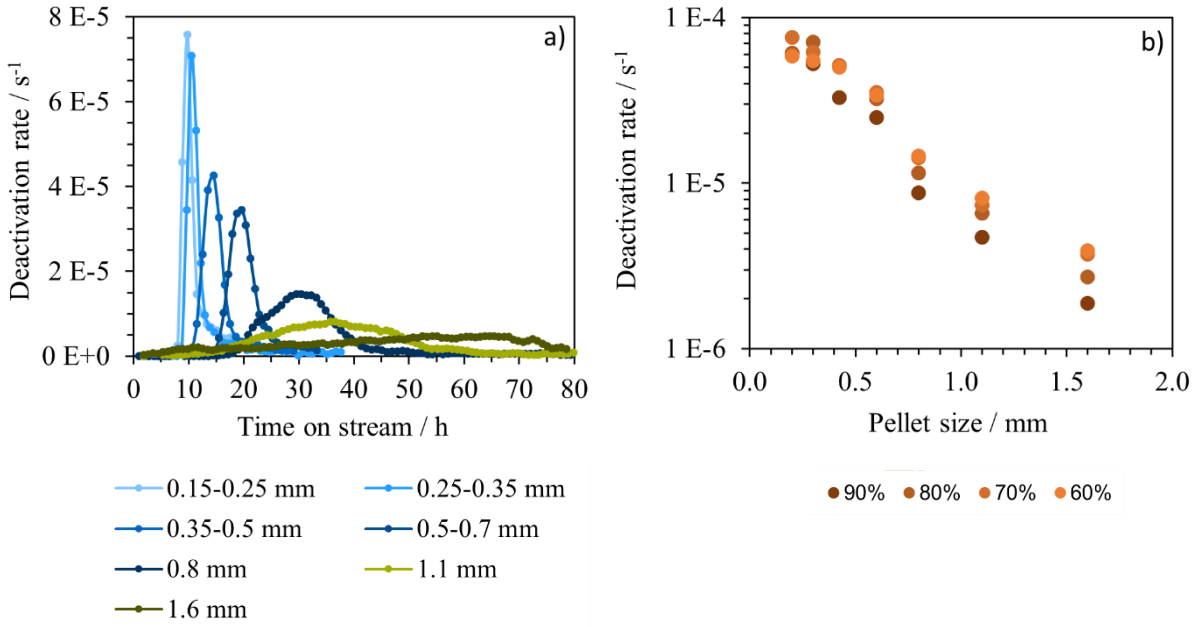

Figure 2.3. a) Evolution of catalyst deactivation rates with time on stream on LaX with different pellet sizes b) Deactivation rate as a function of LaX pellet size at butene conversions of 90%, 80%, 70% and 60%, respectively. (Reaction condition: 0.1 g catalyst, 75°C, 25 bar, Isobutane to cis-2-butene with a molar ratio of 200:1, olefin space velocity 0.2 $g_{butene} \cdot g_{catalyst}^{-1} \cdot h^{-1}$.)

The slower deactivation with large pellets increased the integral alkylate yield (Figure 2.4a) from 3.3 $g_{alkylate} \cdot g_{cat}^{-1}$ for the smallest pellets (0.15-0.25 mm) to 16.8 $g_{alkylate} \cdot g_{cat}^{-1}$ for the largest pellets (1.6 mm). The shorter period of full conversion with the largest pellets is compensated by the very low deactivation rate, leading, thus, to the highest integral alkylate yield. Overall, a linear correlation between integral yield and the pellet size of LaX was observed (Figure 2.4b).

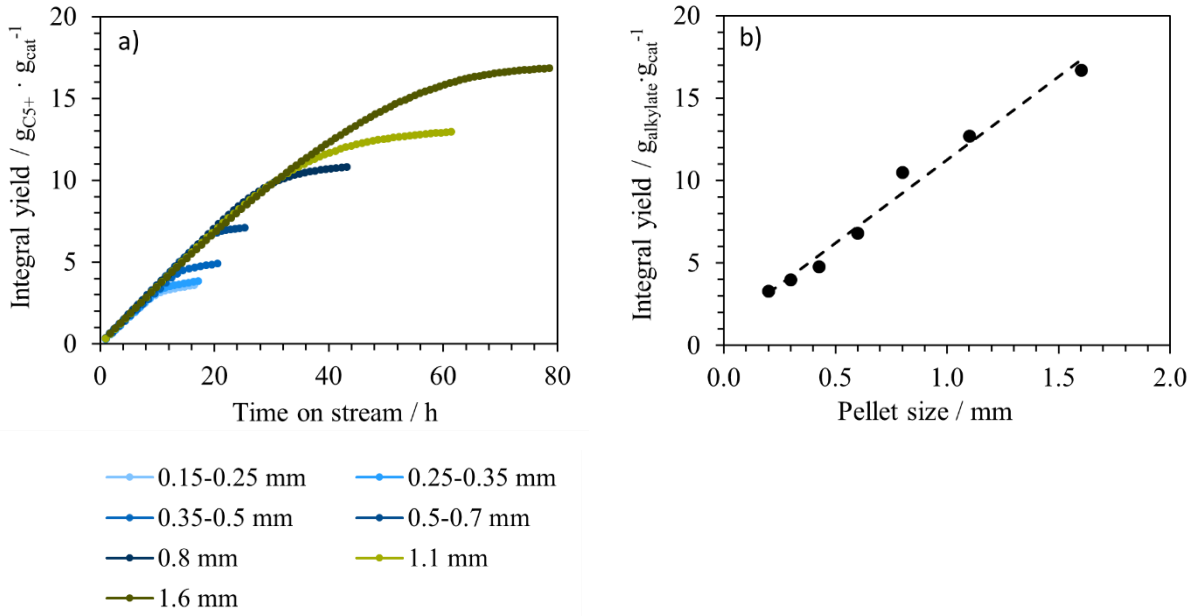

Figure 2.4. a) Integral yield of alkylate (C_{5+}) with time on stream and b) Integral yield for different pellet sizes in the cis-2-butene/isobutane alkylation. (Reaction condition: 0.1 g catalyst, 75°C, 25 bar, Isobutane to cis-2-butene with a molar ratio of 200:1, olefin space velocity 0.2 $g_{butene} \cdot g_{catalyst}^{-1} \cdot h^{-1}$.)

2.3.2. Effect of pellet size on product selectivity

The main products of 2-butene/isobutane alkylation were branched octanes, i.e., isomers of trimethylpentane (TMP) and dimethylhexane (DMH). The byproducts were C_9 or higher hydrocarbons (C_{9+}), C_{5-7} hydrocarbons and n-butane. Figure 2.5 compares the selectivity of catalysts with TOS. With all catalyst pellets, the selectivity of C_8 alkanes decreased with TOS, and in parallel C_{9+} hydrocarbons as well as C_{5-7} products increased. With the increase of catalyst pellet sizes, the initial selectivity towards octanes increased from approximately 70 wt% to 85 wt% and the selectivity of C_{9+} byproducts was reduced from approximately 12 wt% to 3 wt%. In parallel, the selectivity of C_{5-7} hydrocarbons decreased from around 14 wt% to 7 wt% (Figure 2.5b). Moreover, the n-butane selectivity was enhanced by larger pellets from 2 wt% to 5 wt%. These changes indicate that large pellets reduce multiple alkylation, as well as cracking and increase the hydride transfer to adsorbed n-butene.

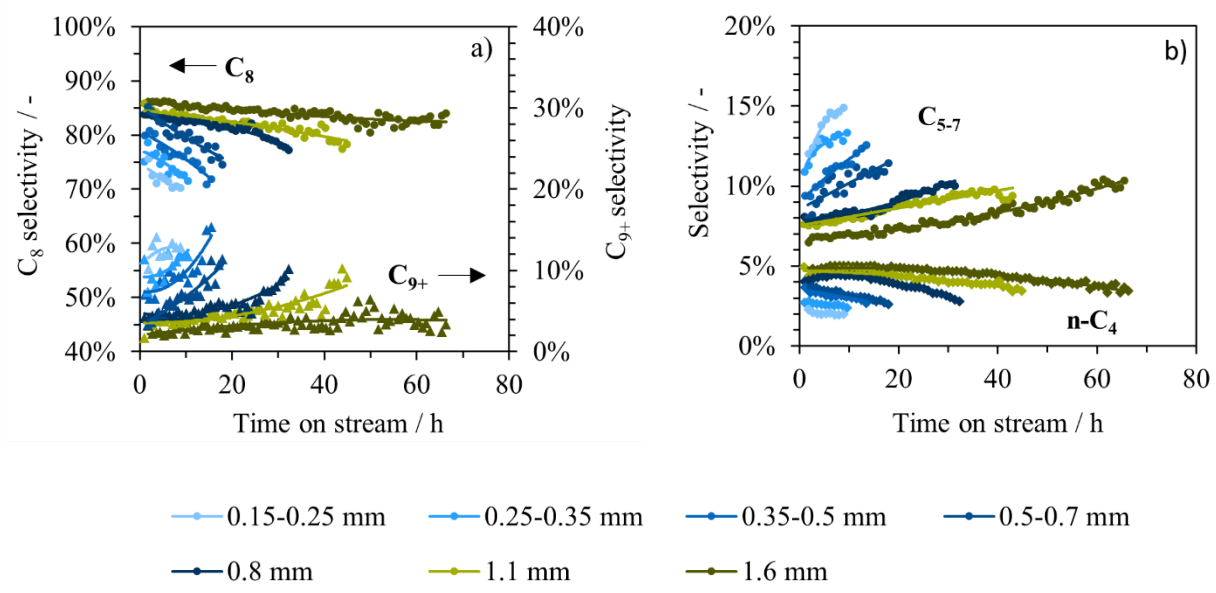

Figure 2.5. a) Selectivity of C_8 and C_{9+} hydrocarbons over time on stream for different pellet sizes. b) Selectivity of n-Butane and C_{5-7} hydrocarbons over time on stream for different pellet sizes. (Reaction condition: 0.1 g catalyst, 75°C, 25 bar, isobutane to cis-2-butene with a molar ratio of 200:1, olefin space velocity 0.2 $g_{butene} \cdot g_{catalyst}^{-1} \cdot h^{-1}$.)

Within the C_8 products, the overall selectivity to TMPs increased from approximately 60% with the smallest pellets to 80% with the largest (Figure 2.6a); the DMH selectivity decreased from 11% to 7%. Thus, the composition within the C_8 products shifted towards more TMP and less DMH with larger pellet size, i.e., the main alkylation reaction increased and all other reactions decreased in importance.

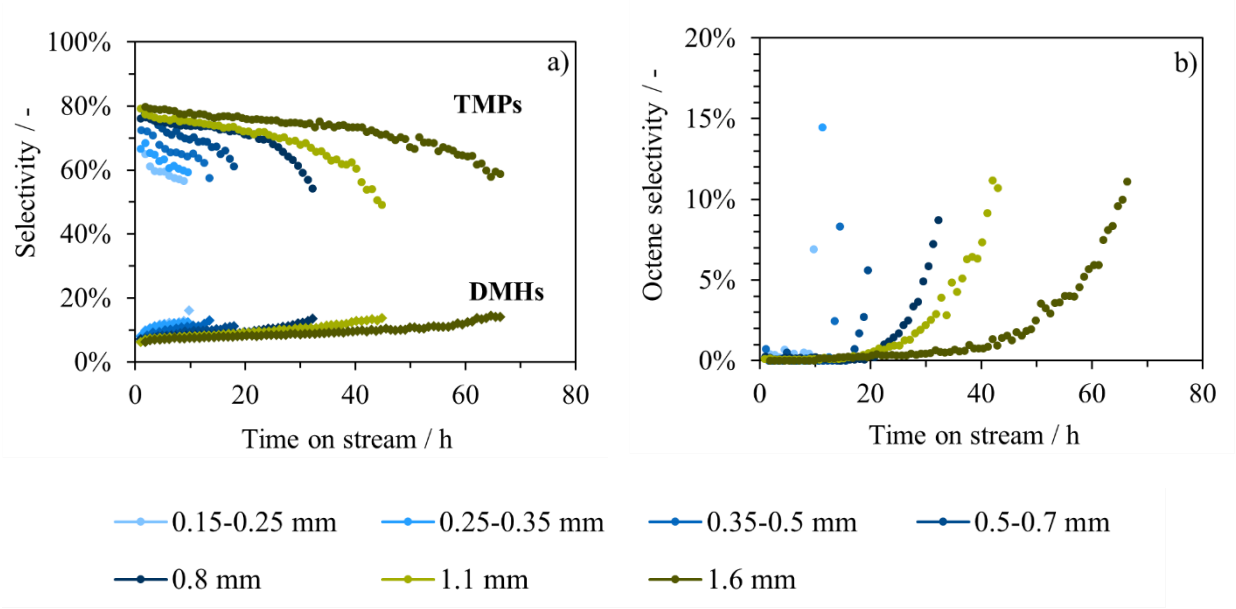

Figure 2.6. a) Selectivity of trimethylpentane (TMP) isomers and dimethylhexane (DMH) isomers with time on stream for different pellet sizes. b) Octene selectivity with time on stream for different pellet sizes. (Reaction condition: 0.1 g catalyst, 75°C, 25 bar, Isobutane to cis-2-butene with a molar ratio of 200:1, olefin space velocity 0.2 $g_{butene} \cdot g_{catalyst}^{-1} \cdot h^{-1}$.)

Octenes are formed via deprotonation of C_8^+ carbenium ions desorbing from catalytic surface before hydride transfer from isobutane took place. Because isomers of 3,4-dimethylhexenes were the most abundant alkenes, the reaction of 2-butene with a secondary carbenium ion ($CH_3CH_2^+CH_3CH_3$) denoted as dimerization is hypothesized to be the main reaction pathway during partial conversion of butene. Thus, we conclude that dimerization begins to dominate, as alkylation deactivates, i.e., when butene conversion drops below full conversion. The rise in concentration of alkenes is hypothesized to further enhance deactivation.[8] The formation of octenes occurred at a slower rate and at a later TOS for the larger pellets (Figure 2.6b) perfectly correlated with the lower rate of deactivation.

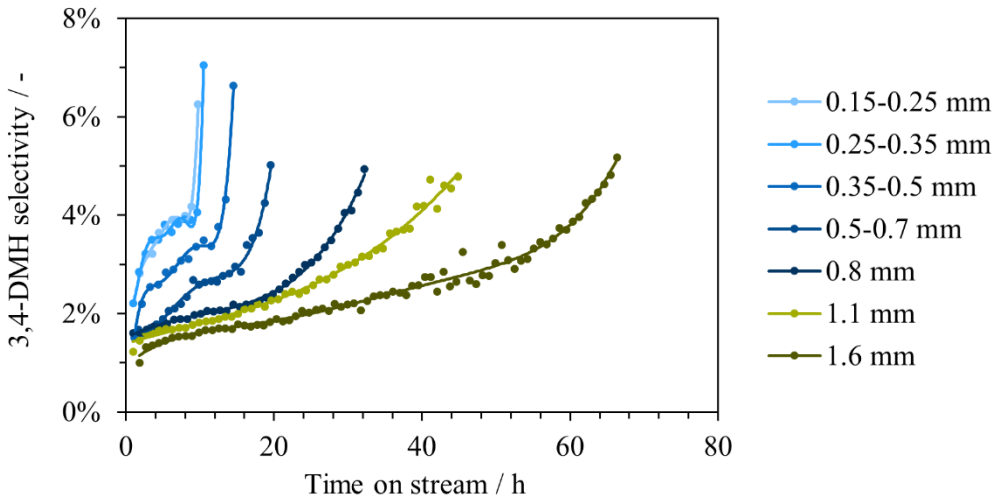

Figure 2.7. 3,4-DMH selectivity with time on stream for different pellet sizes.

Even though octenes were not detected at full conversion, the presence of DMH suggests that these alkenes formed transiently and that the alkanes formed by re-adsorption and hydride transfer from isobutane (Scheme 2.1). Both, the total selectivity to all DMH isomers (Figure 2.6a) and the selectivity to 3,4-DMH (Figure 2.7), i.e., the primary DMH isomer from 2-butene dimerization and a hydride transfer, showed a strong decrease with increasing pellet size. Thus, we conclude that the decrease of the local 2-butene concentration caused by the gradient in the pellet minimizes the rate of dimerization, which is bimolecular in 2-butene in the pores, versus the rate of alkylation, which depends only linearly on 2-butene.

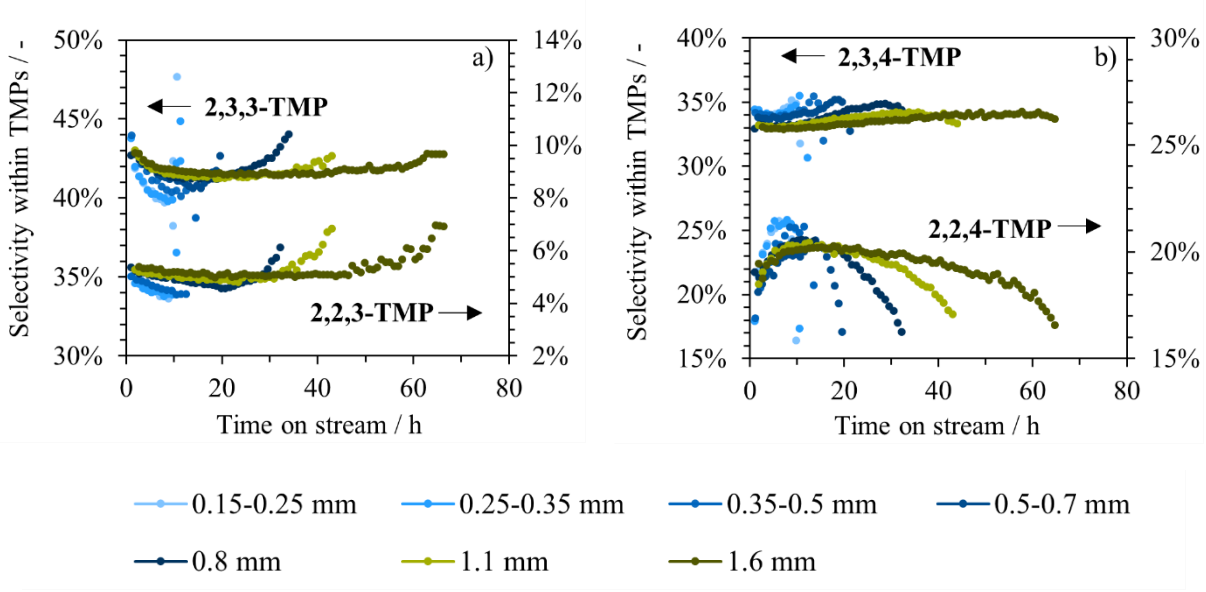

Figure 2.8. Selectivity within C_8 fraction with time on stream for different pellet sizes for a) 2,2,3- and 2,3,3-TMP and b) for 2,2,4- and 2,3,4-TMP. (Reaction condition: 0.1 g catalyst, 75°C, 25 bar, isobutane to cis-2-butene with a molar ratio of 200:1, olefin space velocity 0.2 $g_{butene} \cdot g_{catalyst}^{-1} \cdot h^{-1}$.)

Figure 2.8 compiles the selectivity to different products within TMPs. The main products were 2,3,3-TMP (40-45%) and 2,3,4-TMP (33-35%), both being secondary products that underwent skeletal isomerization from 2,2,3-TMP and 2,2,4-TMP (Scheme 2.2). The primary product formed by alkylation of isobutane with n-butene is 2,2,3-TMP (Scheme 2.2, route I). It had the lowest abundance within TMPs with only 4-6%. The isomer 2,2,4-TMP, formed by isomerization of 2,2,3-TMP and alkylation of isobutane with isobutene (formed by deprotonation of the tert-butyl carbenium ion, i.e., via "self-alkylation"; Scheme 2.2, route II) had an abundance of 20-25%. The higher selectivity of secondary products (2,3,3-TMP & 2,3,4-TMP) than primary products (2,2,3-TMP & 2,2,4-TMP) indicates that 1-2 turnovers of isomerization occurred for a C_{8+} carbenium ion before it accepted a hydride and desorbed as TMP.

The selectivity to 2,2,4-TMP and 2,3,4-TMP within TMPs decreased for larger pellets and in parallel 2,2,3-TMP and 2,3,3-TMP decreased (Figure 2.8). These apparently linked variations, allow us to hypothesize that 2,3,3-TMP is mainly formed by isomerization of 2,2,3-TMP, while 2,3,4-TMP is formed mainly by isomerization of 2,2,4-TMP. The hypothesis is based on the

minimum number of methyl shifts in the absorbed state, i.e., as carbenium ion before a hydride transfer from isobutane takes place.

With increasing TOS, the selectivity to 2,2,3-TMP and 2,3,3-TMP (products from route I in Scheme 2.2 decreased, while those to 2,2,4-TMP and 2,3,4-TMP (products from route II in Scheme 2.2) increased on all pellet sizes until the onset of octene formation. The trend inverted as the catalyst is deactivated to the extent that 2-butene conversion was incomplete. The changes of the relative importance of the two routes are clearer in Figure 2.9, which shows the ratio of self-alkylation (Route II, 2,2,3-TMP + 2,3,3-TMP) vs. n-butene alkylation (Route I, 2,2,4-TMP + 2,3,4-TMP) with TOS. Initially, the ratio was 1.05 for all pellet sizes. Then the ratio first increased with TOS but dropped when catalyst deactivation became severe. It is notable that the (moderate) changes were more pronounced with the smaller pellets than with the larger.

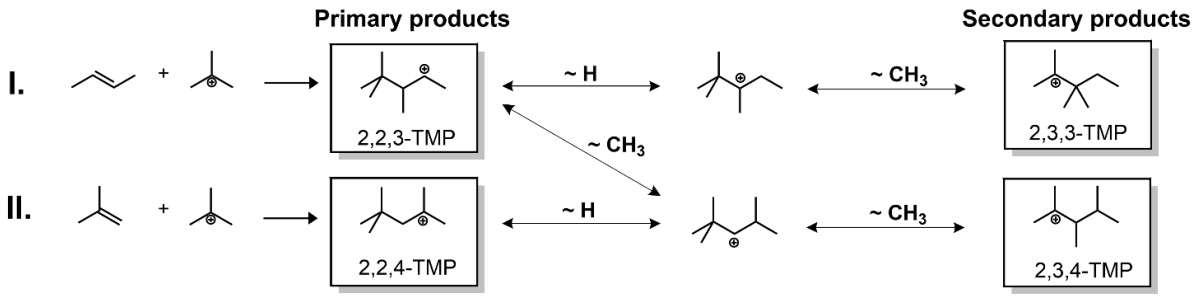

Scheme 2.2. Formation routes for trimethylpentane isomers. Route I (standard alkylation): Reaction of n-butene with tertiary carbenium ion forming 2,2,3-TMP as primary product and 2,3,3-TMP by isomerization. Route II (Self-alkylation): Reaction of isobutene with tertiary carbenium ion forming 2,2,4-TMP as primary product and 2,3,4-TMP as secondary product.

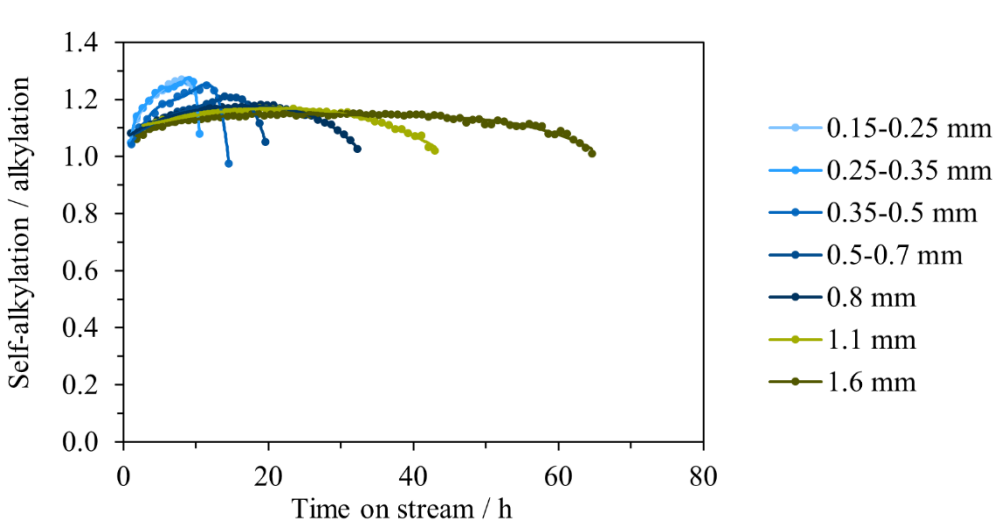

Figure 2.9. Ratio of main products from self-alkylation (S(2,2,4-TMP) + S(2,3,4-TMP)) to the main products from n-butene alkylation (S(2,2,3-TMP) + S(2,3,3-TMP)).

The higher rate of self-alkylation (Route II in Scheme 2) on smaller pellets or at higher TOS is hypothesized to indicate a higher isobutene concentration at the catalytic site. Isobutene is formed via two pathways: (1) hydrogen transfer from isobutane to n-butyl carbenium ion (n-C_4^+), leading to n-butane and isobutyl carbenium ion (iso-C_4^+) that desorbs as isobutene; (2) cracking of carbenium ions stemming from cracking of multiple alkylates forming to C_{5-7} alkenes, which react with isobutane to C_{5-7} alkanes and isobutene (Scheme 2.2). The two pathways produce n-butane (Scheme 2.2, Pathway 1) and C5-7 alkanes (Scheme 2.2, Pathway 2) as byproducts, respectively. Small pellets showed lower n-butane selectivity and higher C_{5-7} hydrocarbon selectivity than large pellets (Figure 2.5b), indicating that more pronounced cracking of higher alkylates causes its higher relevance for small pellets and the higher fluctuation in the selectivity to Route II. In contrast, the multiple alkylation was much slower with large pellets (lower concentration of n-butene in the inner of the large particles), which in turn leads to less cracking of higher alkylates and, hence, a lower concentration of isobutene and lower selectivity to Route II. The same was observed during catalyst deactivation. n-Butane decreased while C_{5-7} hydrocarbon increased with TOS, indicating that cracking of multiple alkylates (Scheme 2.2, Pathway 2) was the main contributor for the increase of self-alkylation during catalyst deactivation. Accumulation of multiple alkylate in the zeolite pore not only

deactivates catalysts, but also leads to higher concentration of isobutene and consequently a higher probability of self-alkylation.

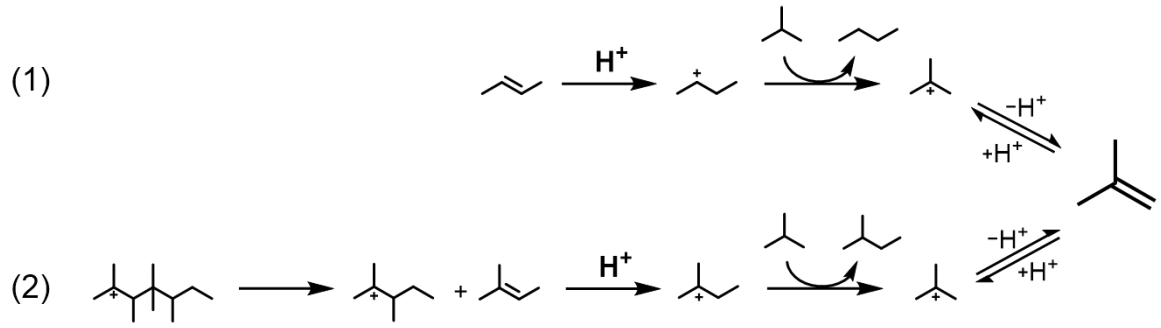

Scheme 2.3. Pathways for the formation of isobutene in 2-butene/isobutane alkylation. (1) Hydride transfer from isobutane to butene. (2) Hydride transfer from isobutane to C_{5-7} alkenes from cracking. The two pathways produce n-butane and C_{5-7} alkanes as byproducts, respectively.

The yield of alkylate per converted butene improved with increasing pellet size as a direct result of the decrease in multiple alkylation (Figure 2.10). The alkylate yield (at approximately 5 h TOS) was 1.84 $g_{alkylate} \cdot g_{butene}^{-1}$ for very small pellets (0.15-0.25 mm) and increased to 2.03 $g_{alkylate} \cdot g_{butene}^{-1}$ for 1.6 mm pellets. Considering that alkylation of isobutane with n-butene results in a theoretical yield of 2.04 $g_{alkylate} \cdot g_{butene}^{-1}$ under stoichiometry of 1 isobutane to 1 butene, multiple alkylation or oligomerization consumes more than one butene molecule per converted isobutane.

It should be noted in passing that also lighter alkanes (C_{5-7} hydrocarbons) must originate from C_{9+} hydrocarbons as they are generated by cracking and, therefore, also lower the process efficiency by consuming more than one butene molecule per isobutane converted.

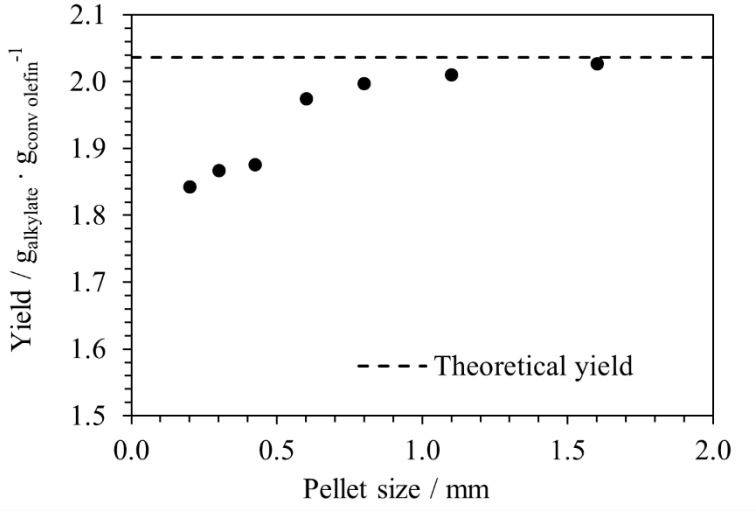

Figure 2.10. Yield of alkylate (C_5 or larger hydrocarbons) per converted butene (at 5 h time on stream) at different pellet sizes.

Overall, the catalytic performance (catalyst deactivation, product selectivity and alkylate yield) of identical catalysts improved towards the theoretical optimum value with increasing catalyst pellet size. This supports the hypothesis that 2-butene transport limitations are beneficial for the reaction, i.e., the side-reactions (oligomerization, multiple alkylation) depend to a higher degree on the local concentration of 2-butene than alkylation. Because the hydride transfer reactions (activating isobutane) are a material property they are not influenced by the pellet size.

2.3.3. Characterization of used catalyst pellets

It has been argued so far that the reduced catalyst deactivation and the improved TMP selectivity with large catalyst pellets are caused by the averaged lower 2-butene concentration at the acid sites. To analyze the impact of this lower concentration, the adsorbed hydrocarbon species on used catalysts was investigated using model catalyst pellets of cubic shape with 2 mm side length. Figure 2.11 shows images of cross-sections of such catalyst pellets of different times on stream. The used catalysts show two zones, an outer dark shell and a lighter colored inner. With increasing TOS the fraction of the dark shell grew (Figure 2.12) and the coloring occurred after exposure to atmosphere within minutes with intensification up to 24 hours (see section 2.6 supporting information Figure S2.7).

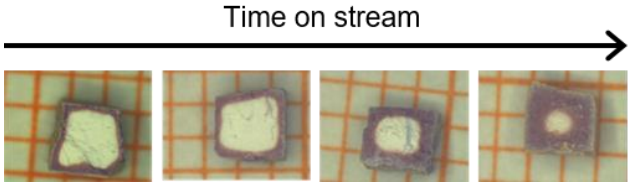

Figure 2.11. Microscope images of cross-sections of used 2 mm cubes at different time on stream (10, 20, 50 and 78 h TOS from left to right). Background net scales 1 mm x 1mm for each square.

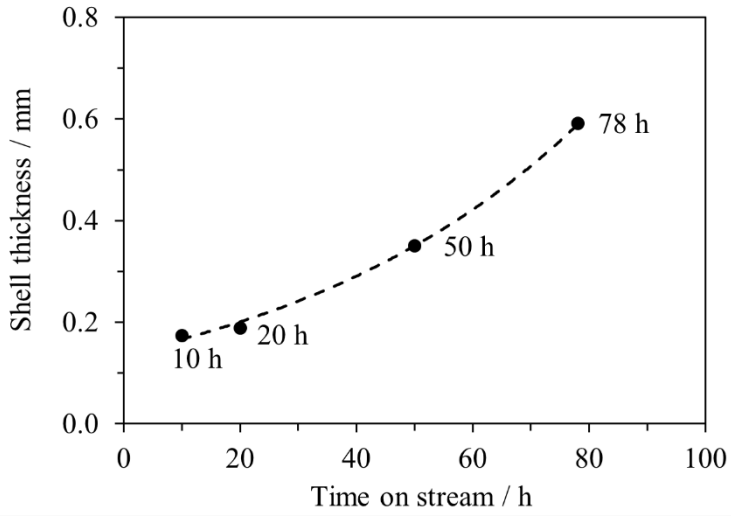

Figure 2.12. Development of dark shell zone diameter with time in stream.

For detailed analysis, the dark shell and light core of used pellets were mechanically separated and characterized by IR spectroscopy in Figure 2.13. The bands at 2922 and 2877 cm^{-1} are assigned to the asymmetric and symmetric stretching vibrations of CH_3 groups (ν_aCH_3, ν_sCH_3), while bands at 2930 and 2838 cm^{-1} correspond to the asymmetric and symmetric stretching vibrations of CH_2 groups (ν_aCH_2, ν_sCH_2).

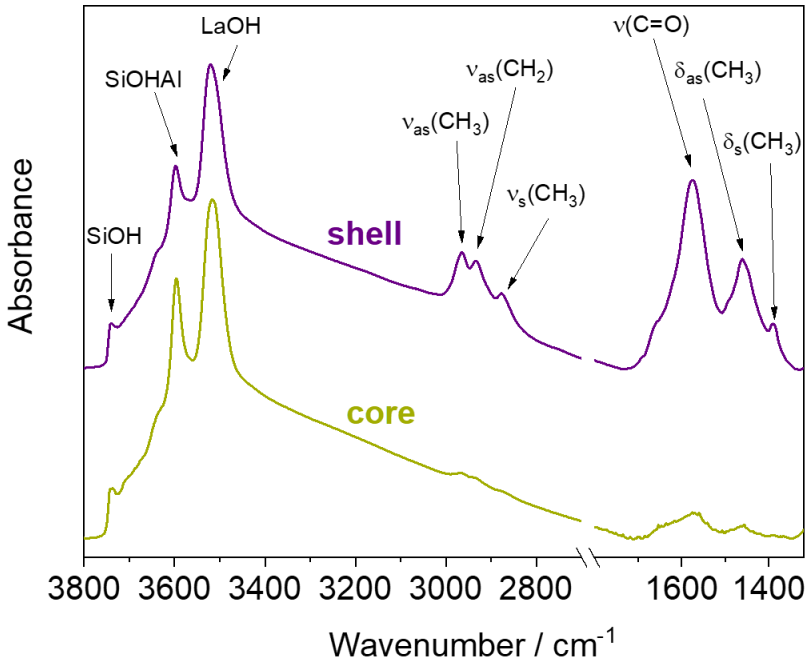

Figure 2.13. Infrared spectra of used catalysts with separated core and shell part of pellet.

Bands at 1376 and 1460 cm^{-1} correspond to deformation vibrations (δCH_3, δCH_2). The shell of the pellet showed strong CH vibration bands in the region between 2800 and 3000 cm^{-1} and 1350 to 1700 cm^{-1} suggesting the presence of largely saturated hydrocarbons. The core fraction of pellets on the other hand has a much lower concentration of hydrocarbons indicated by the weaker bands of 2800-3000, 1376 and 1460 cm^{-1}.

In particular, the very strong band at 1578 cm^{-1} on the shell part is difficult to assign. Some literatures attributed it to polycyclic aromatic hydrocarbons [23], however, this possibility was excluded by the GC-MS analysis of the organic deposits after dissolving the used zeolite in HF which showed no presence of polycyclic aromatic hydrocarbons (see section 2.6 supporting information Figure S2.6). Instead, the long-chain oxygenates (C15-C22) and in particular alkyl

carboxylates were identified on the GC-MS of the organic deposits. This led us to speculate that the band at 1578 cm^{-1} was indicating the presence of carboxylate species. They are hypothesized to form via carboxylation or oxidation of the deposited hydrocarbons by the exposure of the used catalyst to ambient environment during the handling process. This hypothesis is also supported by the observation of gradually intensified coloring of used catalyst with ongoing exposure to atmosphere (see section 2.6 supporting information Figure S2.7) which implies a transformation of species via reaction with air that is likely to be oxidation or carboxylation.

The dark shell of the pellet still shows free BAS (i.e., the OH band at 3600 cm^{-1}) as well as free LaOH groups (OH band at 3520 cm^{-1}), while these bands are significantly higher in the core fraction, indicating less blockage of active sites in the latter volume. As shown in Table 2.1 fresh catalysts have a BAS concentration of 0.76 $mmol \cdot g^{-1}$ and LAS concentration of 0.35 $mmol \cdot g^{-1}$. The dark shell volume showed a BAS concentration of 0.42 $mmol \cdot g^{-1}$ and a LAS concentration of 0.20 $mmol \cdot g^{-1}$ indicating a loss of slightly less than half of both acid site concentrations. In contrast, the acid site loss was much smaller for the catalysts in the fraction with a lighter color.

Table 2.1. Acid site concentration of fresh and different parts of used catalyst pellets.*

	Fresh LaX	Light core	Dark shell
BAS [$mmol \cdot g^{-1}$]	0.76	0.65	0.42
LAS [$mmol \cdot g^{-1}$]	0.35	0.28	0.20

* Acid site concentration determined by IR spectra of adsorbed pyridine

Further investigation of the dark shell fraction by IR spectroscopy showed that the bands in the region 1350 to 1700 cm^{-1} changed during heating from 150 to 450°C (Figure 2.14). The band at 1641 cm^{-1} is primarily attributed to the stretching mode of the C=C double bonds. However, it is assumed to be partly also caused by the deformation vibration of H_2O, as molecular water is still adsorbed on LaX when outgassed at 150°C. The broad OH band in the region from 3000 to 3600 cm-1 (see section 2.6 Figure S2.5) supports this assumption.

The spectra taken at 150°C also showed a band at 1536 cm^{-1} attributed to cyclopentenyl cations.[11] After thermal treatment at 450°C the bands at 1641 and 1536 cm^{-1} disappeared, indicating the complete removal of water as well as a transformation of olefinic species. The bands at 1580 cm^{-1} and 1450 cm^{-1} are attributed to the antisymmetric and symmetric vibration of carboxylates, typically generated by transformation of functional groups on zeolites during deactivation.[25]

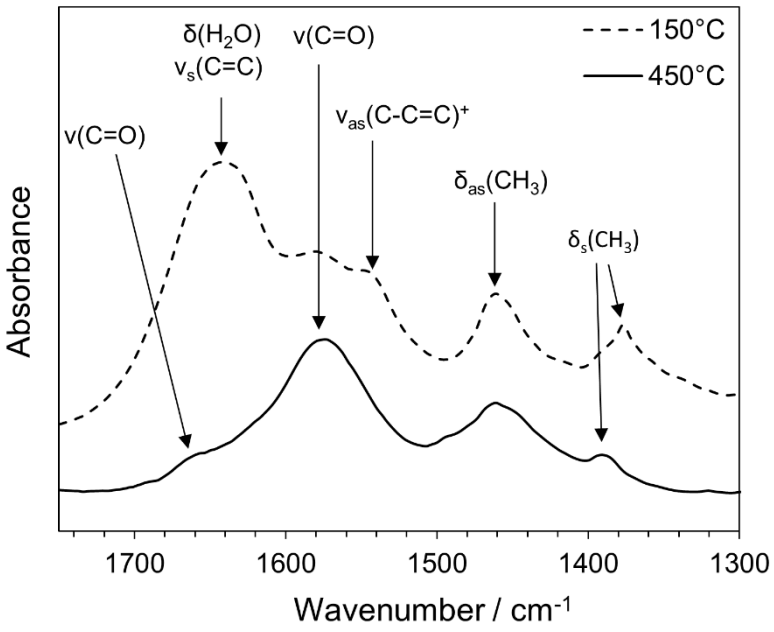

Figure 2.14. IR spectra of dark-colored shell at 150°C and 450°C in the region 1300-1750 cm^{-1}.

The IR spectra clearly shows that the dark shell of used pellets is deactivated by the organic deposits. In liquid acid catalyzed alkylation conjunct polymers also known as acid-soluble oil (ASO) or red oil are known to cause brownish coloring.[26] Especially conjugated diene hydrocarbons of ASO are stated to cause catalyst deactivation by poisoning without affecting product distribution.[27] Therefore, it is plausible to assume unsaturated hydrocarbons generated from multiple alkylation and deprotonation are built up and causes the darkening of the catalyst. The observed coloring with time on stream in Figure 2.11 proves the nonuniform deactivation of catalyst pellets from outside towards pellet core, in line with the predicted reactant concentration gradient along the radius of pellets in Figure 2.1. The catalyst at the core of large pellets still has the color of fresh catalyst and very less deactivated, thus capable to operate with long lifetime.

2.4. Conclusions

The pellet size of La^{3+} exchanged X zeolite strongly influences the alkylation of isobutane with 2-butene. Increasing from pellets with diameters of 0.15-0.25 mm to ones of 1.6 mm markedly decreased the deactivation rate of LaX for alkylation of n-butene and iso-butane. Not only was the lifetime prolonged by more than 3-fold, the yield of alkylate products during the catalyst activity increased 6-fold. The higher productivity was accompanied by a higher selectivity to trimethylpentanes (TMP) and the concomitantly lower selectivity to cracked products (C_{5-7}) and larger hydrocarbons (C_{9+}) resulting from multiple alkylation. Within the octanes, lower concentrations of dimethylhexanes (i.e., the product of 2-butene dimerization and of the minor rates of isomerization of TMP) was reduced with increasing pellet size. Within the TMPs, the route from primary alkylation products, 2,2,3- and 2,3,3-TMP (Route 1), grew in prominence over the route resulting from alkylation from intermediately formed isobutene, i.e., 2,2,4- and 2,3,4-TMP (Route 2) as the particle size increased.

Simulation of 2-butene concentration gradient along the radius of catalyst pellets using the Thiele model shows that pellets with small radius had a more homogenous distribution of butene inside the pellet, while pellets with large radius had a steeper drop of butene concentration at the boundary of pellet causing a very low butene concentration inside catalyst pellet. Therefore, we conclude that side reaction pathways including multi-alkylation, dimerization and self-alkylation in large catalyst pellets are significantly retarded by the low concentration of butene and the resulting high P/O ratio at the catalytic active site.

The differences in butene concentration profiles are also manifested in the formation of a dark-colored outer shell and lighter-colored core in used catalyst pellets. The dark-colored fraction increased with time on stream. Multiply unsaturated hydrocarbon species that are transformed partly to carboxylates (identified by IR spectroscopy and GC-MS analysis) are concluded to dominate in the dark-colored volume, while the light inner core of pellets showed only minor traces of hydrocarbon compounds.

These results demonstrate that adjusting the pellet size is a successful path to locally minimize the concentration of butene at catalytically active site and to improve catalyst properties for solid acid alkylation catalyst independent of the mode of operation.

2.5. References

1. Weitkamp, J.; Traa, Y., Isobutane/butene alkylation on solid catalysts. Where do we stand? *Catal. Today* **1999,** *49* (1), 193-199.
2. Albright, L. F., Alkylation of Isobutane with C3−C5 Olefins To Produce High-Quality Gasolines: Physicochemical Sequence of Events. *Ind. Eng. Chem. Res.* **2003,** *42* (19), 4283-4289.
3. Corma, A.; Martínez, A., Chemistry, Catalysts, and Processes for Isoparaffin–Olefin Alkylation: Actual Situation and Future Trends. *Catal. Rev.* **1993,** *35* (4), 483-570.
4. Feller, A.; Lercher, J. A., Chemistry and Technology of Isobutane/Alkene Alkylation Catalyzed by Liquid and Solid Acids. In *Advances in Catalysis*, Academic Press: 2004; Vol. Volume 48, pp 229-295.
5. Yoo, K.; Burckle, E. C.; Smirniotis, P. G., Comparison of protonated zeolites with various dimensionalities for the liquid phase alkylation of i-butane with 2-butene. *Catal. Lett.* **2001,** *74* (1), 85-90.
6. Sievers, C.; Liebert, J. S.; Stratmann, M. M.; Olindo, R.; Lercher, J. A., Comparison of zeolites LaX and LaY as catalysts for isobutane/2-butene alkylation. *Appl. Catal. A* **2008,** *336* (1–2), 89-100.
7. Yoo, K.; Smirniotis, P. G., The influence of Si/Al ratios of synthesized beta zeolites for the alkylation of isobutane with 2-butene. *Appl. Catal. A* **2002,** *227* (1), 171-179.
8. Diaz-Mendoza, F. A.; Pernett-Bolaño, L.; Cardona-Martínez, N., Effect of catalyst deactivation on the acid properties of zeolites used for isobutane/butene alkylation. *Thermochim. Acta* **1998,** *312* (1), 47-61.
9. Guzman, A.; Zuazo, I.; Feller, A.; Olindo, R.; Sievers, C.; Lercher, J. A., On the formation of the acid sites in lanthanum exchanged X zeolites used for isobutane/cis-2-butene alkylation. *Microporous Mesoporous Mater.* **2005,** *83* (1–3), 309-318.
10. Sievers, C.; Onda, A.; Olindo, R.; Lercher, J. A., Adsorption and Polarization of Branched Alkanes on H−LaX. *J. Phys. Chem. C* **2007,** *111* (14), 5454-5464.
11. Feller, A.; Barth, J.-O.; Guzman, A.; Zuazo, I.; Lercher, J. A., Deactivation pathways in zeolite-catalyzed isobutane/butene alkylation. *J. Catal.* **2003,** *220* (1), 192-206.
12. Klingmann, R.; Josl, R.; Traa, Y.; Gläser, R.; Weitkamp, J., Hydrogenative regeneration of a Pt/La-Y zeolite catalyst deactivated in the isobutane/n-butene alkylation. *Appl. Catal. A* **2005,** *281* (1), 215-223.
13. Pater, J.; Cardona, F.; Canaff, C.; Gnep, N. S.; Szabo, G.; Guisnet, M., Alkylation of Isobutane with 2-Butene over a HFAU Zeolite. Composition of Coke and Deactivating Effect. *Ind. Eng. Chem. Res.* **1999,** *38* (10), 3822-3829.
14. Sievers, C.; Zuazo, I.; Guzman, A.; Olindo, R.; Syska, H.; Lercher, J. A., Stages of aging and deactivation of zeolite LaX in isobutane/2-butene alkylation. *J. Catal.* **2007,** *246* (2), 315-324.
15. Albright, L. F.; Li, K., Alkylation of isobutane with light olefins using sulfuric acid. Reaction mechanism and comparison with HF alkylation. *Ind. Eng. Chem. Prod. Rd.* **1970,** *9* (3), 447-454.

16. Yoo, K.; Namboodiri, V. V.; Varma, R. S.; Smirniotis, P. G., Ionic liquid-catalyzed alkylation of isobutane with 2-butene. *J. Catal.* **2004,** *222* (2), 511-519.

17. Li, Y.; Liu, R.; Zhao, G.; Zhou, Z.; Zhang, J.; Shi, C.; Liu, X.; Zhang, X.; Zhang, S., Simulation and optimization of fixed bed solid acid catalyzed isobutane/2-butene alkylation process. *Fuel* **2018,** *216*, 686-696.

18. Feller, A.; Guzman, A.; Zuazo, I.; Lercher, J. A., On the mechanism of catalyzed isobutane/butene alkylation by zeolites. *J. Catal.* **2004,** *224* (1), 80-93.

19. Kirsch, F. W.; Potts, J. D.; Barmby, D. S., Isoparaffin-olefin alkylations with crystalline aluminosilicates: I. Early studies—C4-olefins. *J. Catal.* **1972,** *27* (1), 142-150.

20. Taylor, R. J.; Sherwood, D. E., Effects of process parameters on isobutane/2-butene alkylation using a solid acid catalyst. *Appl. Catal. A* **1997,** *155* (2), 195-215.

21. Nivarthy, G. S.; Seshan, K.; Lercher, J. A., The influence of acidity on zeolite H-BEA catalyzed isobutane/n-butene alkylation1Dedicated to Professor Lovat V.C. Rees in recognition and appreciation of his lifelong devotion to zeolite science and his outstanding achievements in this field.1. *Microporous Mesoporous Mater.* **1998,** *22* (1), 379-388.

22. Schüßler, F.; Pidko, E. A.; Kolvenbach, R.; Sievers, C.; Hensen, E. J. M.; van Santen, R. A.; Lercher, J. A., Nature and Location of Cationic Lanthanum Species in High Alumina Containing Faujasite Type Zeolites. *J. Phys. Chem. C* **2011,** *115* (44), 21763-21776.

23. Park, J. W.; Seo, G., IR study on methanol-to-olefin reaction over zeolites with different pore structures and acidities. *Appl. Catal. A* **2009,** *356* (2), 180-188.

24. Guzman, A.; Zuazo, I.; Feller, A.; Olindo, R.; Sievers, C.; Lercher, J. A., Influence of the activation temperature on the physicochemical properties and catalytic activity of La-X zeolites for isobutane/cis-2-butene alkylation. *Microporous Mesoporous Mater.* **2006,** *97* (1), 49-57.

25. Bauer, F.; Karge, H. G., Characterization of Coke on Zeolites. In *Characterization II*, Karge, H. G.; Weitkamp, J., Eds. Springer Berlin Heidelberg: Berlin, Heidelberg, 2007; pp 249-364.

26. Albright, L.; Spalding, M.; Kopser, C.; Eckert, R., Alkylation of isobutane with C4 olefins. 2. Production and characterization of conjunct polymers. *Ind. Eng. Chem. Res.* **1988,** *27*.

27. Berenblyum, A.; Ovsyannikova, L. V.; Katsman, E.; Zavilla, J.; Hommeltoft, S.; Karasev, Y. Z., Acid soluble oil, by-product formed in isobutane alkylation with alkene in the presence of trifluoro methane sulfonic acid: Part I Acid soluble oil composition and its poisoning effect. *Appl. Catal. A* **2002,** *232*, 51–58.

2.6. Supporting information

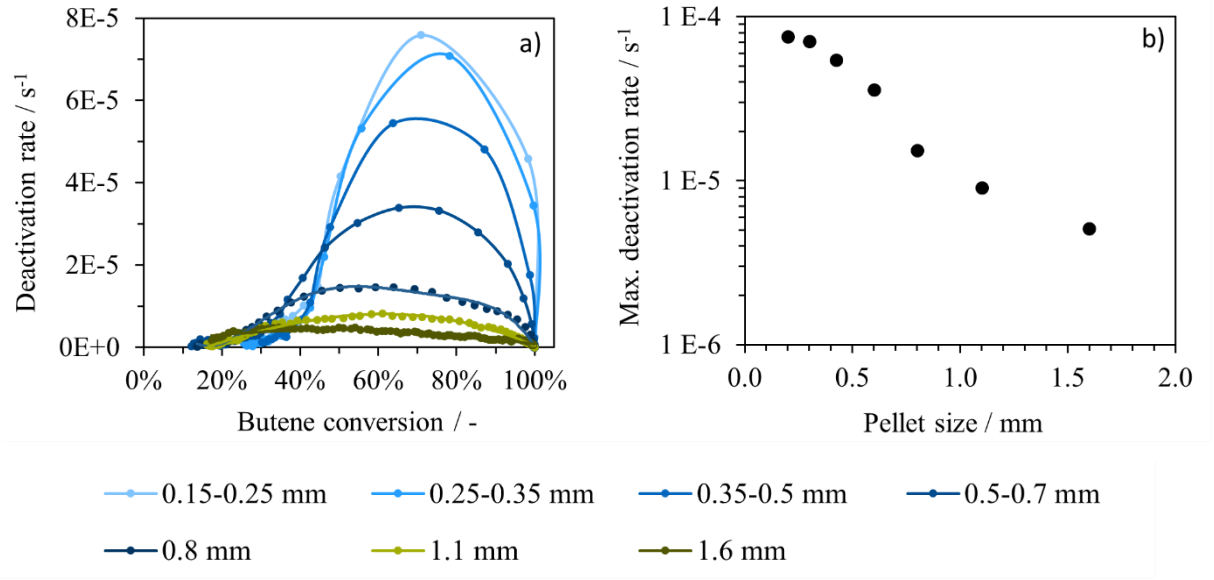

Figure S2.1. a) Evolution of deactivation rate with butene conversion for different pellet sizes and b) Maximum deactivation rates of different pellet sizes.

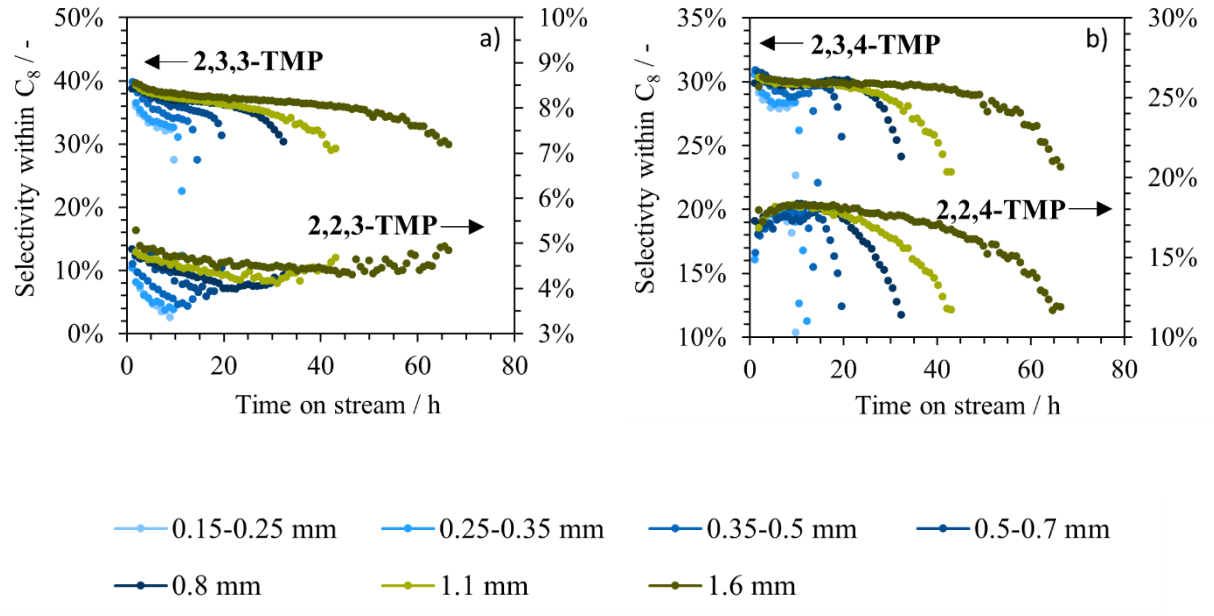

Figure S2.2. Trimethylpentane isomer selectivity within C_8 fraction for different pellet sizes with time on stream. a) 2,3,3-TMP and 2,2,3-TMP, b) 2,3,4-TMP and 2,2,4-TMP.

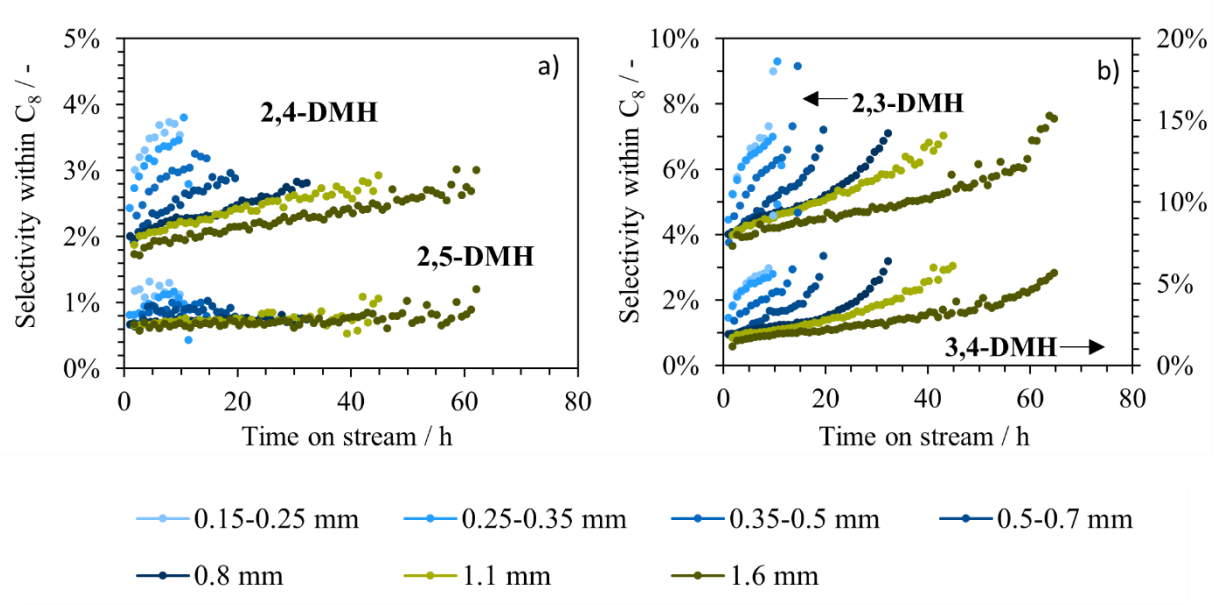

Figure S2.3. Dimethylhexane isomer selectivity within C_8 fraction for different pellet sizes with time on stream. a) 2,4-DMH and 2,5-DMH, b) 2,3-DMH and 3,4-DMH.

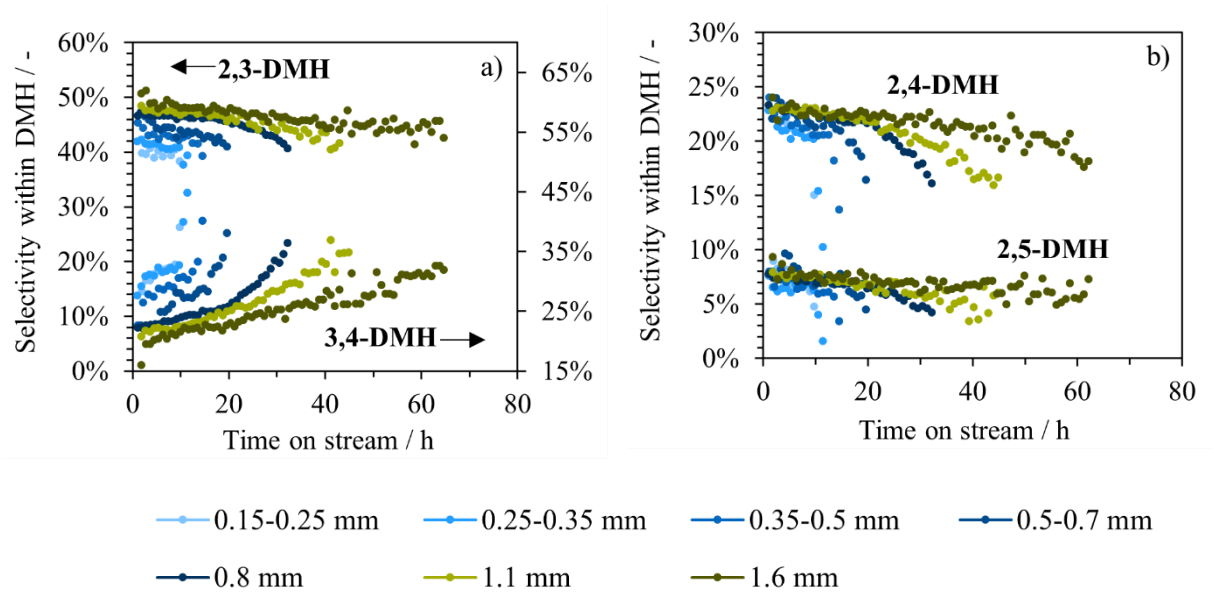

Figure S2.4. Isomer distribution of dimethylhexanes with time on stream for different pellet sizes. a) 2,3-DMH and 3,4-DMH, b) 2,4-DMH and 2,5-DMH.

Table S2.1. Summary of catalytic performance results for LaX zeolite pellets of different size.

Pellet size [mm]	Full conversion period (X > 99%) [h]	Max. deactivation rate [s^{-1}]	Conv. at max deact. rate [%]	Integral yield [$g_{alkylate} \cdot g_{cat}^{-1}$]
0.15-0.25	8.5	75.9×10^{-6}	71	3.3
0.25-0.35	10	70.8×10^{-6}	78	4.0
0.35-0.50	12.5	54.4×10^{-6}	64	4.8
0.50-0.70	15.5	35.7×10^{-6}	65	6.8
0.8	19.5	15.3×10^{-6}	64	10.5
1.1	15	9.1×10^{-6}	58	12.7
1.6	6.5	5.1×10^{-6}	55	16.6

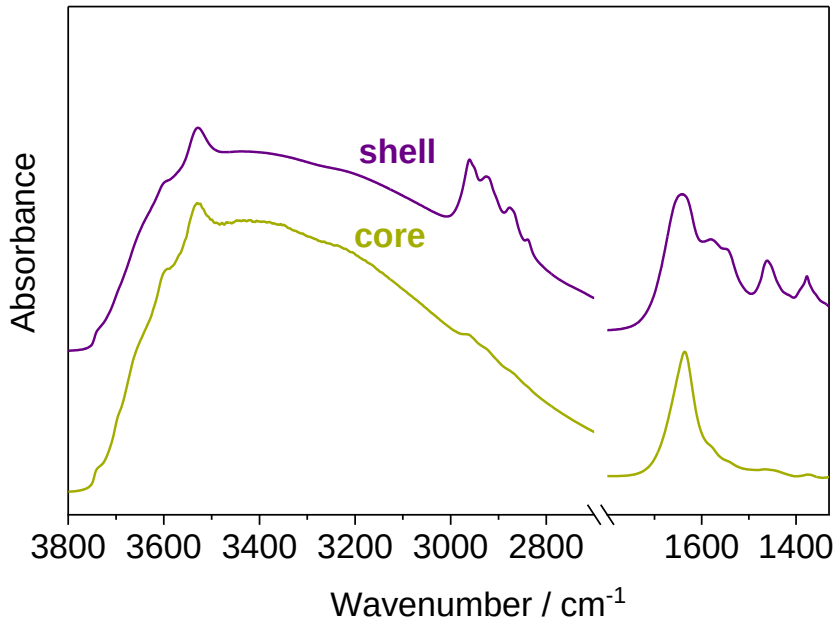

Figure S2.5. IR spectra of used catalysts in the core and shell part of pellet in the region after activation at 150°C for 2 h in 20 ml/min N_2 flow.

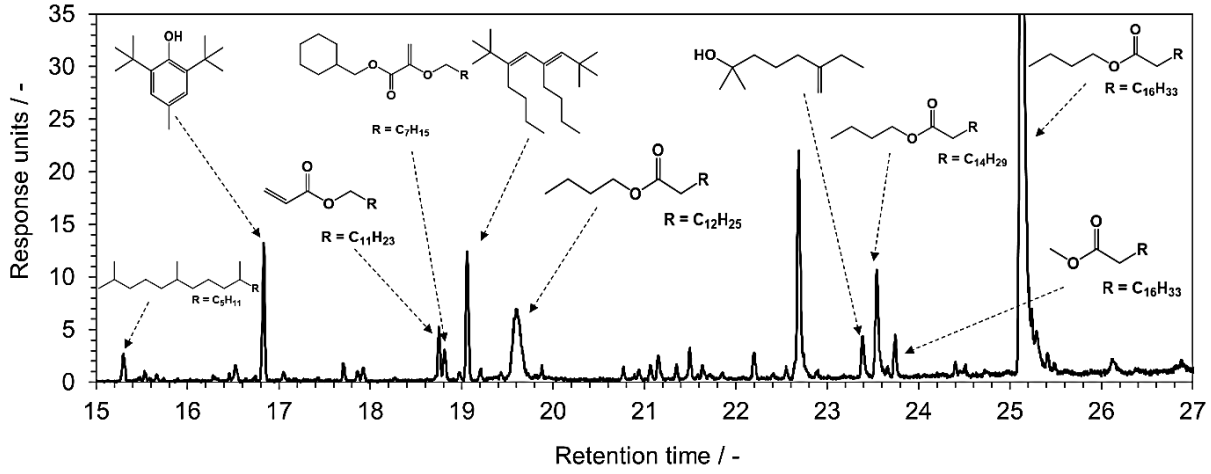

Figure S2.6. GC chromatogram of shell pellet fraction after dissolving zeolite in HF and extracting organic compounds with DCM. Compounds identified via mass spectroscopy.

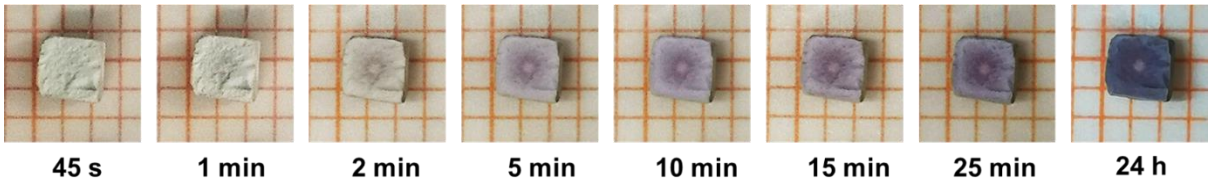

Figure S2.7. Images of cross-sections of LaX cubes used for isobutane/2-butene alkylation. Evolution of dark shell during exposure to atmosphere.

Derivation of intrapellet concentration profile of butene

Here, Fick's diffusion law in presence of chemical reactions is used to derive the butene concentration inside the catalyst pellet. Equation S1 shows the time-dependent concentration evolution (***∂C/∂t***) as a function of both diffusion under concentration gradient (***DΔC***) and conversion by alkylation reaction (rate), in which ***C*** is the butene concentration, ***D*** is its diffusion coefficient in the catalyst pellet.

$$\frac{\partial C}{\partial t} = D\Delta C - rate \qquad \text{(S1)}$$

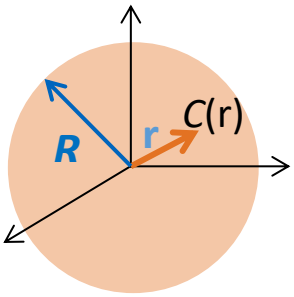

For simplicity, a spherical pellet model is used. The pellet has a radius of *R*. The butene concentration ***C*(*r*)** is then a function of its distance to the center of the pellet ***r***. Treating the diffusion term by using Laplace operator in spherical coordinates:

$$\Delta C = \frac{\partial^2 C}{\partial r^2} + \frac{2}{r}\frac{\partial C}{\partial r} \qquad \text{(S2)}$$

The term of alkylation reaction rate is expressed as Equation S3, in which ***k*** is the rate constant, **ρ** is the acid site concentration of the catalyst. Here the reaction is treated as first order of butene because all the acid sites are covered by carbenium ions under reaction condition and rate is proportional to the encounter frequency of butene.

$$rate = k\rho C \qquad \text{(S3)}$$

Then Equation S1 is transformed into Equation S4.

$$\frac{\partial C}{\partial t} = D\left(\frac{\partial^2 C}{\partial r^2} + \frac{2}{r}\frac{\partial C}{\partial r}\right) - k\rho C \qquad \text{(S4)}$$

Under steady state, the change of butene concentration in pellet with time is very small (***∂C/∂t* = 0**), thus Equation S5 is obtained from Equation S4.

$$k\rho C = D\left(\frac{\partial^2 C}{\partial r^2} + \frac{2}{r}\frac{\partial C}{\partial r}\right) \qquad \text{(S5)}$$

The general solution of Equation S5 is

$$\left(\frac{\partial(Cr)}{\partial r}\right)^2 = \frac{k\rho}{D}(Cr)^2 + A \qquad \text{(S6)}$$

Take into account the boundary condition that when butene concentration (***C***) is 0, its gradient (***∂C/∂r***) is 0. Therefore, the value of A should be 0. With A = 0, Equation S6 has the solution:

$$\ln(Cr) = \sqrt{\frac{k\rho}{D}} \cdot r + B \qquad \text{(S7)}$$

Take into account the second boundary condition that at the pellet surface, the butene concentration is equal to that outside the pellet, i.e. $C = C_0$ when $r = R$ (C_0 is the butene concentration outside pellet). Therefore, the value of B is obtained (Eq. S8a) and the solution is obtained as well (Eq. S8b).

$$B = \ln(C_0 R) - \sqrt{\frac{k\rho}{D}} \cdot R \qquad \text{(S8a)}$$

$$C = \frac{C_0 R}{r} \exp\left[\sqrt{\frac{k\rho}{D}}(r - R)\right] \qquad \text{(S8b)}$$

Define $x = R - r$, i.e. the distance from the sphere boundary towards inside, the concentration is finally expressed as

$$C = \frac{C_0 R}{R - x} \exp\left[-\sqrt{\frac{k\rho}{D}} \cdot x\right] \qquad \text{(S9)}$$

Figure 1 in the maintext is drawn with choosing a representative small radius (R_{small}) and a big radius (R_{big}) shown below.

$$R_{small} = 2.6 \Big/ \sqrt{\frac{k\rho}{D}} \qquad \text{(S10a)}$$

$$R_{big} = 10 \cdot R_{small} = 10 \times 2.6 \Big/ \sqrt{\frac{k\rho}{D}} \qquad \text{(S10b)}$$

2.7. Associated content

Publication

This chapter is based on a peer reviewed article. Reprinted with permission from Verena B. Höpfl, Teresa Schachtl, Yue Liu, and Johannes A. Lercher; "Pellet Size-Induced Increase in Catalyst Stability and Yield in Zeolite-Catalyzed 2-Butene/Isobutane Alkylation" *Industrial & Engineering Chemistry Research,* 2022, 61 (1), 330-338. Copyright 2022 American Chemical Society. Minor layout changes have been made.

Contributions

V.B.H. shaped catalysts, planned, designed and carried out the catalytic experiments, analyzed and interpreted the data and wrote the manuscript.

T.S. synthesized catalysts, performed analysis of acid site concentration including data processing and contributed to the scientific discussion. Y.L. and J.A.L. supported experiment design, contributed to the scientific discussion and corrected the manuscript. All authors have given approval to the final version of the manuscript.

Acknowledgements

The authors acknowledge financial supports from Flint Hills Resources LLC and INVISTA Textiles (U.K.) Ltd and beneficial discussion with Will Cross and Keith Whiston.

Chapter 3

3. The opposing impact of pellet size in PFR and CSTR in zeolite-catalyzed 2-butene/isobutane alkylation

Abstract

The pellet size induced effect on catalyst stability and selectivity of LaX zeolite in isobutane/2-butene alkylation reveals opposing impacts of pellet size in different reactor types. The performance of LaX is in both reactors strongly dependent on acid site accessibility and mass transport limitation, whereas both parameters are affected by pellet size. In CSTR, small pellets are preferred as the amount of accessible sites is crucial dominating over beneficial effect of pore diffusion. The reduction of pellet size range from 1.0-2.0 to 0.35-0.5 mm resulted in an improved catalytic performance of LaX zeolite evidenced by lifetime prolongation and increase of integral alkylate yield. The higher selectivity to desired C_8 products and suppression of side-products is attributed to increased external surface of smaller pellets leading to higher acid site accessibility, which enhances hydride transfer. In fixed-bed reactor, LaX catalyst showed improved performance when pellet size was increased due to the formation of an intrapellet gradient as well as a bed gradient of butene compensating decreased site accessibility and making mass transport limitation the dominant factor.

3.1. Introduction

Alkylate as a mixture of highly branched alkanes mainly consisting of C_8 is very much in demand as a blending feedstock in gasoline pool. Besides its devoid of sulphur, nitrogen and aromatic compounds it also offers a high-octane number and low vapour pressure making alkylate perfectly applicable as clean-burning gasoline.[1-2] Industrially it is produced by proton induced alkylation of isobutane with butenes catalyzed by liquid acids HF and H_2SO_4. Their obvious drawbacks related to handling, refrigeration and environmental issues are the reason for intense research on substitutes being able to replace established catalysts.[3-4]

Decade-long investigation of possible candidates rendered zeolites, especially faujasite-type X and Y[5-6] as well as BEA[7-8], as the most promising catalysts. Current research is mainly focused on overcoming their still present disadvantages, which diminish alkylate yield of solid acids in alkylation.[9] Greatest challenge is preventing catalyst deactivation caused by pore and acid site blocking due to side-products formed via multiple alkylation and butene polymerization.[10-13] Therefore, there is a general agreement, that high concentration and strength of Brønsted acid sites[14-15] as well as low olefin space velocity and high paraffin to olefin ratio are crucial to achieve satisfying catalytic performance. Especially the last parameter is improved by using a back-mixed CSTR type reactor, which keeps olefin concentration homogeneously at a low level.[16-17]

Despite required reaction parameters making CSTR by far the favoring reactor type for alkylation, fixed bed or plug flow reactors (PFR) are more preferred for practical applications. Their construction is much simpler as they do not require any moving parts and therefore it is generally a low-cost, low-maintenance design. As a result only fixed bed reactors are applied in first commercial solid catalyzed alkylation processes like CB&I AlkyClean[18], or AlkyRAN pilot plants[19].

Previously, we identified a beneficial effect of pellet size when increasing LaX zeolite pellets from 0.15-0.25 mm up to 1.6 mm using a ¼” fixed-bed reactor for isobutane/2-butene alkylation at an olefin space velocity of 0.2 h^{-1} with a feeding P/O ratio of 200. The improved catalytic performance was caused by an intra-pellet reactant gradient according to Thiele modulus, which reduces the local butene concentration at the active sites suppressing undesired side-reactions. In this study, we will use this pellet size effect to reveal details of different catalyst deactivation in CSTR and PFR. Moreover, running fixed-bed reactor under CSTR-like conditions with very

high paraffin to olefin ratio enables a direct comparison of dominating parameters for each of the two reactor types.

3.2. Experimental

3.2.1. Catalyst preparation

La-exchanged zeolite X (LaX) was prepared from NaX (Si/Al = 1.2) provided by Chemische Werke, Bad Köstritz. The parent material was ion exchanged four times with 0.2 M $La(NO_3)_3$ solution at 70°C for 2 h with a liquid-to-solid ratio of 10 ml/g. The material was washed subsequently with bidistilled water and dried at room temperature. After the second and fourth ion exchange the sample was calcined in 100 ml/min syn air at 450°C for 1 h with a heating ramp of 0.5 $°C \cdot min^{-1}$. The prepared catalyst was stored under saturated water vapor pressure.

In order to form pellets in the range of 0.35-0.5, 0.5-0.7, 0.7-1.0 and 1.0-2.0 mm the catalyst powder was pressed to wafers using a hydraulic press, crushed and sieved. Pellet sizes 0.8, 1.1, 1.6, 2, 2.5 and 3 mm were formed in the shape of cubes by pressing zeolite wafers in the thickness of the desired edge length and cutting them.

3.2.2. Catalytic experiments

The alkylation of isobutane with 2-butene was performed at 75°C and 25 bar and carried out either in a fixed-bed reactor with ¼ inch diameter (PFR) or a 50 ml Micro Robinson-Mahoney catalytic packless reactor from Autoclave engineers operating in continuous mode (CSTR).

In CSTR, the double-walled catalyst basket was filled with 1.0 g pressed and sieved catalyst pellets. Prior to reaction, the catalyst was activated *in situ* in 100 $ml \cdot min^{-1}$ N_2 at 150°C for 12 h with a heating ramp of 2 $°C \cdot min^{-1}$. After cooling to reaction temperature, the reactor was filled with liquefied isobutane (purity 3.5, Westfalen GmbH) at a pressure of 25 bar. The reaction was started by feeding a liquefied mixture of cis-2-butene (purity 2.0, Rießner Gase GmbH) and isobutane with a molar paraffin-to-olefin (P/O) ratio of 10 and an olefin space velocity (OSV) of 0.2 $g_{butene} \cdot g_{catalyst}^{-1} \cdot h^{-1}$ using high-pressure syringe pumps from Teledyne ISCO. The product mixture was expanded after the reactor by a back-pressure regulator and passed through

a six-port valve with a 0.1 ml sample loop. The product distribution was measured using a 60 m DB-1 column (ID = 0.32 mm, film thickness = 1.00 μm) in an Agilent 6890B gas chromatograph equipped with a FID detector.

In PFR, 0.1 g catalyst was activated *in situ* in H_2 at 250°C for 1 h with a heating ramp of 2 °C·min^{-1}. The reaction was started by feeding a mixture of isobutane and cis-2-butene with a molar ratio of 200:1 (Rießner Gase GmbH) using a high-pressure Teledyne ISCO 500D syringe pump. The olefin space velocity was 0.2 $g_{butene} \cdot g_{catalyst}^{-1} \cdot h^{-1}$. The reaction mixture was expanded after the reactor by a backpressure regulator and passed through a six-port valve with a 0.1 ml sample loop. The product distribution was measured using a 60 m DB-1 column (ID = 0.32 mm, film thickness = 1.00 μm) in an Agilent 7890B gas chromatograph equipped with a FID detector.

For catalyst bed deactivation study, the reactor loading was varied from 0.025 - 0.1 g, while keeping flow rate and feeding P/O ratio constant.

The external surface area of pellets in different size was estimated by evaluation of microscopic images.

3.3. Results and Discussion

3.3.1. Pellet size effect in CSTR

Decreasing pellet size in CSTR from the range 1.0-2.0 mm stepwise down to 0.35-0.5 mm lead to an increase of high conversion period (X>98%) defined as catalyst lifetime. As seen in Figure 3.1b lifetime increased from 10.5 h using largest pellet fraction up to 16 h when smallest pellets were applied. This lifetime prolongation by 45% came along with an increased turnover number per Brønsted acid site up to 88 $mol_{alkylate} \cdot mol_{BAS}^{-1}$ and increase of integral alkylate yield up to 7.0 $g_{alkylate} \cdot g_{catalyst}^{-1}$. Subsequently, by changing the macroscopic shape of solid acid catalyst pellets the productivity in alkylation reaction was improved. Due to the typical steep decrease of butene conversion after catalyst lifetime was observed for all ranges (Figure 3.1a), pellet size seems to have less effect on general catalyst deactivation behavior. This assumption is also feasible as there were only minor differences comparing deactivation rate at certain butene conversion (see section 3.6, Figure S3.1).

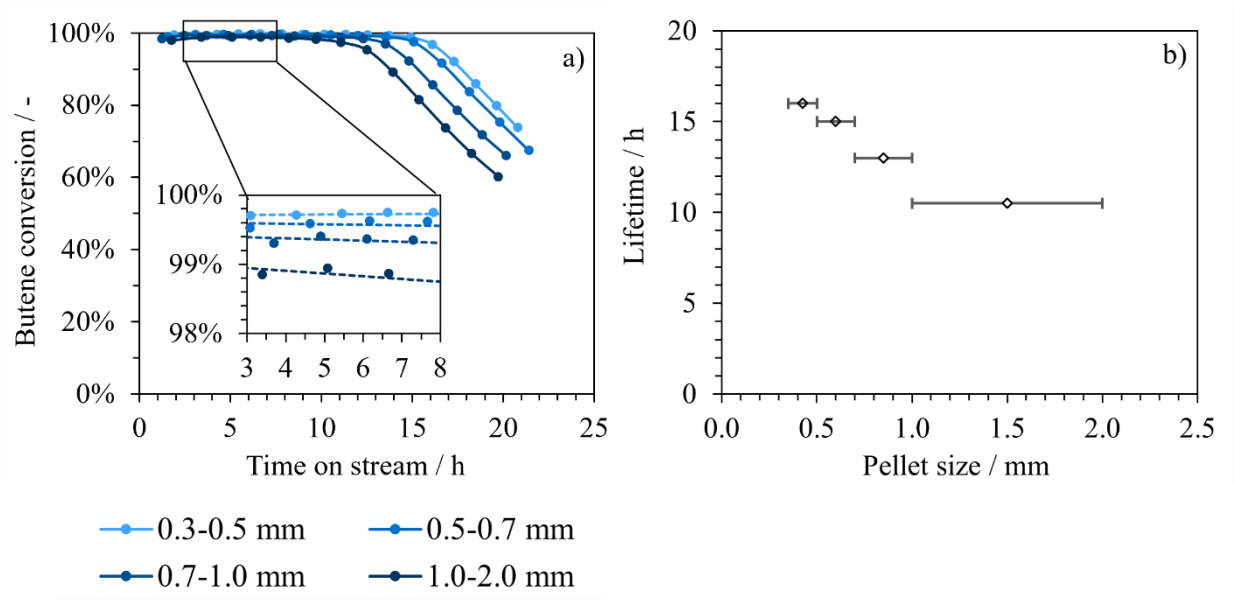

Figure 3.1. a) Butene conversion with time on stream for different pellet sizes in CSTR (Reaction conditions: 1.0 g catalyst, 75°C, 25 bar, feeding isobutane to cis-2-butene molar ratio of 10:1, olefin space velocity 0.2 $g_{butene} \cdot g_{catalyst}^{-1} \cdot h^{-1}$) and b) Dependence of catalyst lifetime on pellet size of LaX.

However, applied pellet size strongly affected the conversion level during catalyst lifetime as seen in Figure 3.1a enlarged period). While largest pellet fraction (1.0-2.0 mm) showed an average conversion of 98.90%, the smallest size in the range of 0.35-0.5 mm converted 99.75% of fed butene. This enhancement of conversion resulted in a drastic increase of *in situ* paraffin to olefin (P/O) ratio in the CSTR from barely 2800 to almost 9600 in the beginning of the alkylation reaction (see Figure 3.2a). Keep in mind only isobutane is considered as paraffin in this case and all butene isomers contribute to olefin fraction.

With time on stream P/O ratio is constantly decreasing due to product accumulation. The reason for enhanced conversion level is attributed to decreased pellet size coming along with increased external surface area by a factor of around 5 comparing largest and smallest fraction as Figure 3.2b shows. This results in a larger interface of solid catalyst and liquid reaction mixture, which facilitates the entrance of compounds into porous zeolite pellets. As consequence, accessibility of acid sites is enhanced and more reactant is converted simultaneously.

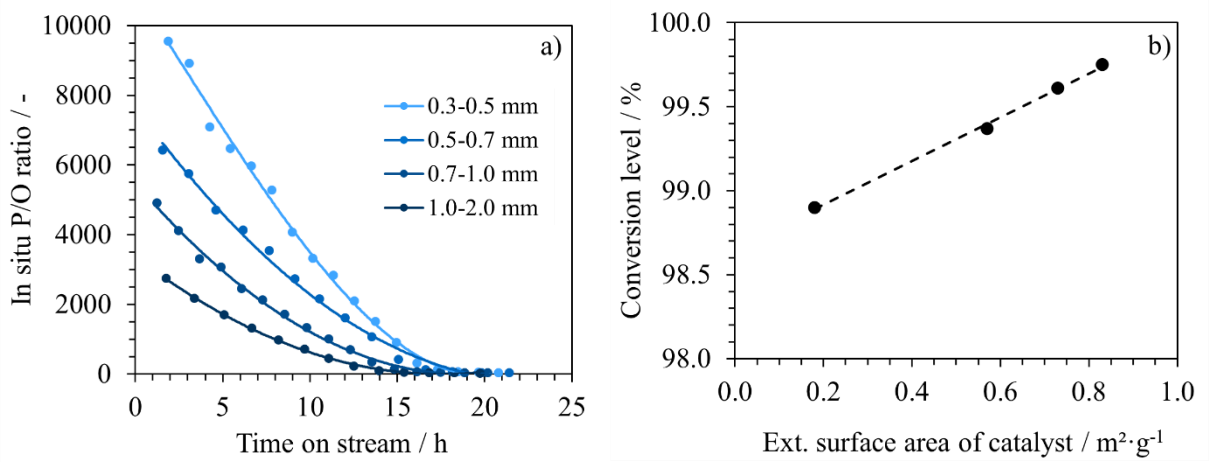

Figure 3.2. a) Development of in situ paraffin to olefin ratio (P/O; isobutane/butenes) with time on stream for different pellet sizes and b) Dependence of butene conversion level on total external surface area of loaded catalyst.

Figure 3.3 shows overall selectivity of zeolite pellets improved with decreasing size as preferred products in C_8 fraction increased by around 2.5%, while selectivity towards undesired larger (C_{9+}) or smaller (C_{5-7}) side-products decreased by 2.5% and 2% respectively.

The change in selectivity is attributed to enhanced *in situ* P/O ratio leading to lower local butene concentration at the active site, which suppresses side-reactions like multiple alkylation and cracking as well as dimerization. By-products are supposed to be responsible for catalyst deactivation because large compounds can block pores, while unsaturated products can block sites by strong adsorption.[12] Therefore, improved selectivity results in prolonged lifetime and increased productivity for smaller pellets

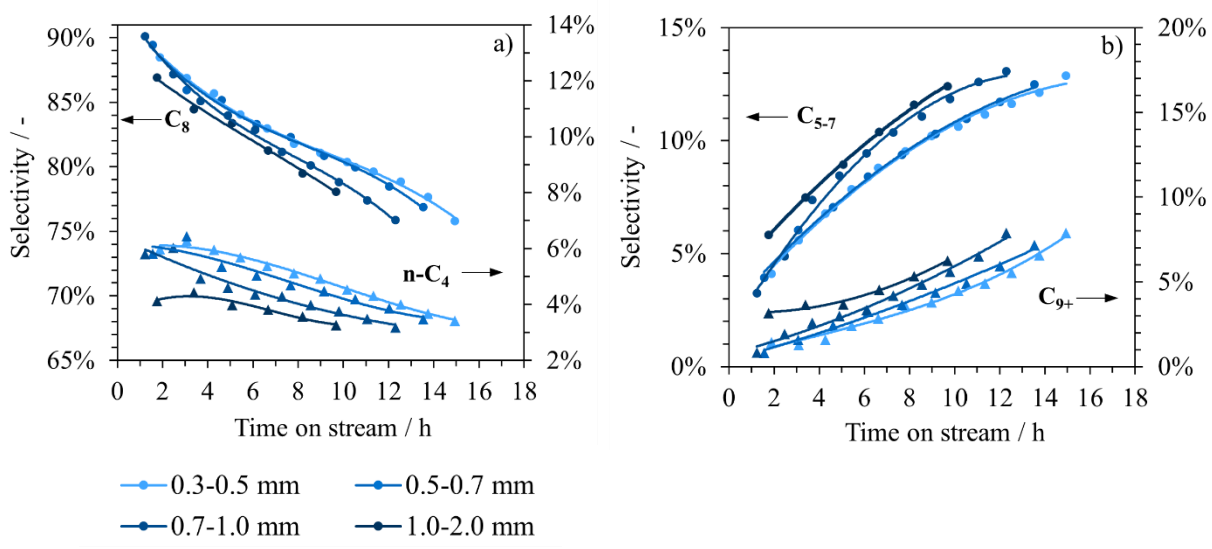

Figure 3.3. Selectivity of products for different pellet sizes a) C_8 isomers and n-butane, b) C_5 to C_7 and C_9 or larger hydrocarbons.

Figure 3.3a shows overall n-butane selectivity increased with decreasing pellet size by around 2% from largest to smallest fraction. Due to n-butane being formed when hydride transfer from isobutane to *n*-butyl carbenium ion ($CH_3CH^+CH_2CH_3$) occurs, it can be generated during initiation after butene adsorption on fresh BAS as shown in Scheme 3.1.

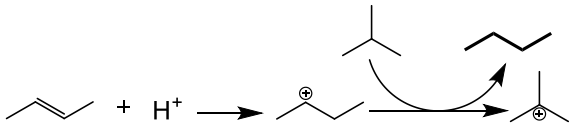

Scheme 3.1. Formation of n-butane during initiation step.

The ratio of isomers 2,2,3-TMP and 3,4-DMH can be used as indicator for hydride transfer rate compared to olefin addition as these two are the primary products from alkylation and dimerization route (Scheme 3.2). Correlating with the observation of higher n-butane selectivity for decreasing pellet size the ratio of hydride transfer rate to olefin addition increased.

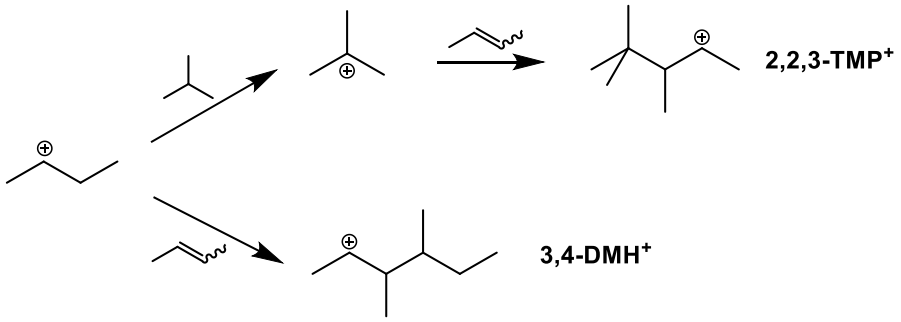

Scheme 3.2. Reaction pathways of secondary C_4 carbenium ions.

A faster reaction of secondary carbenium ions with isobutane to tertiary carbenium ions than the addition of another butene is crucial for catalyst lifetime as the formation of oligomers has to be prevented in order to avoid heavy hydrocarbon deposits. The low 3,4-DMH formation tendency clearly points to a reduced local butene concentration as dimerization rate is highly dependent on butene concentration.

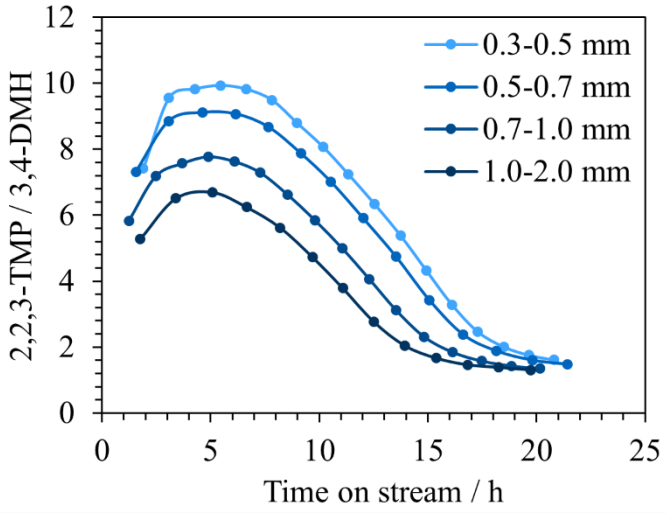

Figure 3.4. 2,2,3-TMP / 3,4-DMH ratio for different pellet size ranges in CSTR.

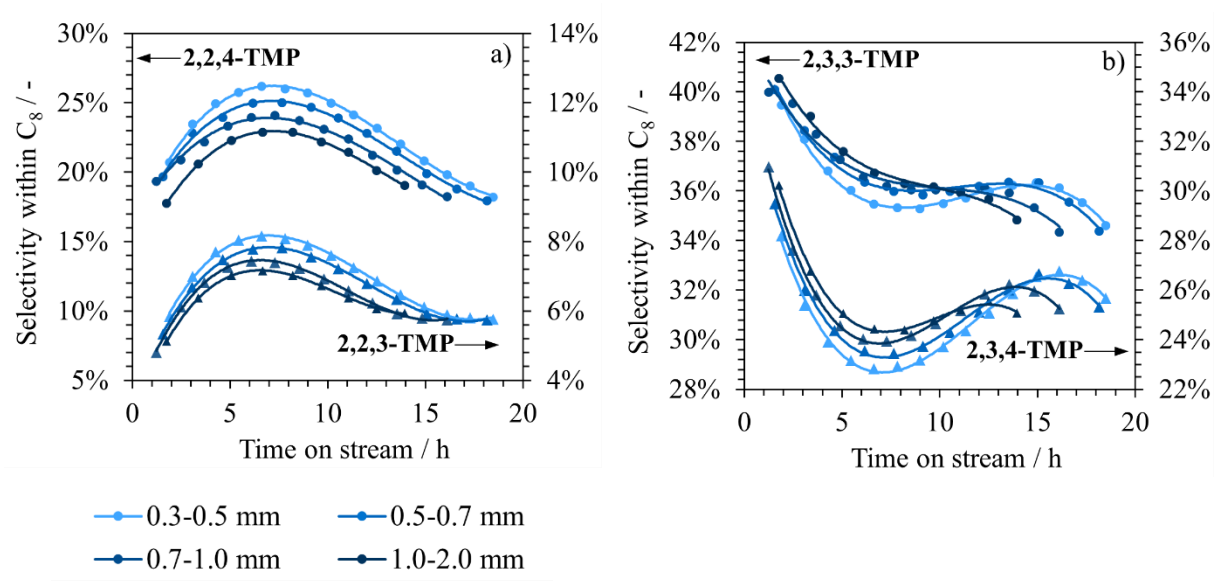

Figure 3.5. Trimethylpentane isomer selectivity within C_8 fraction dependency on pellet sizes a) primary isomers 2,2,3-TMP and 2,2,4-TMP b) secondary isomers 2,3,3-TMP and d) 2,3,4-TMP.

Besides overall C_8 selectivity improved by applying smaller pellets the composition within this fraction also shifted towards more high-octane isomers being trimethylpentanes and less undesired dimethylhexanes (see SI Figure S2). Moreover, changed selectivity of different TMP isomers within C_8 fraction shown in Figure 3.5 indicates a shorter residence time of C_{8+} carbenium ions on catalytic surface as primary TMP isomers, 2,2,3-TMP from n-butene alkylation and 2,2,4-TMP from isobutene alkylation, both increase with decreasing pellet size range. Subsequently, selectivity of secondary isomers, 2,3,3-TMP and 2,3,4-TMP, is lower for smaller pellets as they are formed by skeletal isomerization via methyl- and/or hydride shifts, which requires interaction with active sites before hydride transfer of isobutane occurs. This change in isomer distribution is in accordance with overall selectivity changes, both proving enhanced hydride transfer as well as lower butene concentration at smaller pellets.

3.3.2. Pellet size effect in fixed-bed reactor

The impact of pellet size on the alkylation reaction in PFR is shown in Figure 3.6. The smallest sieve fraction tested was 0.35-0.5 mm, the largest cube shaped pellets had an edge length of 3.0 mm. In contrast to CSTR, the effect of pellet size in PFR is much more pronounced and decreasing pellet size led to shorter catalyst lifetime for pellets smaller 0.8 mm. The characteristic reaction conditions in a fixed-bed reactor enable full conversion. The correlating period is defined as catalyst lifetime. Our previous study identified the formation of an intra-pellet butene gradient being the reason for improved catalytic performance of pellets up to 1.6 mm under fixed-bed reaction conditions, where feeding P/O ratio was 200 at an olefin space velocity of 0.17 h^{-1}.

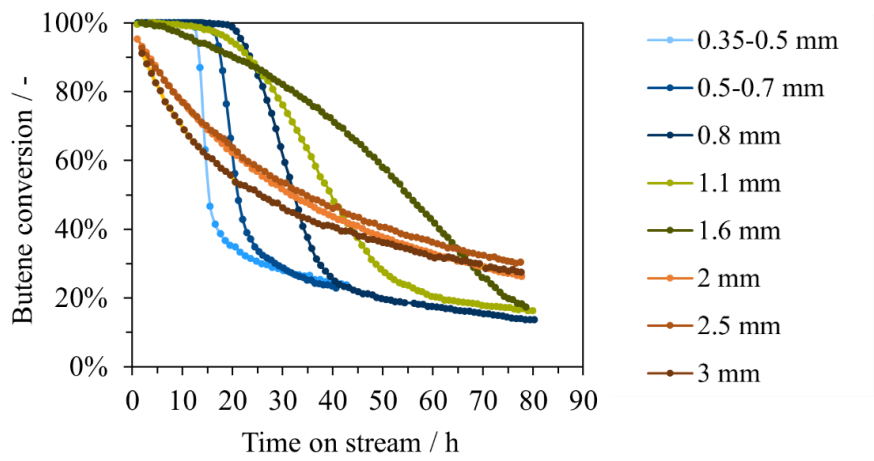

Figure 3.6. Butene conversion with time on stream for different pellet sizes of LaX zeolite (Reaction condition: 0.1 g catalyst, 75°C, 25 bar, Isobutane to cis-2-butene with a molar ratio of 200:1, olefin space velocity 0.2 $g_{butene} \cdot g_{catalyst}^{-1} \cdot h^{-1}$).

Keeping catalyst loading constant, pellets larger than 1.6 mm showed a drastic change in deactivation behavior with time on stream. While pellets smaller or equal 1.6 mm reach full conversion in the beginning and deactivation occurred in a convex shape, large pellets in the size of 2.0 mm up to 3.0 mm showed a concave shaped deactivation curve, which does not depend on pellet size anymore. Additionally, the last stage typical for solid acid alkylation catalysts where deactivation is slow and dimerization is dominating is only observed for pellets up to 1.6 mm within measured time on stream.

The shape of catalyst deactivation curve changed with olefin space velocity and can therefore be influenced by the amount of catalyst (Figure 3.7a) or feeding flow rate (see section 3.6, Figure S3). Decreasing olefin space velocity by a factor of 2 enables the change from convex to concave shape deactivation behavior, whereas still no full conversion of butene could be achieved. Lowest olefin space velocity applied showed a butene conversion of 99.8% measured at 1 h TOS. This leads to the conclusion, that the amount of accessible acid sites is dramatically decreased with increasing pellet size and exceeding 1.6 mm comes along with insufficient active sites for full conversion.

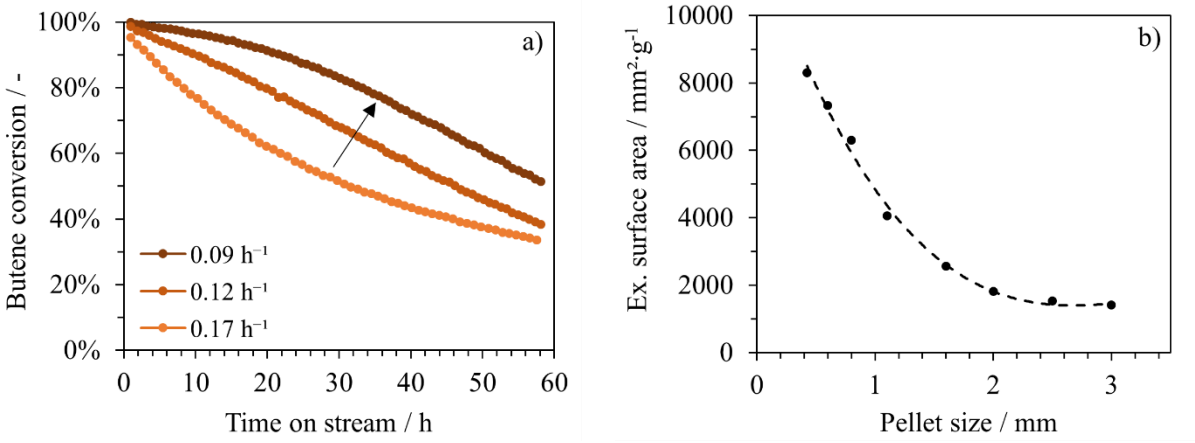

Figure 3.7. Influence of olefin space velocity varied by catalyst loading on shape of butene conversion curve of 2.0 mm pellets (Reaction conditions: 0.1-0.2 g catalyst, 75°C, 25 bar, Isobutane to cis-2-butene with a molar ratio of 200:1) b) Dependence of external surface area on pellet size.

Due to the formation of a butene gradient within catalyst pellets accroding to Thiele modulus the amount of accessible sites is highly dependent on external surface area which decreases exponteniell with pellet size (Figure 3.7b). The external surface area per g catalyst changes only marginally when exceeding a pellet size of 1.6 mm, which correlates with almost overlapping TOS behaviour of pellet sizes 2.0, 2.5 and 3.0 mm.

In PFR, trimethylpentane (TMP) selectivity at certain butene conversion constantly increased with pellet size, though, less changes were detected for cubes larger than 1.6 mm (Figure 3.8). Small pellets in the range of 0.35-0.5 mm showed a steep decrease of selectivity of TMP with the drop of conversion. In contrast, cubes larger or equal 2.0 mm still had a very high TMP selectivity around 70% even at butene conversion below 30%. This indicates that very large

pellets have not yet reached the last period of alkylation where dimerization is dominating and unsaturated C_8 products are formed preferentially.

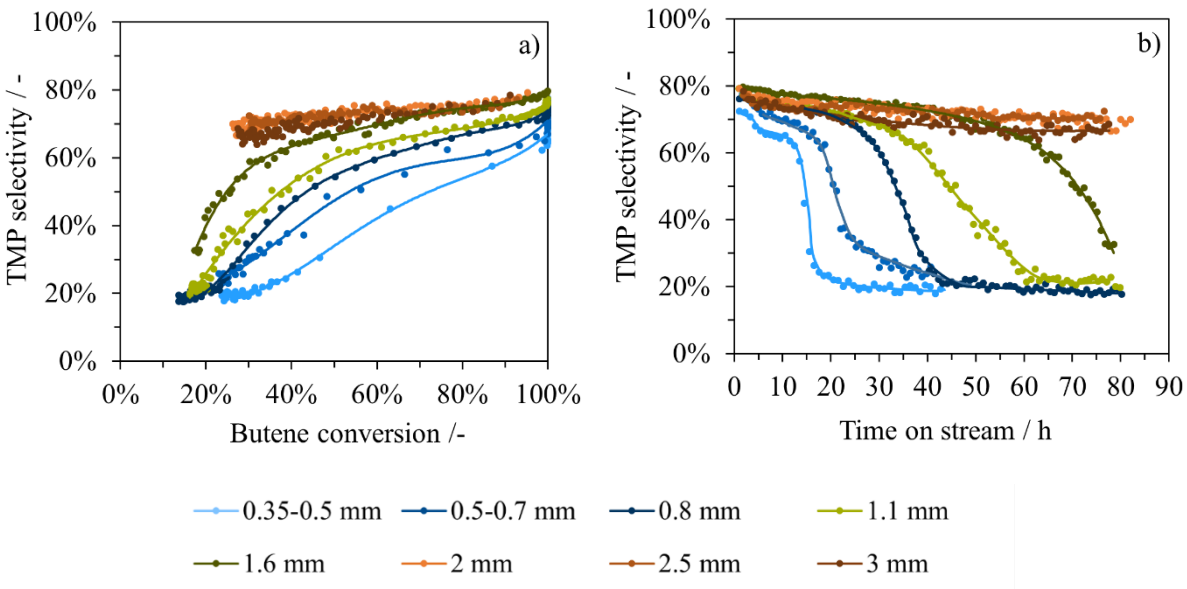

Figure 3.8. Trimethylpentane selectivity vs. butene conversion for different pellet sizes in fixed-bed reactor. (Reaction condition: 0.1 g catalyst, 75°C, 25 bar, Isobutane to cis-2-butene with a molar ratio of 200:1, olefin space velocity 0.17 $g_{butene} \cdot g_{catalyst}^{-1} \cdot h^{-1}$.)

However, it has to be considered, that the low conversion of very large pellets is also caused by butene bypassing the catalyst bed. This assumption is supported by trans-2-butene showing an increasing deviation from equilibrium composition after period of full conversion ends. As seen in Figure 3.9 the thermodynamical equilibrium composition is reached for small pellets but deviates strongly when large pellets are used. The isomerization of cis-2-butene to the favored trans-isomer is assumed to be very fast on LaX zeolite, therefore, it is highly likely that significant amount of detected cis-2-butene has never seen an active site.

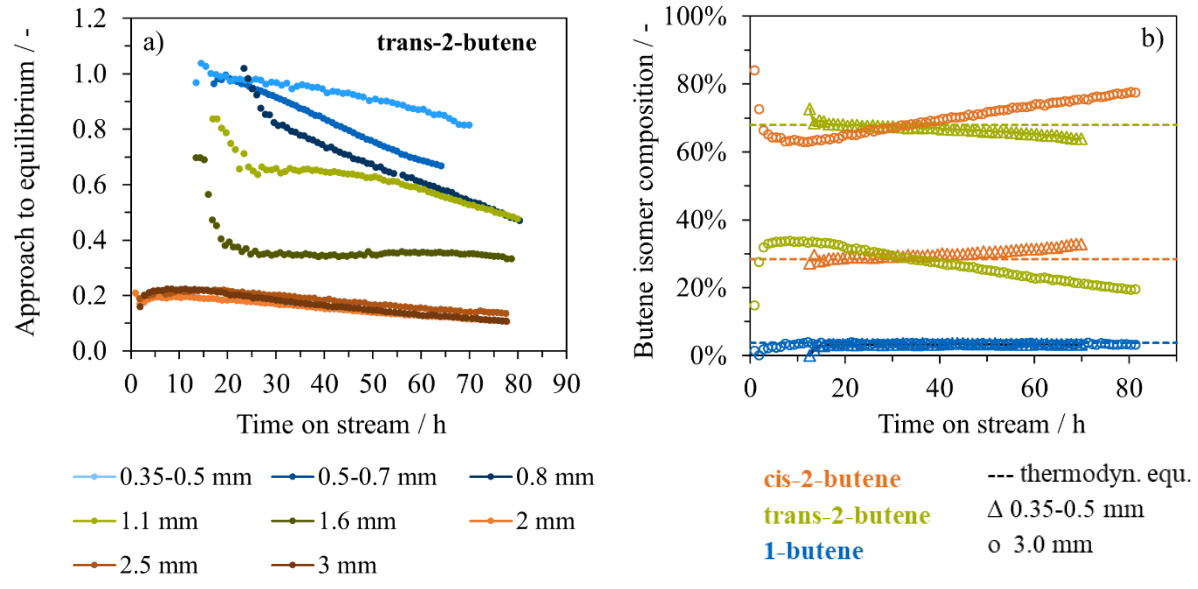

Figure 3.9. Butene isomerization a) Approach to equilibrium of trans-2-butene for different pellet sizes and b) Butene isomer composition for pellet sizes 0.35-0.5 and 3.0 mm

The deactivation rates decreased with increasing pellet size as seen in Figure 3.10. During the second period of alkylation reaction, where butene conversion decreases from 99% to 30-40%, pellets smaller than 2.0 mm showed almost constant deactivation rate whereas pellets larger or equal 2.0 mm showed a decelerating deactivation rate due to concave butene conversion development with time on stream. Consequently, there is a threshold of pellet deactivation mechanism between 1.6 and 2.0 mm under chosen alkylation conditions.

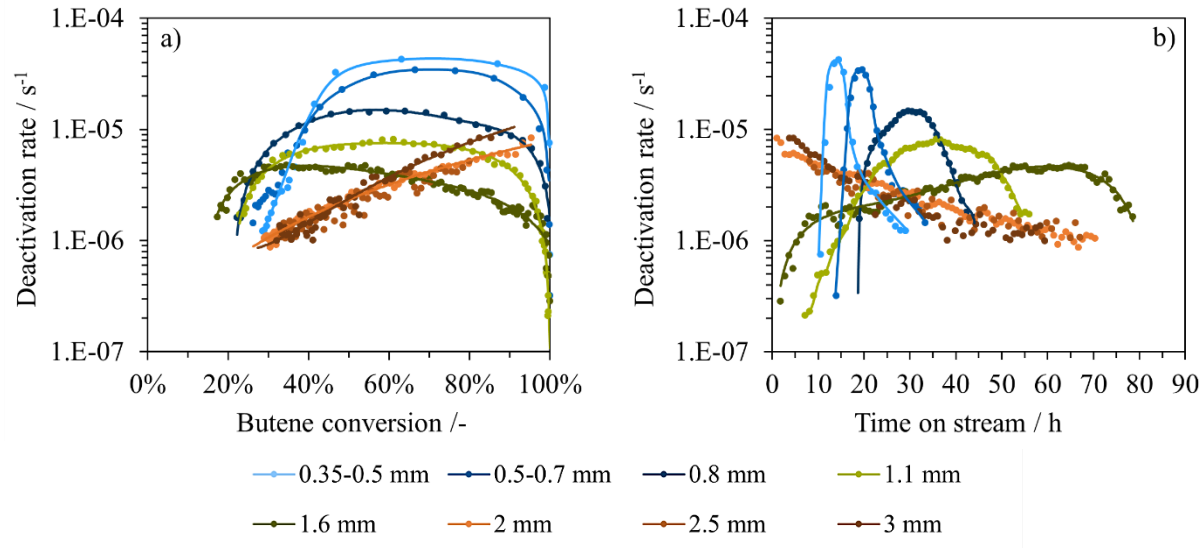

Figure 3.10. Deactivation rate development for different pellet size in fixed-bed reactor a) with butene conversion and b) with time on stream (Reaction condition: 0.1 g catalyst, 75°C, 25 bar, Isobutane to cis-2-butene with a molar ratio of 200:1, olefin space velocity 0.17 $g_{butene} \cdot g_{catalyst}^{-1} \cdot h^{-1}$.)

3.3.3. Influence of feeding P/O ratio on pellet size effect in PFR

The effect of pellet size in PFR is further investigated at two different feeding P/O ratios, 100 and 200, for four chosen pellet sizes while keeping olefin space velocity constant. Applying higher butene concentration in the feed resulted for pellet sizes 0.35-0.5, 1.1 and 1.6 mm in shorter periods of full conversion and faster deactivation in the second reaction period (Figure 3.11a-c), whereas the effect was most pronounced for 1.6 mm pellets. For pellets in the size of 2.0 mm, which showed a concave deactivation curve shape, the loss of butene conversion per time was steeper using lower P/O feeding ratio (Figure 3.11d).

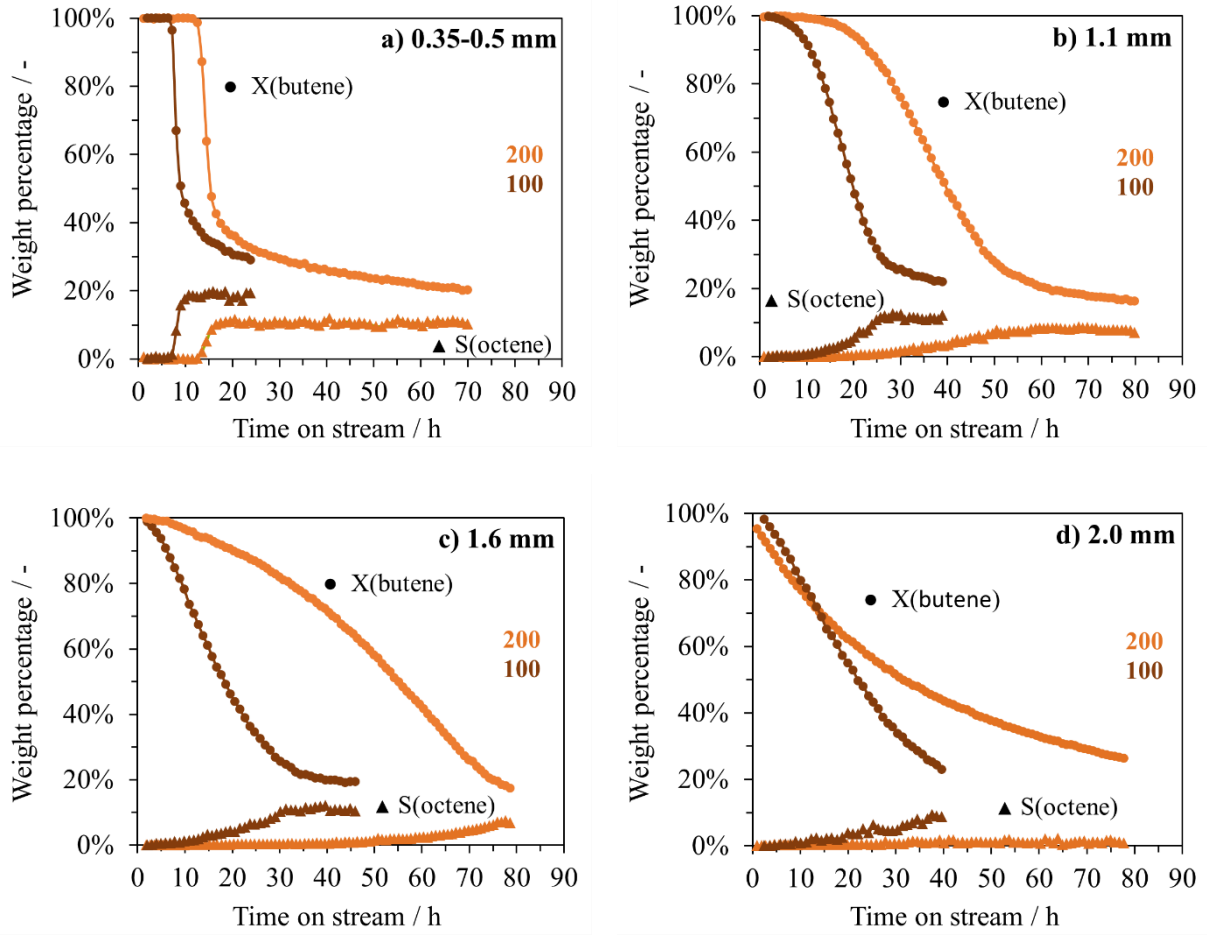

Figure 3.11. Effect of feeding P/O ratio 100 and 200 on butene conversion for pellets in the size of a) 0.35-0.5 mm, b) 1.1 mm, c) 1.6 mm and d) 2.0 mm. (Reaction condition: 0.1 g catalyst, 75°C, 25 bar, olefin space velocity 0.17 $g_{butene} \cdot g_{catalyst}^{-1} \cdot h^{-1}$.)

Moreover, higher initial butene conversion could be achieved in case of 2.0 mm pellets by using higher butene concentration in the feed pointing to a higher amount of simultaneously accessible sites. The increased conversion is attributed to be the result of faster intra-pellet diffusion being dependent on butene concentration outside the pellet as external surface area is unmodified.

The formation of octenes also shown in Figure 3.11 is highly dependent on butene conversion as seen at the parallel development with time on stream. As long as full conversion is achieved no octenes are detected and as soon as conversion drops below 100% octene formation sets in. In case of largest pellets studied here (2.0 mm), the selectivity of unsaturated C_8 products increased steadily from the beginning. Furthermore, faster loss of butene conversion per time leads to faster increase of octenes, therefore, octene selectivity is paralleled with catalyst deactivation. Consequently, the expected faster deactivation at lower feeding P/O ratio is attributed to higher local butene concentration at the active site leading to more side-products by oligomerization and multiple alkylation.

3.3.4. Deactivation over catalyst bed

Detailed study of catalyst bed deactivation by segmentation is used to further investigate the unexpected conversion behavior of very large catalyst pellets in isobutane/2-butene alkylation over LaX. The effect of contact time on catalytic performance of 0.35-0.5 mm pellets showing typical alkylation reaction periods being full conversion, sharp loss of conversion and a final period of slow deactivation, as well as on the behavior of 2.0 mm pellets deactivating continuously in a convex shape of conversion curve are compared by varying olefin space velocity via catalyst loading keeping flow rate and feeding P/O ratio constant.

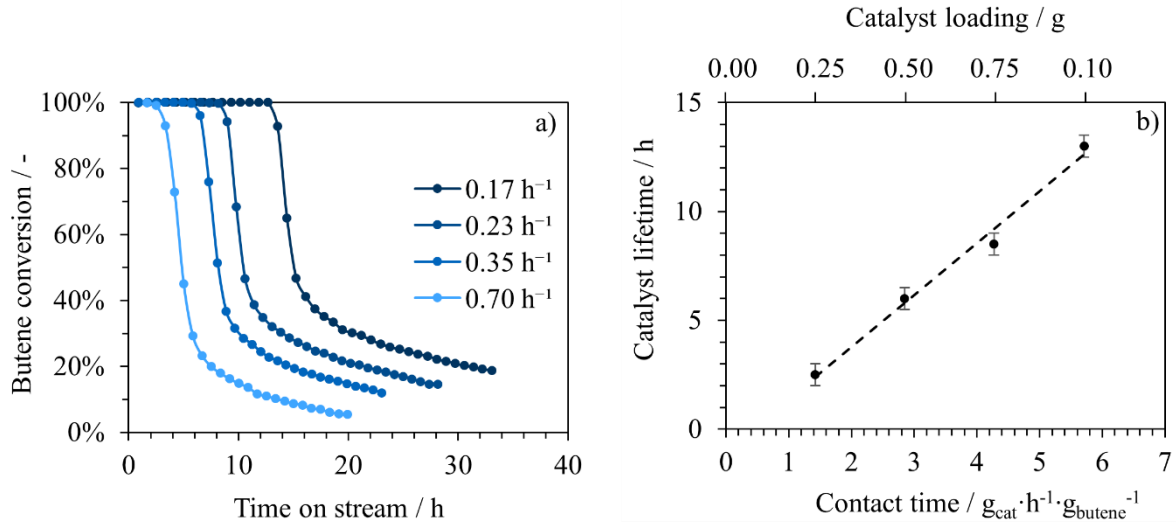

Figure 3.12. a) Influence of olefin space velocity varied by catalyst loading on butene conversion of pellets in the range 0.35-0.5 mm b) Correlation between catalyst lifetime and contact time. (Reaction condition: 0.025-1 g catalyst, 75°C, 25 bar, Isobutane to cis-2-butene with a molar ratio of 200:1)

The catalyst lifetime of pellets in the range 0.35-0.5 mm showed a linear correlation with contact time varied by catalyst loading (Figure 3.12b) indicating less influence of products formed in the beginning of the catalyst bed on the catalytic activity of later bed sections. As deactivation of the first catalyst bed section started directly after the first measurement point we conclude that there is no stable period of alkylation reaction without catalyst deactivation by byproducts. Consequently, the lifetime of a catalyst is determined as the time the whole catalyst bed needs to deactivate comparable to a cigarette burning down. The remaining activity of the last reaction stage increased with increasing reactor loading as the deactivation in this period is much slower and therefore residual activity of several catalyst bed sections

accumulates. Figure 3.14a shows when applying 0.35-0.5 mm pellets every bed section has the same conversion level of around 10% after 20 h TOS when the last reaction stage is reached. As conversion of succeeding section sets in when conversion of previous catalyst fraction drops the deactivation of early bed sections is not visible during catalyst lifetime due to still enough active sites being accessible in later bed sections enabling full conversion. Unsaturated products formed in early and already deactivating catalyst bed sections have to be saturated via hydrogen transfer on upcoming and still active sites. The end of lifetime correlates with a fast increase of octene selectivity (see section 3.6, Figure S3.7) indicating a change of the dominating reaction pathway.

As hinted by untypical convex butene conversion curve in case of 2 mm pellets seen in Figure 3.6 we observed a completely different deactivation behavior of the catalyst bed with changing olefin space velocity varied by catalyst loading. In contrast to small pellets Figure 3.13a shows catalyst cubes of later bed sections converted butene simulataneously with early catalyst bed.

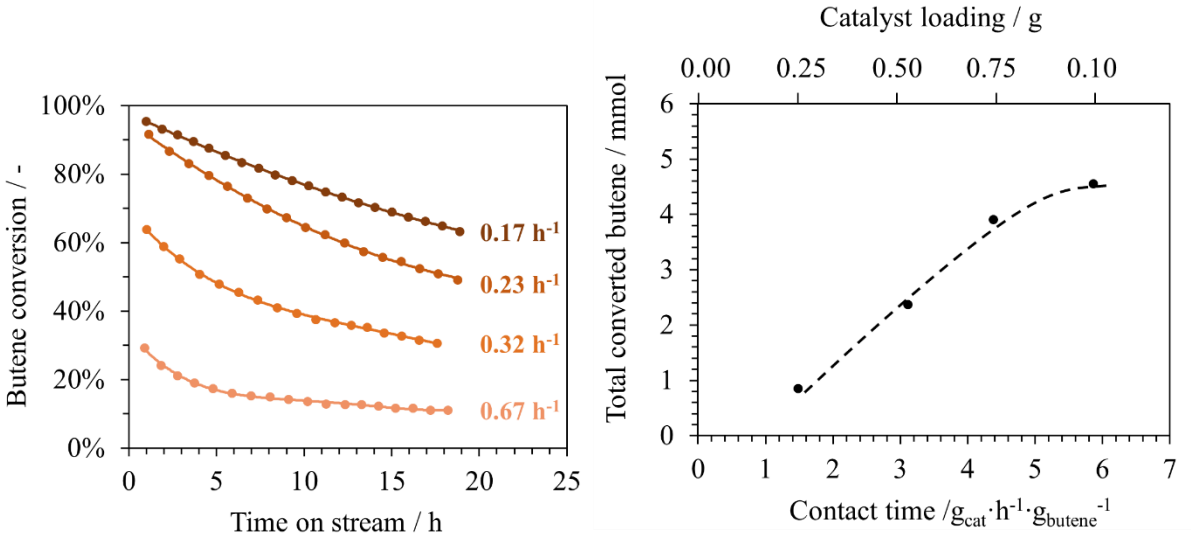

Figure 3.13. a) Influence of olefin space velocity varied by catalyst loading on butene conversion of pellets in the size of 2.0 mm. b) Dependency of total amount of converted butene on contact time at similar time on stream.

However, 2.0 mm pellets did not show a continuous consumption of catalyst bed visible at the non-linear dependency of total amount of converted butene on contact time displayed in Figure 3.13b. As 8 single cubes were applied at this size the separation of different bed setions was easy, whereas each section consists of 2 cubes. The first three sections (cubes 1-6) converted in the very beginning of the reaction very similar amounts of C_4 being around 30% conversion in each section (Figure 3.13b). This points to an equal distribution of reactant over these sections. For the last two cubes, though, very low butene conversion was detected at the beginning of the reaction, however it was increasing with time on stream.

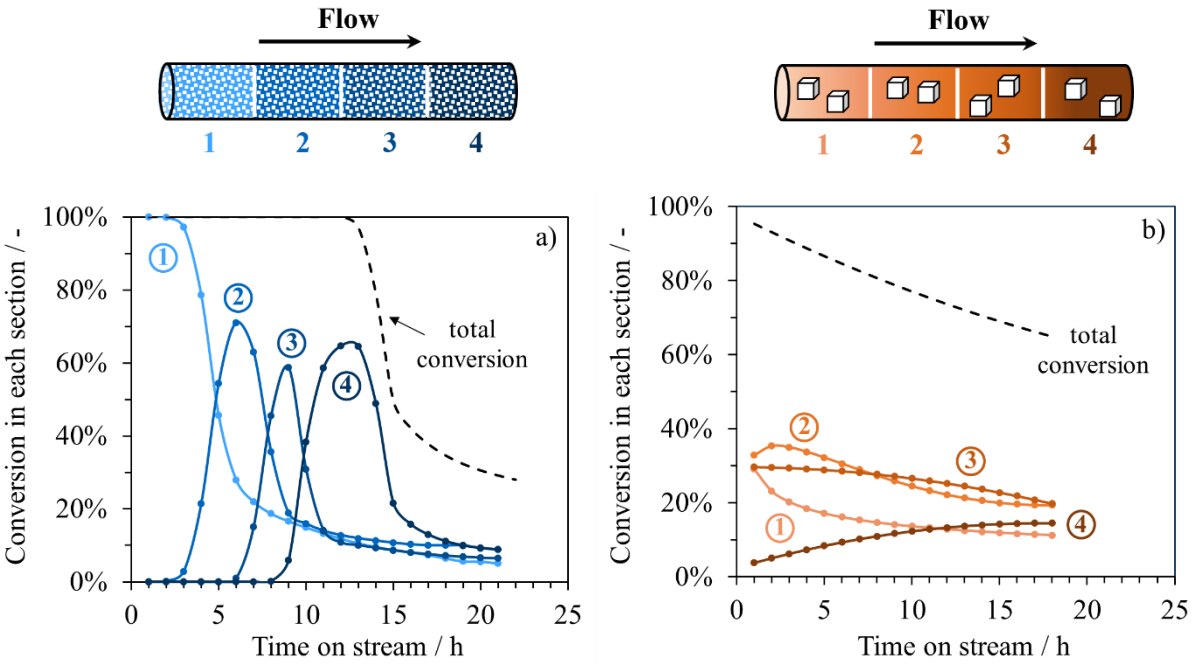

Figure 3.14. Butene conversion for each catalyst bed section in case of a) 0.35-0.5 mm and b) 2.0 mm pellets.

Despite all sections showing different deactivation behavior in the beginning they all reached a similiar butene conversion level of 10-15% after around 18 h TOS paralled with very slow deactivation. It has to be mentioned that the first section being cubes 1 and 2 showed the fastest loss of conversion, while section 2 (cubes 3 and 4) underwent a s-shaped behavior. The last two bed sections showed opposite deactivation, particularly the conversion of cubes 5 and 6 constantly decreased, while conversion of cubes 7 and 8 increased.

The changing conversion and deactivation behaviour of different catalyst bed sections indicates that in contrast to smaller pellets we do not have a continuous deactivation of pellets in flow direction with time on stream, but rather parallel deactivation of all pellets in different deactivation stages. As previously shown a butene gradient is formed within catalyst pellets leading to a shell-core deactivation mechanism of single catalyst pellets clearly visible at images of cross sections of 2.0 mm cubes. As seen in Figure 3.15 the colored shell grew with time on stream for all cubes simultaneously, however, shell of first ones in flow direction showed fastest growing. Subsequently, images of cross section support the assumption of parallel deactivation of complete catalyst bed in case of large pellets.

We have already pointed out in section 3.3.3 that different P/O ratios in feeding mixtures effects catalyst deactivation markely leading to the conclusion that butene concentration at pellet outside determines deactivation rate, which correlates with faster growing of colored shell when lower P/O ratios were applied (see Figure S3.6 in section 2.6).

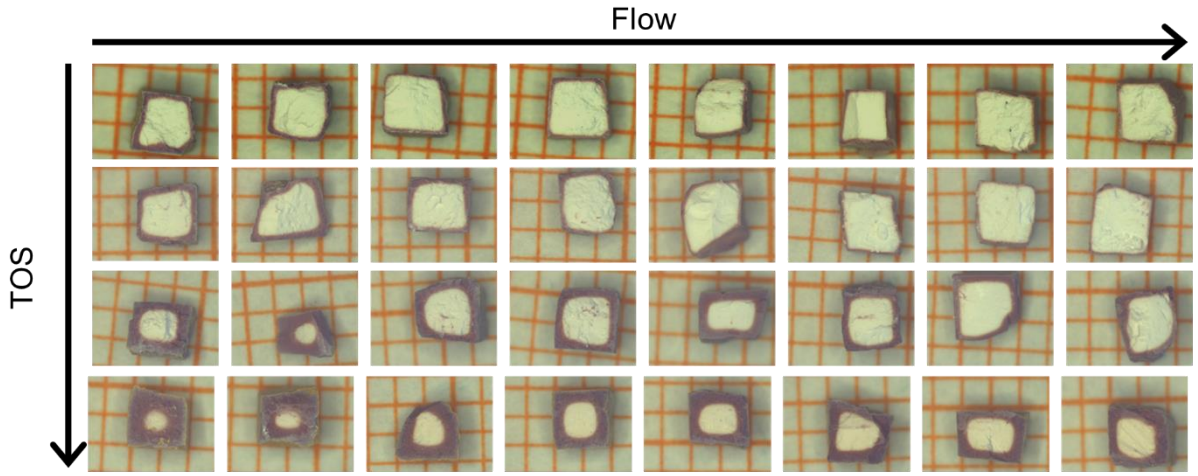

Figure 3.15. Microscopic images of cross sections of 2.0 mm pellets at different time on stream (10, 20, 46 and 78 h). Development of colored shell with time on stream dependent on catalyst bed position. (Butene conversion with time on stream and evolution of shell thickness with converted amount of butene are shown in Figure S3.6 in section 3.6.)

Considering these results it is plausible that different butene concentration at pellet outside is also the reason for changing deactivation behavior of different catalyst bed sections for 2.0 mm pellets. Therefore, the simulatenous deactivation of whole catalyst bed implies a reactant gradient over complete catalyst bed in addition to already proved butene gradient within pellets.

Calculating the concentration gradient of butene over the catalyst bed for these two pellet sizes (Figure 3.16) the presumption of a gradient broadening can be confirmed with experimental data. Especially at early time on stream the difference between concentration profiles is clearly visible observing a much steeper gradient for 0.35-0.5 mm pellets compared to the gradient formed for cataylst bed consiting of 2.0 mm pellets. It takes only 25% of catalyst bed for small pellets to achieve complete conversion, while large pellets achieve highest conversion only when butene has passed 75% of catalyst bed. The dramatically lower conversion per gramm catalyst in different catalyst bed sections when 2.0 mm pellets are applied is mainly attributed to reaction mixture bypassing catalyst pellets. It has to be considered that the external surface area is extremely decreased for pellets exceeding 1.6 mm and therefore entering zeolite pellets becomes much more hindered.

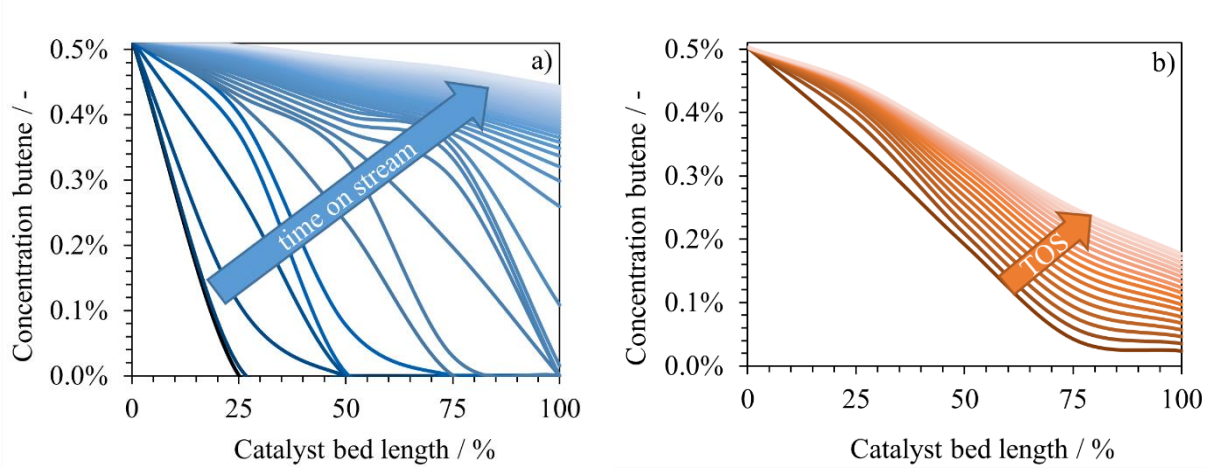

Figure 3.16. Calculated butene concentration gradient over catalyst bed with TOS for a) 0.35-0.5 mm and b) 2.0 mm pellets. Concentration at 25, 50, 75 and 100% bed length results from dividing catalyst bed in 4 sections each consisting of 25 mg catalyst and subtracting unconverted amount of butene.

The broadening of butene gradient over catalyst bed leads to a more homogenous distribution of reactant resulting in simultaneous consumption of the whole catalyst loading instead of consecutively catalyst bed deactivation in flow direction like known so far. The very steep butene gradient over catalyst bed for pellets in the size of 0.35-0.5 mm correlates with linear correlation of lifetime and contact time. The surprising deactivation mechanism found for large pellets in PFR provoked by both, a intra-pellet reactant gradient as well as a reactant gradient over catalyst bed allows the direct comparison of zeolite pellet deactivation in fixed-bed reactor and CSTR, where reaction mixture is homogeneously in contact with all catalyst pellets.

3.3.5. Fixed-bed reactor operated under P/O ratio typical for CSTR

The imitation of CSTR-like conditions in fixed-bed reactor by using a feeding P/O ratio of 2000 for four pellet sizes ranges between 0.15-0.1.0 mm keeping OSV constant allows the combination of pellet size effect in these two reactor types. While the period of full conversion was prolonged for very small pellets (0.15-0.25 mm) similar to findings for the effect of pellet size in CSTR (see Figure 3.17a), the deactivation behavior with time on stream is still related to observed behavior in fixed-bed reactor where increasing pellet size resulted in a decreased deactivation rate (see section 3.6 Figure S3.5**)**

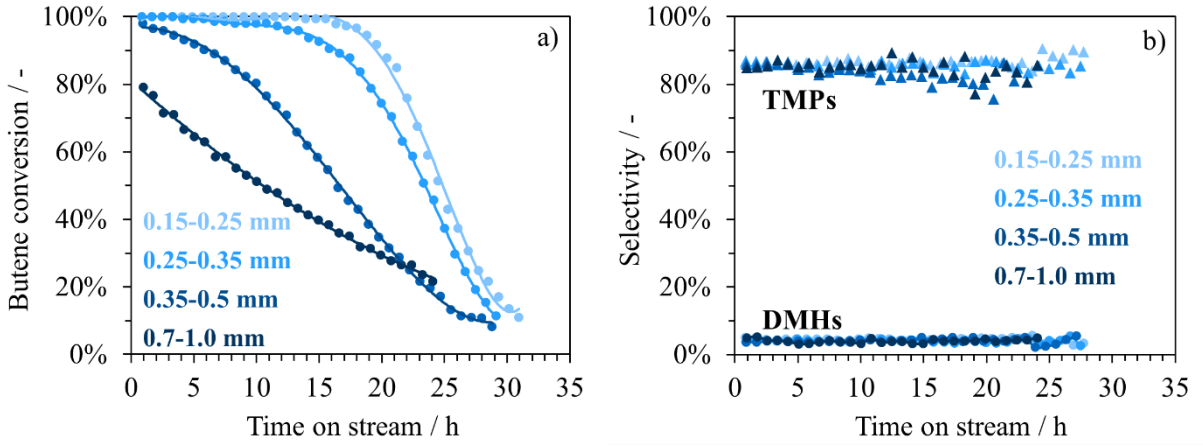

Figure 3.17. a) Butene conversion and b) Trimethylpentane and dimethylhexane selectivity of different pellet size ranges in fixed-bed reactor at P/O = 2000, OSV = 0.2 h^{-1}.

Regarding product distribution in Figure 3.17b feeding P/O ratio of 2000 leads to outstanding high and constant TMP selectivity of 86% independent on pellet size. There are only slight differences when conversion drops. However, larger pellets in the range of 0.7-1.0 mm were still able to generate around 80% TMPs at 50% conversion, while very small pellets (0.15-0.25 mm) even kept the high TMP selectivity until almost no butene is converted anymore.

The deactivation of solid acid catalyst pellets has to be differentiated in the two reactor types. In CSTR, all pellets are in contact with homogeneous reaction mixture leading to a simultaneous reaction and deactivation of all catalyst pellets.

Besides already discussed effects of pellet size in CSTR on catalyst lifetime and selectivity (see Section 3.3.1) the influence of in situ P/O ratio in the stirred tank reactor can be seen when comparing TMP selectivity at similar P/O ratios (see Figure 3.18 black and green marks).

Due to the P/O ratio being dependent on conversion level (Figure 3.2) the average trimethylpentane selectivity is taken at different time on streams for different pellet sizes. At a paraffin to olefin ratio of around 2000 in CSTR small pellets from 0.35-0.5 mm had only 71.8 wt% average TMP abundancy, while the largest fraction of 1.0-2.0 mm showed a much higher selectivity of 78.3 wt%. For a higher in situ P/O ratio of 4000 the increase of TMP selectivity with pellet size was even more pronounced.

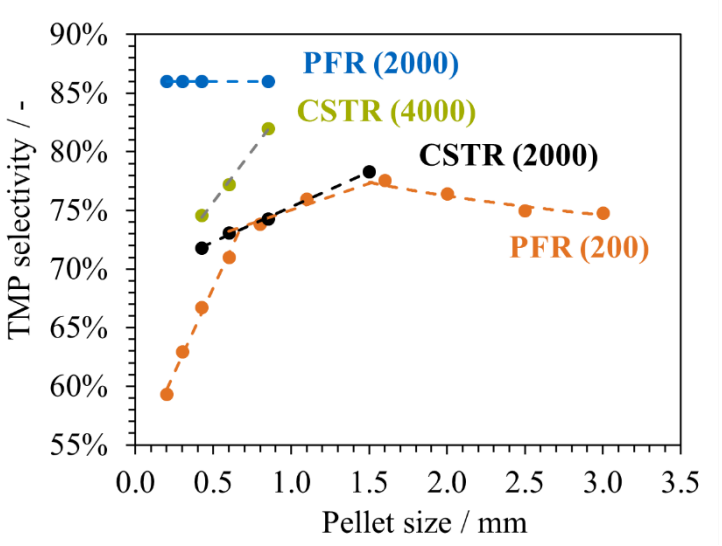

Figure 3.18. Dependence of average TMP selectivity on pellet size for different reactor types. In case of fixed-bed reactor feeding P/O ratio is taken (PFR (XXX), for stirred tank reactor the in situ P/O ratio in the reactor is taken CSTR(XXX).

Subsequently, similar butene concentration in reaction mixture resulted in improved product selectivity when larger pellets are applied. It is plausible to assume an intra-pellet gradient being the reason for this dependency. Therefore, two counteracting effects are balanced in stirred tank reactor when pellet size changes. On the one hand, decreasing pellet size comes along with enlarged external surface area, which enables a higher accessibility of reactants to active sites resulting in lower butene concentration, which is crucial in order to avoid deactivating side-products. On the other hand, increasing pellet size supports the formation of a butene

gradient within the catalyst pellet also being beneficial to reduce local butene concentration. However, pore diffusion is highly dependent on reactant concentration, therefore, the enormous dilution with isobutane by back-mixing reduces the driving force for diffusion to enter the pellet. Additionally, the higher conversion level in case of smaller pellets reduces reactant concentration even more making the effect of mass transport limitation much less effective. As consequence, the improved catalytic performance of smaller pellets in CSTR is attributed to increased amount of acid sites by higher surface area being more beneficial than the intra-pellet gradient for large pellets.

In contrast to CSTR, linear correlation of lifetime and catalyst bed length has shown that catalysts pellets in fixed-bed reactor are consumed successively in flow direction making the change of external surface area less effective for this reactor type. However, the two opponent effects of accessibility and gradient are also competing when pellet size is changed in fixed-bed reactor.

Lower accessibility of active sites for large pellets results in the formation of an additional concentration gradient over catalyst bed due to pellet bypassing. Thus, besides an intra-pellet gradient also a bed gradient is formed which becomes broader with decreasing pellet size. Both gradients are beneficial for catalytic performance in alkylation as local butene concentration is reduced. Though, there is an optimum pellet size dependent on feeding P/O and olefin space velocity. Exceeding this size, the accessibility to active sites is reduced dramatically by huge pore diffusion limitation and massive bypassing resulting in incomplete butene conversion which diminishes integral alkylate yield markedly.

3.4. Conclusion

In CSTR, the reduction of pellet size range from 1.0-2.0 to 0.35-0.5 mm results in an improved catalytic performance of LaX zeolite in isobutane/2-butene alkylation. Catalyst lifetime was prolonged from 10.5 to 16 h and integral alkylate yield raised up to 7.0 $g_{alkylate} \cdot g_{catalyst}^{-1}$. As there are no markely differences in deactivation behavior we conclude that general deactivation mechanism of zeolite pellets is the same for all pellet sizes. The higher external surface area of smaller pellets leads to higher acid site accessibility which enables a higher butene conversion level accompanied by a drastic increase of in situ P/O ratio in the reactor. As the local butene concentration is crucial for ratio of hydride transfer vs. olefin addittion, the selectivity is improved towards more desired C_8 products and less side-products from multiple alkylation and cracking. In addition, dimerization is suppressed by enhanced P/O ratio indicated by increased 2,2,3-TMP vs. 3,4-DMH ratio. The TMP isomer distribution within C_8 fraction reveals less formation of secondary TMP isomers, which brings us to the conclusion that residence time of C_{8+} carbenium ions on the catalytic surface is reduced by faster hydride transfer resulting from increased isobutane concentration.

In PFR, the change of pellet size has a much stronger effect on alkylation performance of solid acid catalysts than in CSTR. Increasing pellets up to 3.0 mm results in steady increase of TMP selectivity, however, less changes are observed exceeding 1.6 mm. Butene conversion curve also shows a drastic change between 1.6 and 2.0 mm from concave to convex shape with time on stream. Experiments at lower olefin space velocity proved the dependence on deactivation curve behavior. Furthermore testing different feeding P/O ratios showed a faster loss of conversion per time for higher P/O ratio in feeding mixtures underlining butene concentration at pellet outside determines deactivation rate.

The deactivation of catalyst bed was investigated for two different pellet sizes by segmentation revealing successive consumption of zeolite catalyst like a cigarette burning in case of 0.35-0.5 mm pellets. The butene concentration profile over catalyst bed for small and large pellets demonstrated a much more homogeneous distribution of reactant in case of 2 mm pellets leading to simultaneous deactivation of all catalyst pellets induced by the formation of a bed gradient.

Running fixed-bed reactor at conditions normally found in CSTR, where P/O ratio is extremely high due to back-mixing, allowed the direct comparison of pellet size effect in two different

reactor types. The performance of LaX in isobutane/2-butene alkylation is in both reactors strongly dependent on site accessibility and mass transport limitation tunable by pellet size. However, in CSTR small pellets are preferred as the amount of accessible site is crucial dominating over beneficial effect of pore diffusion. On the other hand, fixed-bed reactor showed improved performance when pellet size was increased due to intra-pellet and bed gradient of butene compensating decreased site accessibility.

All in all, the combination of large pellets in mm size with fixed-bed reactor using P/O ratio of 100-200 makes solid acid catalysts much more economically competitive to established liquid acid technology by increased lifetime and integral alkylate yield as well as higher selectivity towards desired high-octane products in an industrially more relevant reactor type.

3.5. References

1. L. F. Albright, *Industrial & Engineering Chemistry Research* **2003**, *42*, 4283-4289.
2. A. Corma, A. Martínez, *Catalysis Reviews* **1993**, *35*, 483-570.
3. A. Feller, J. A. Lercher, in *Advances in Catalysis, Vol. 48*, Academic Press, **2004**, pp. 229-295.
4. K. W. Li, R. E. Eckert, L. F. Albright, *Industrial & Engineering Chemistry Process Design and Development* **1970**, *9*, 434-440.
5. I. M. Gerzeliev, V. A. Temnikova, M. N. Baskhanova, A. L. Maksimov, *Russian Journal of Applied Chemistry* **2020**, *93*, 1578-1585.
6. C. Sievers, J. S. Liebert, M. M. Stratmann, R. Olindo, J. A. Lercher, *Applied Catalysis A: General* **2008**, *336*, 89-100.
7. G. S. Nivarthy, A. Feller, K. Seshan, J. A. Lercher, *Microporous and Mesoporous Materials* **2000**, *35-36*, 75-87.
8. K. Yoo, E. C. Burckle, P. G. Smirniotis, *Catalysis Letters* **2001**, *74*, 85-90.
9. J. Weitkamp, Y. Traa, *Catalysis Today* **1999**, *49*, 193-199.
10. A. Feller, I. Zuazo, A. Guzman, J. O. Barth, J. A. Lercher, *Journal of Catalysis* **2003**, *216*, 313-323.
11. J. Pater, F. Cardona, C. Canaff, N. S. Gnep, G. Szabo, M. Guisnet, *Industrial & Engineering Chemistry Research* **1999**, *38*, 3822-3829.
12. C. A. Querini, E. Roa, *Applied Catalysis A: General* **1997**, *163*, 199-215.
13. C. Sievers, I. Zuazo, A. Guzman, R. Olindo, H. Syska, J. A. Lercher, *Journal of Catalysis* **2007**, *246*, 315-324.
14. A. Guzman, I. Zuazo, A. Feller, R. Olindo, C. Sievers, J. A. Lercher, *Microporous and Mesoporous Materials* **2005**, *83*, 309-318.
15. F. Schüßler, E. A. Pidko, R. Kolvenbach, C. Sievers, E. J. M. Hensen, R. A. van Santen, J. A. Lercher, *The Journal of Physical Chemistry C* **2011**, *115*, 21763-21776.
16. K. P. de Jong, C. M. A. M. Mesters, D. G. R. Peferoen, P. T. M. van Brugge, C. de Groot, *Chemical Engineering Science* **1996**, *51*, 2053-2060.
17. R. J. Taylor, D. E. Sherwood, *Applied Catalysis A: General* **1997**, *155*, 195-215.
18. E. T. C. Vogt, G. T. Whiting, A. Dutta Chowdhury, B. M. Weckhuysen, in *Advances in Catalysis, Vol. 58* (Ed.: F. C. Jentoft), Academic Press, **2015**, pp. 143-314.

19. S. N. Khadzhiev, I. M. Gerzeliev, O. S. Vedernikov, A. V. Kleymenov, D. O. Kondrashev, N. V. Oknina, S. E. Kuznetsov, Z. A. Saitov, M. N. Baskhanova, *Catalysis in Industry* **2017**, *9*, 198-203.

3.6. Supporting information

Related to section 3.3.1: Pellet size effect in CSTR

Reaction conditions: 1.0 g catalyst, 75°C, 25 bar, feeding isobutane to cis-2-butene molar ratio of 10:1, olefin space velocity 0.2 $g_{butene} \cdot g_{catalyst}^{-1} \cdot h^{-1}$).

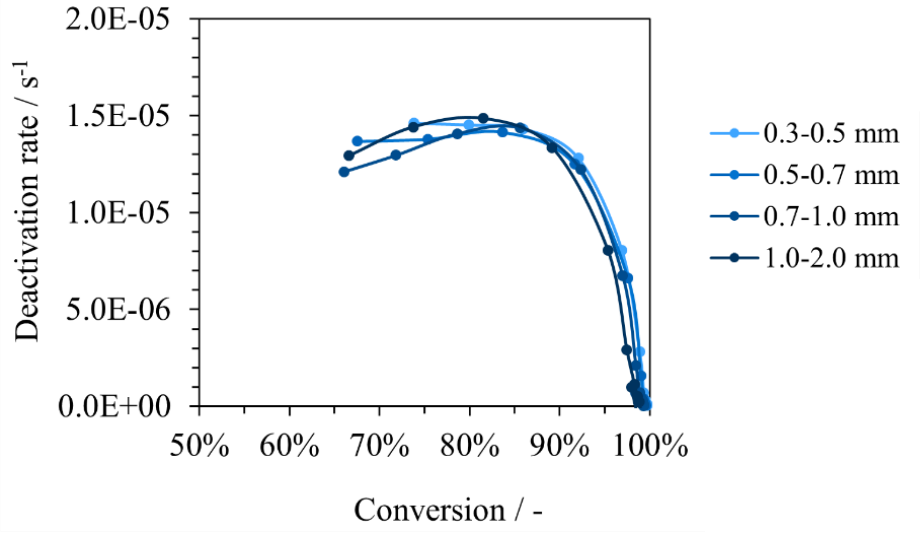

Figure S3.1. Dependence of deactivation rate on butene conversion for different pellet sizes CSTR.

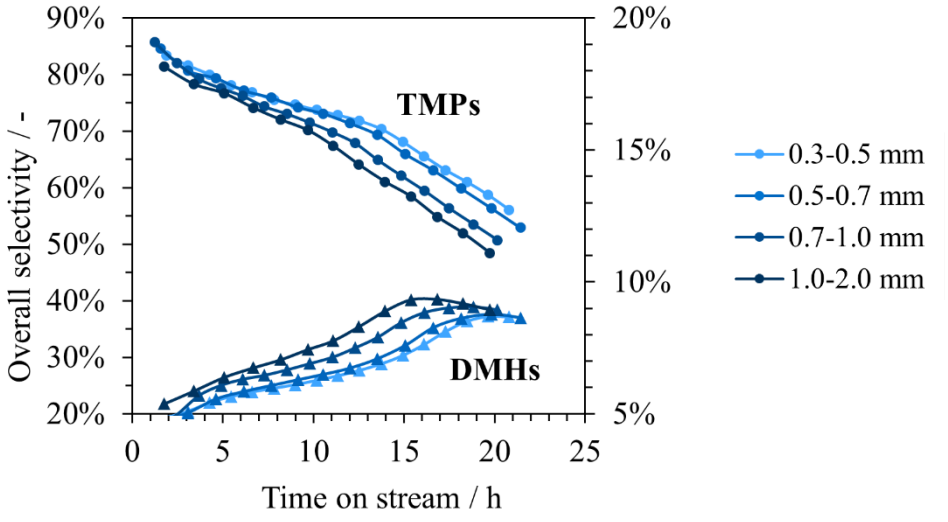

Figure S3.2. Overall TMP and DMH selectivity of different pellet size ranges in CSTR.

Table S3.1. Catalytic performance results of different pellet size ranges in CSTR.

Pellet size range [mm]	Turnover number* [$mol_{alkylate} \cdot mol_{BAS}^{-1}$]	Lifetime [h]	Integral yield [$g_{alkylate} \cdot g_{cat}^{-1}$]
0.35 - 0.5	88	16	7.0
0.5 - 0.7	83	15	6.6
0.7 - 1.0	76	13	6.1
1.0 - 2.0	67	10.5	5.4

* taken at remaining conversion of 66-67%

Related to section 3.3.2: Pellet size effect in fixed-bed reactor

Reaction conditions (if not defined otherwise): 0.1 catalyst, 75°C, 25 bar, Isobutane to cis-2-butene with a molar ratio of 200:1, olefin space velocity 0.2 $g_{butene} \cdot g_{catalyst}^{-1} \cdot h^{-1}$).

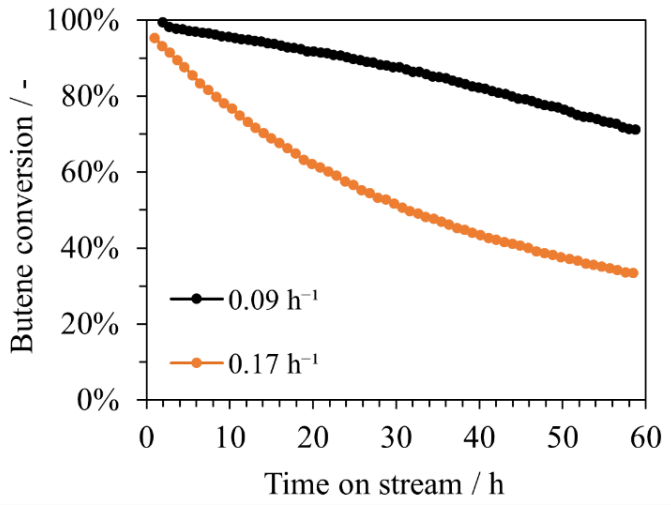

Figure S3.3. Influence of olefin space velocity varied by flow rate on shape of butene conversion curve of 2.0 mm pellets.

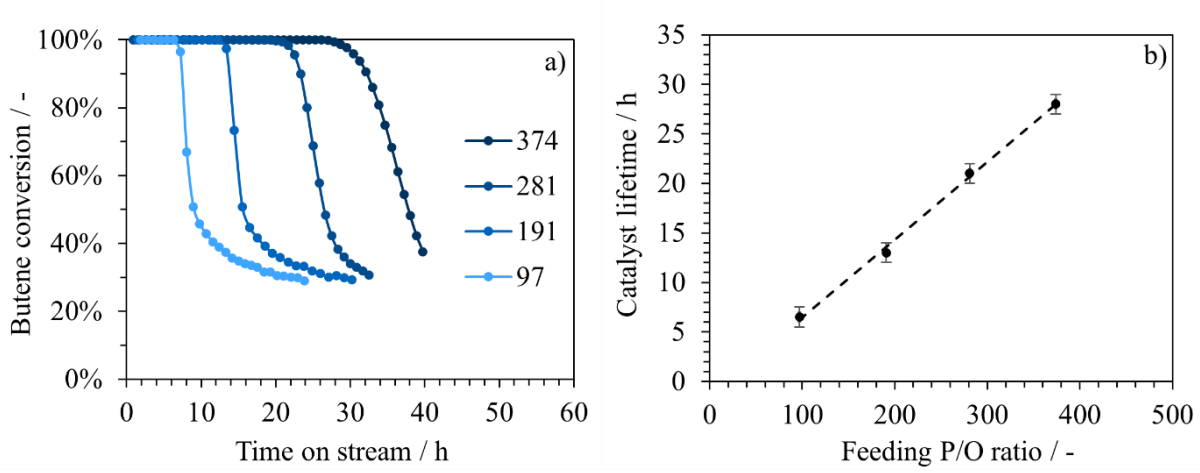

Figure S3.4 a) Influence of paraffin to olefin ratio on butene conversion of pellets in the range 0.35-0.5 mm keeping olefin space velocity constant and b) Correlation between catalyst lifetime and feeding P/O ratio.

Table S3.2. Catalytic performance results of different pellet size ranges in PFR.

Pellet size [mm]	Number of pellets	External surface area [$mm^2 \cdot g^{-1}$]
0.35 - 0.5	~ 2000	8303
0.5 - 0.7	640	7328
0.8	68	6301
1.1	33	4058
1.6	14	2563
2.0	8	1808
2.5	5	1532
3.0	3	1417

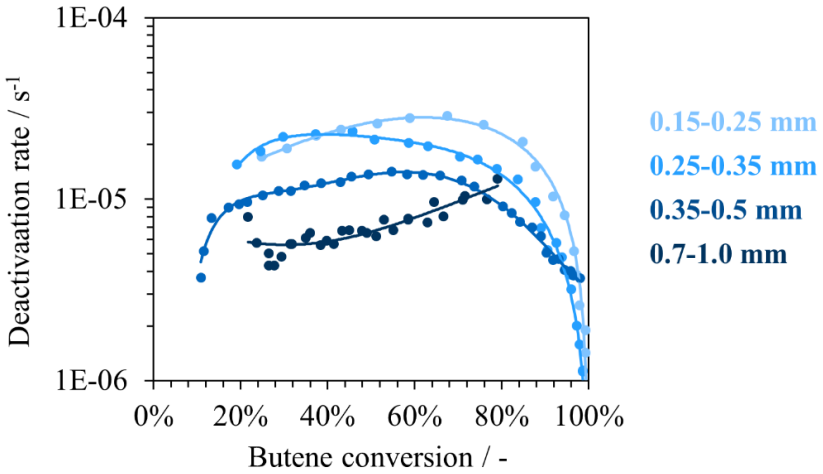

Figure S3.7. Deactivation rate with butene conversion for different pellet sizes under CSTR-like conditions in PFR at P/O = 2000.

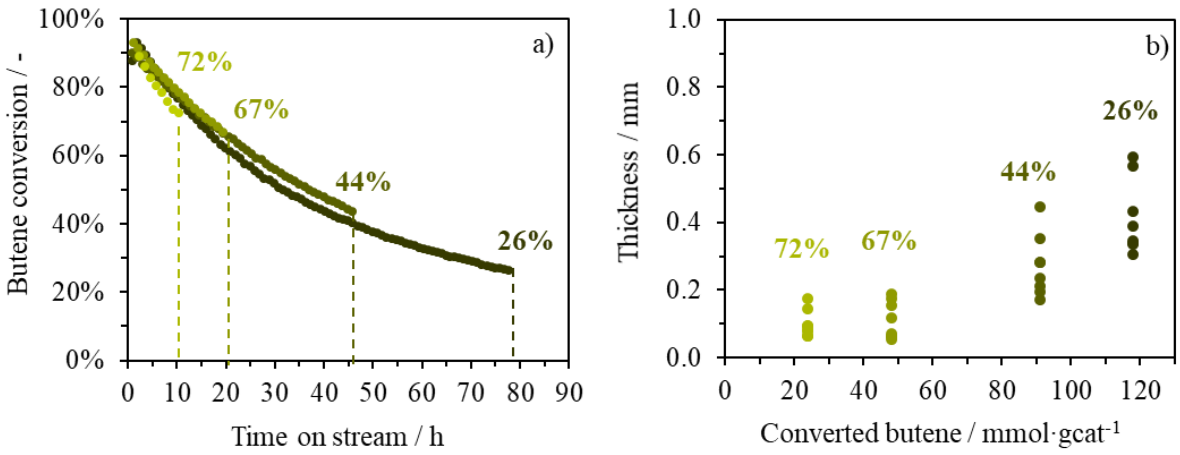

Figure S3.6. a) Butene conversion with time on stream for 2.0 mm cubes interrupted at different remaining conversion and b) Evolution of shell thickness with converted amount of butene measured at remaining butene conversion using microscopic images of cross sections.

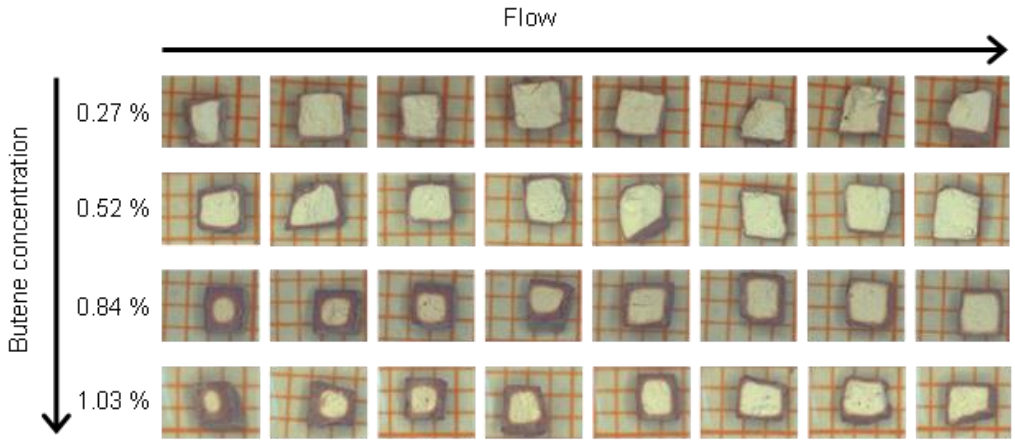

Figure S3.5. Microscopic images of cross-sections of used 2.0 mm cubes in flow direction after same time on stream varying feeding butene concentration.

Chapter 4

4. Understanding the role of residue water on catalytic performance of LaX zeolite in isobutane/2-butene alkylation

Abstract

The optimum activation of lanthanum exchanged X zeolite used in alkylation of isobutane with 2-butene is crucial to reach the maximum alkylate yield per life cycle. In order to make this catalyst economically competitive, the most favorable water content has to become independent on individual reactor characteristics to be universally applicable. Varying the amount of residue water by activation temperature in a fixed-bed reactor effects dramatically catalyst lifetime and selectivity of high-octane products. A volcano-like dependency of alkylate yield on water content was found with a maximum at 250°C. Acid site quantification as well as in situ studies using IR spectroscopy revealed two different factors causing deactivating. Insufficient water removal when choosing low activation temperature results in low Brønsted acid site concentration. Additionally, water weakens the beneficial effect of La^{3+} induced hydrocarbon polarization enhancing hydride transfer. If water content drops below the threshold of around 20 H_2O/UC catalyst lifetime is reduced due to partial dehydroxylation leading to decreased BAS concentration and strong interaction of heavy hydrocarbons with LAS.

4.1. Introduction

Rare-earth ion-exchanged faujasite type zeolites like LaX and LaY have shown remarkable catalytic activity in isobutane/n-butene alkylation.[1-3] La^{3+}cations are claimed to have several beneficial effects such as zeolite framework stabilization as well as the enhancement of Brønsted acid site strength by additional polarization of the bridging OH group.[4-5] Unfortunately, their industrial application as alkylation catalyst is compromised by rapid deactivation due to undesired side-products blocking pore and acid sites.[6-7]

To prevent the formation of deactivating heavy hydrocarbons the ratio of hydride transfer rate vs the rate of oligomerization is decisive. As the alkylation reaction occurs via addition of butene to an isobutyl carbenium ion, the resulting octyl carbenium ion has to undergo hydride transfer from isobutane in order to be removed from the active site. The resulting trimethylpentanes are high-octane alkylate products and additionally generated isobutyl ion closes the catalytic cycle. [8]

Two main strategies are followed to improve solid acid catalyted technology: first, the usage of well-stirred tank reactors operating at huge paraffin to olefin ratios helps to maximize hydride transfer rate as local butene concentration is minimized.[9-10] Second, applied catalyst has to offer high concentration and strength of Brønsted acid sites, which effectively catalyze hydride transfer reactions suppressing the formation of oligomers, which strongly adsorb on the catalyst and, thus, lead to deactivation.[11]

Numerous studies were made to understand the nature of acid sites in rare-earth exchanged FAU zeolites.[4, 12-13] In case of LaX, Brønsted acid sites are generated by dissociation of water from hydrated La^{3+} cations generating bridging OH as well as LaOH groups based on Hirschler-Plank-mechanism[14-16]: .

$$[La(H_2O)_n]^{3+} \leftrightarrow [La(OH)(H_2O)_{n-1}]^{2+} + H^+$$

Several studies claimed catalytic performance of LaX in isobutane/2-butene alkylation is strongly affected by activation temperature indicating a crucial role of remaining water in the reaction.[2, 17] Previous work in our group identified an optimum activation temperature of 423-453 K applied for 16 h for LaX catalyst.[18] However, these conditions were investigated using a stirred-tank reactor, where flow conditions and catalyst accessibility are quite different compared to a fixed-bed reactor. Subsequently, direct correlation of defined water content and

catalytic performance is still under investigation. A better understanding of the role of residue water facilitates the adjustment of optimum activation conditions for industrial application independent on reactor type.

Here, by the quantification of residual water of LaX by varying activation temperature using a fixed-bed reactor as well as simulating activation conditions in characterization setups, we investigate the evolution of active sites with the amount of water and how this influences the catalytic performance in isobutane/2-butene alkylation. Moreover, consequences for selectivity after very mild and very harsh treatment gives the possibility to draw conclusions on the nature of sites at different water content.

4.2. Experimental

4.2.1. Catalyst preparation

La^{3+}-exchanged zeolite X (LaX) was prepared from NaX (Si/Al = 1.2) provided by Chemische Werke, Bad Köstritz. The parent material was ion exchanged four times with 0.2 M $La(NO_3)_3$ solution at 70°C for 2 h with a liquid-to-solid ratio of 10 $ml \cdot g^{-1}$. The material was washed subsequently with bidistilled water and dried at room temperature. After the second and fourth ion exchange the sample was calcined in 100 $ml \cdot min^{-1}$ syn air at 450°C for 1 h with a heating ramp of 0.5 $°C \cdot min^{-1}$. The prepared catalyst was stored under constant water vapor pressure over saturated $CaCl_2$ solution. In order to obtain pellets in the range of 0.35-0.5 mm the catalyst powder was pressed to wafers, crushed and sieved.

4.2.2. Catalytic experiments

The alkylation of isobutane with 2-butene was performed in a fixed-bed reactor with ¼ inch diameter at 75°C and 25 bar. Prior to reaction, 0.1 g catalyst was activated *in situ* under 100 $ml \cdot min^{-1}$ nitrogen flow. The activation temperature was varied between 150 and 450°C (heating ramp of 2 $°C \cdot min^{-1}$) kept constant for 1h. The reaction was started by feeding a mixture of isobutane and cis-2-butene with a molar ratio of 200:1 (Rießner Gase GmbH) using a high-pressure Teledyne ISCO 500D syringe pump. The olefin space velocity was 0.2 $g_{butene} \cdot g_{catalyst}^{-1} \cdot h^{-1}$. For analysis the reaction mixture was expanded after the reactor by a backpressure regulator and passed through a six-port valve with a 0.1 ml sample loop. The product distribution was measured using a 60 m DB-1 column (ID = 0.32 mm, film thickness = 1.00 µm) in an Agilent 7890B gas chromatograph equipped with a flame-ionization detector. Data was evaluated using the software OpenLab2.

4.2.3. Catalyst characterization

To simulate activation conditions of catalytic testing setup the exposure of sites during removal of water was recorded by IR spectroscopy, while the amount of water remaining adsorbed on LaX samples as function of activation temperature was investigated by thermogravimetric analysis (TGA) both operated under nitrogen flow.

For IR spectroscopy, catalyst powder was pressed into a thin, self-supporting wafer and installed in the IR cell perpendicular to the beam. It was heated to 150°C with a heating rate of 2° C·min^{-1} under 20 ml·min^{-1} N_2 flow. IR Spectra were taken after 1, 2, 4, 8 and 12 h from 1000 to 4500 cm^{-1} with a resolution of 4 cm^{-1} and an average of 120 scans per spectrum on a Nicolet iS50AEM spectrometer. After activation at 150°C, the sample was heated to 450°C for 1 h, whereas IR spectrum was taken after cooling to 150°C.For thermogravimetric analysis, pressed catalyst pellets (0.35-0.5mm) were activated at 100-450°C with a heating rate of 2°C·min^{-1} for 1 h under nitrogen flow using a SETARAM Sensys Evo TG-DSC. The remaining water content after activation was determined by heating to 450°C with a heating rate of 10 °C·min^{-1}.

Acid site concentration of Brønsted (BAS) and Lewis acid sites (LAS) at certain activation temperatures were determined by IR-spectra of adsorbed pyridine using a Thermo Nicolet 5700 in the range of 400-4000 cm^{-1} with a resolution of 4 cm^{-1}. The samples were pressed into thin, self-supported wafers and activated at 150-450°C for 1 h in vacuum (10^{-6} mbar) with a heating rate of 10°C·min^{-1}. Subsequently, pyridine was adsorbed at 0.5 mbar at 150°C for 1 h. After outgassing in high vacuum for 1 h to remove physisorbed pyridine, a spectrum was taken at 150°C to determine the concentration of adsorbed pyridine. For quantification, molar integral extinction coefficients of 0.73 cm·µmol^{-1} and 0.96 cm·µmol^{-1} were used for pyridine adsorbed on Brønsted and Lewis acid sites, respectively.

The heat of adsorption of water on dry LaX catalyst was measured using a SETARAM TG/DSC 111 connected to a BARATRON 122A. Pressed catalyst pellets were first outgassed in vacuum (10^{-6} mbar) at room temperature till constant weight and then activated at 450°C (heating rate: 5°C·min^{-1}) for 1 h before water was dosed stepwise up to 10 mbar.

4.3. Results and discussion

4.3.1. Effect of activation temperature on catalytic performance of LaX

The conversion of reactant butene in isobutane/butene alkylation catalyzed by LaX zeolite activated for 1 h at different temperatures is shown in Figure 4.1. The catalyst reached independent on activation temperature first a period of full butene conversion defined as catalyst lifetime followed by a sharp drop to 20-30% conversion reaching last reaction stage with slow decrease of conversion. The steep decrease of butene conversion after initial full conversion period is attributed to the deactivation by pore and/or acid site blockage of catalysts caused by heavy hydrocarbon byproducts.[8]

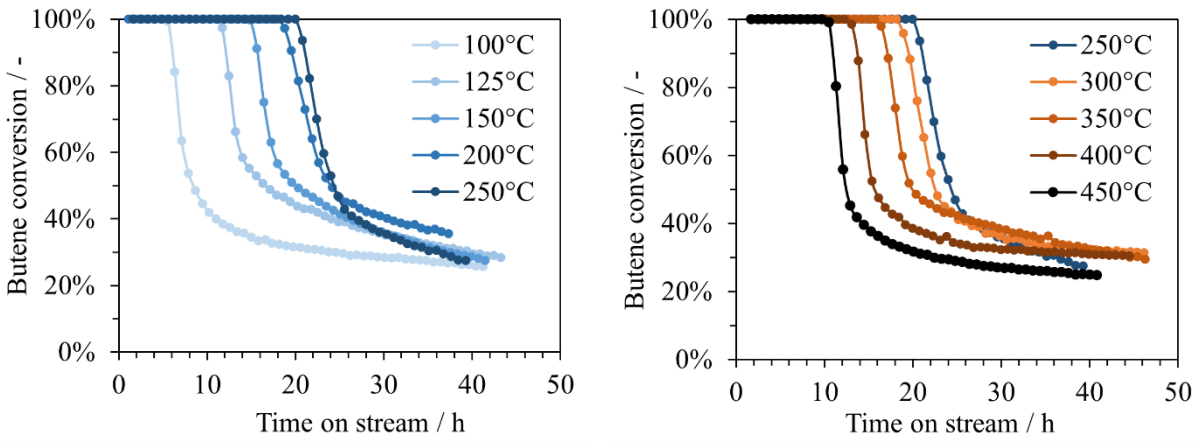

Figure 4.1. Butene conversion with time on stream for activation temperatures from 100 to 450°C.

Applying an activation temperature of 100°C led to shortest catalyst lifetime being only 6 h time on stream. Increasing the activation temperature gradually up to 250°C led to a prolongation of full conversion period to the maximum of 20 hours. Further stepwise intensifying of activation conditions resulted again in the reduction of catalyst lifetime**.** The catalyst treated at most severe activation conditions of 450°C was able to convert 100% butene for 10.5 h before deactivation set in. Consequently, catalyst lifetime shows a volcano-like dependency of activation temperature with a maximum at 250°C (see Figure 4.2a). However, the increase of lifetime when raising the temperature from 100 to 250°C is much steeper than the decline due to harshening activation conditions up to 450°C.

Defining deactivation rate as loss of conversion per time on stream (d *conv*/d *TOS*), the maximum rates for each activation temperature can be seen in Figure 4.2b. showing a reverse volcano-like behavior. Thus, deactivation rates correlate well with catalyst lifetime dependency on activation temperature, whereas lowest maximum deactivation rate was detected for longest catalyst lifetime at 250°C and highest rates were found for most severe activation conditions.

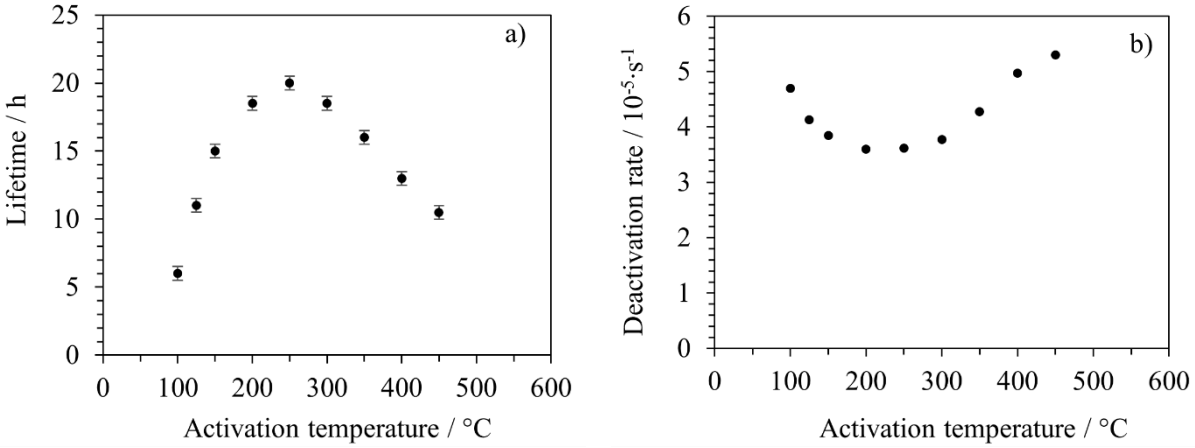

Figure 4.2. Effect of activation temperature on a) catalyst lifetime and b) maximum deactivation rate after end of lifetime.

The average C_8 selectivity during the period of full conversion follows the trend of detected catalyst lifetime having its maximum at 250°C with 76.4 wt% as seen in Figure 4.3a. However, formation of octanes decreased faster for lower activation temperatures than in case of higher ones. The mildest treatment of LaX catalyst at 100°C lead to the lowest average C_8 selectivity during lifetime being only 69.2 wt%. Increasing activation temperature to 125°C also increased octane selectivity up to 71.9 wt%. Exceeding 250°C the abundancy of C_8 was reduced again, however, less difference of octane selectivity is seen for activation temperatures 400 and 450°C. Both conditions lead in average to 74.2 wt% C_8 products.

For mild activation conditions below 300°C the average selectivity towards n-butane also shown in Figure 4.3a agrees with the trend of C_8 selectivity as it increases from 1.4 wt% for 100°C to 2.6 wt% at 250°C. However, in contrast to octane formation n-butane selectivity decreased only slightly exceeding 250°C. This leads to the conclusion, that acid sites involved in n-butane formation step are only minor affected by higher temperatures. As n-C_4 is mainly formed during initiation by hydride transfer from isobutane to secondary C_4^+ carbenium ions generated by butene adsorption on Brønsted acid sites, it is plausible to assume BAS concentration is strongly reduced for mild activation.

In parallel, the selectivity of by-products from multiple alkylation and cracking being hydrocarbons in C_{5-7} range as well as C_9 or larger compounds showed a minimum at 250°C, which can be seen in Figure 4.3b. Applying 100°C resulted in maximum selectivities of 16.3 wt% C_{5-7} and 13.0 wt% C_{9+} hydrocarbons. The increase of activation temperature to 250°C decreased formation of undesired compounds to 11.7 wt% C_{5-7} and 7.8 wt% C_{9+}. Correlating with octane selectivity, the changes of by-product selectivity at harsher conditions are less pronounced than for mild treatment, whereas temperature higher than 400°C do not affect product mixture composition anymore.

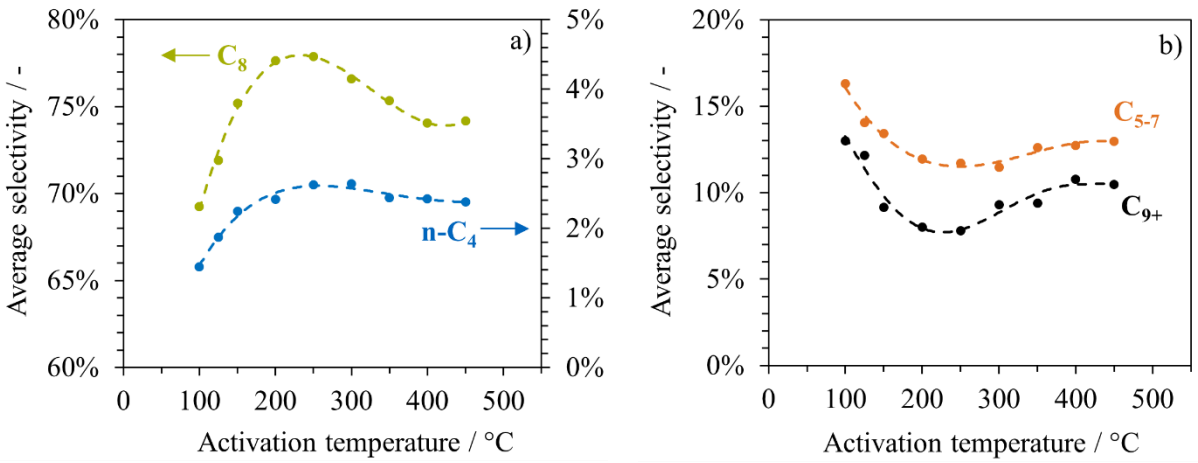

Figure 4.3. Average selectivity during period of full conversion dependent on activation temperature. a) C_8 and n-butane b) C_{5-7} and C_{9+}.

Consequently, lower activation temperatures than 250°C show a strong effect on product selectivity indicating a great impact of activation conditions on active sites catalyzing isobutane/2-butene alkylation. In contrast to that, smaller changes of product distribution were observed for further increasing activation temperature up to 450°C, which points to additional influencing factors being responsible for the decline of catalyst lifetime and correlated alkylate yield for LaX catalyst.

4.3.2. Same lifetime, different selectivity

Based on volcano-like behavior the catalyst lifetime of 125°C and 450°C is almost the same, thus, grouped selectivity towards n-C_4, C_{5-7}, C_8 and C_{9+} is quite different. Therefore, the distribution of different isomers within C_8 fraction is compared for these two reactions to understand the effect of pretreatment on alkylation reaction and its side-pathways.

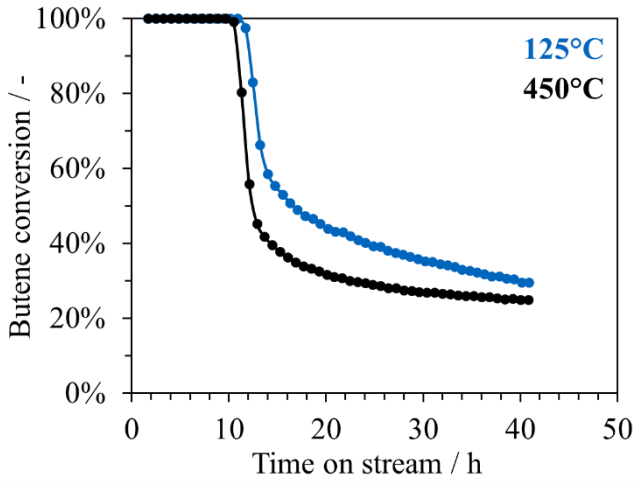

Figure 4.4. Butene conversion of LaX with time on stream after activation at 125°C and 450°C.

Despite both reactions showed a period of full conversion around 11 h (Figure 4.4), there are markedly differences in the development of branched isomers within C8 fraction during catalyst lifetime shown in Figure 4.5. The first measuement point around 1.7 h TOS showed that initial selectivity within octane fraction is independent on activation procedure as both start with similar isomer distribution within C_8 fraction. In the beginning of the reaction highly-branched trimethylpentanes (TMPs) selectivity amounts 90 wt%, dimethylhexane isomers (DMHs) constitute with 10 wt% and 2-methylheptane (2-MHp) selectivty is 0.4 wt%. No unsaturated octenes or other MHp isomers were detected within the period of full conversion. Generally, TMP selectivity decreases while DMH and MHp selectivity increases with ongoing alkylation reaction, however, in case of mild activation at 125°C the decline of high-octane TMP fraction is much steeper compared to harsh treatment at 450°C (Figure 4.2a). At the end of catalyst lifetime when butene conversion drops below 100% the TMP selectivity within C_8 fraction is around 3 wt% higher if an activation temperature of 450°C is applied before starting alkylation

reaction. In parallel, Figure 4.5b shows that selectivity of less branched side-products being DMHs and MHps increased faster after mild activation.

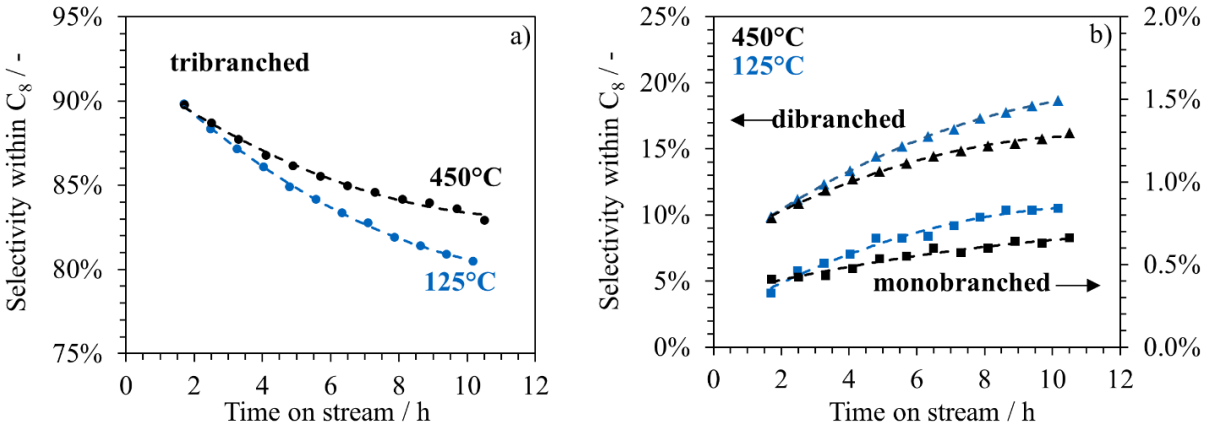

Figure 4.5. Development of selectivity within C_8 fraction with time on stream for reactions after pretreatment at 125 and 450°C. a) Tribranched octane isomers (Trimethylpentanes) and b) Dibranched (Dimethylhexanes) and Monobranched (Methylheptanes, only 2-MHp detectable) octane isomers.

The four tribranched C_8 isomers are summarized as TMP fraction, whereas Figure 4.6 shows their individual content during alkylation reaction. The most abundant isomer, 2,3,3-TMP, decreases generally with time on stream, while 2,2,4-TMP increases steadily. The content of the other two isomers, 2,2,3- and 2,3,4-TMP shows only small changes within catalyst lifetime. Comparing composition of TMP fraction for 125°C and 450°C less differences are observed, which indicates there is no influence of activation temperature on main alkylation mechanism

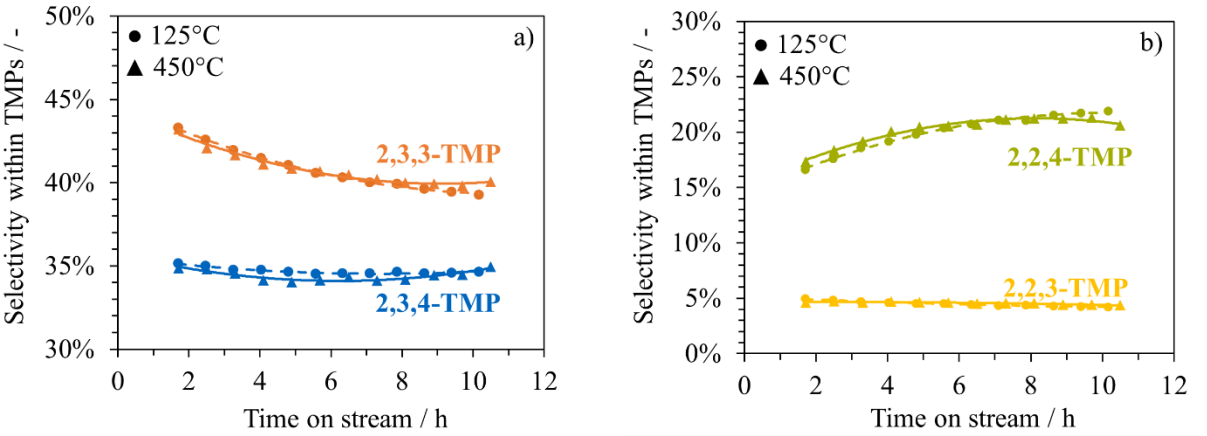

Figure 4.6. Distribution of individual TMP isomers within TMP fraction with time on stream for activation temperatures 125 and 450°C.

or isomerization of C_8 products. Scheme 4.1 illustrates the formation routes of different octane isomers possible in isobutane/2-butene alkylation, whereas skeletal isomerization is considered to be negligible under chosen reaction conditions.

As seen in Scheme 4.1 the formation of different octane isomers is dependent on available butene isomers as well as isomerization of C_{8+} carbenium ions after olefin addition. For TMP formation there are two primary isomers resulting from reaction of 2-butene and isobutene with isobutyl carbenium ions. The latter one is also called self-alkylation as isobutene originates from isobutane which has undergone hydride transfer and deprotonation. In principle, tertiary carbenium ions are more stable than secondary ones, which is the driving force for isomerization towards secondary products, 2,3,3 and 2,3,4-TMP, and therefore being the most abundant products in C_8 fraction.

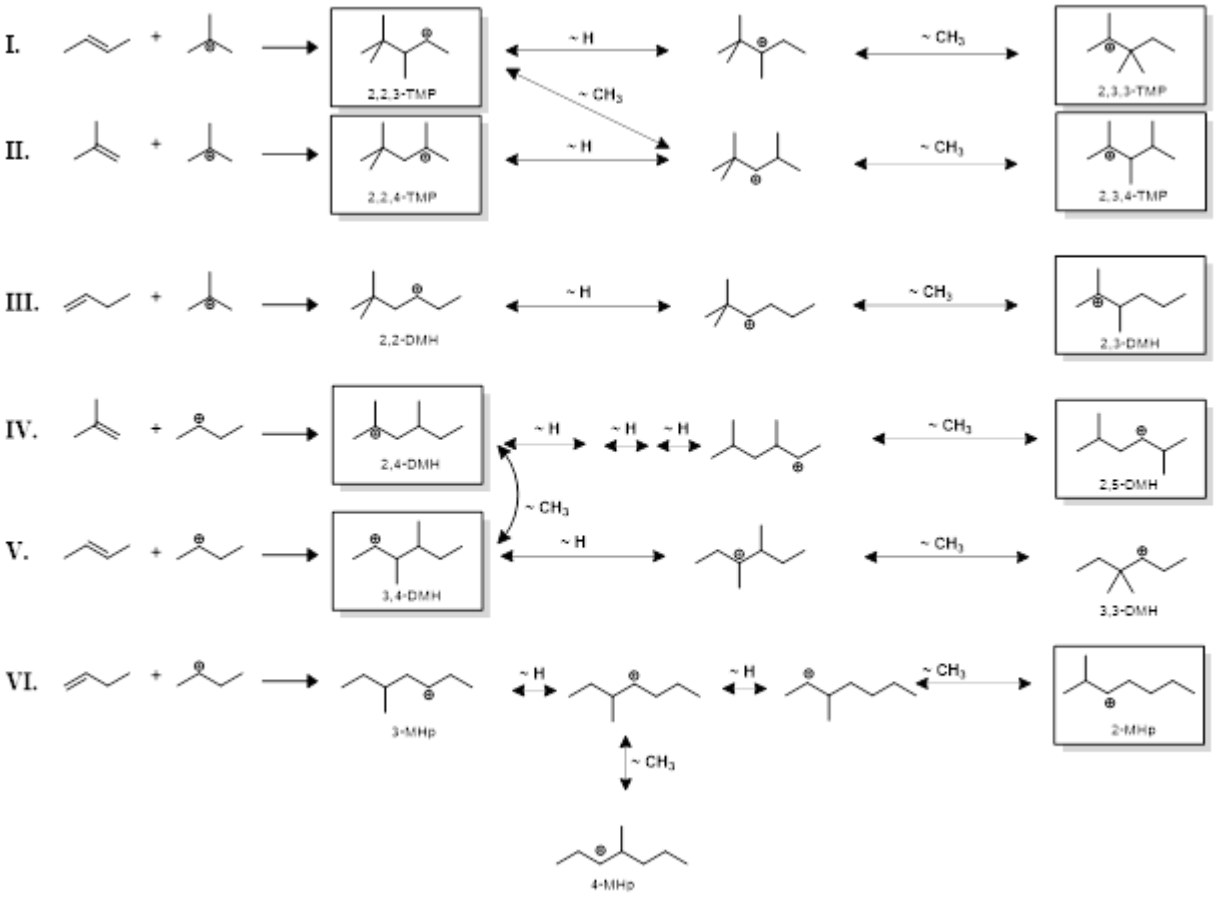

Scheme 4.1. Pathways of octane isomer formation in isobutane/2-butene alkylation. C_{8+} carbenium ions with detectable corresponding octane isomer are marked with boxes.

Contrary to unaffected TMP composition activation procedure has a considerable influence on content of dimethylhexane isomers. Regarding the development of the four detectable DMH

isomers with time on stream for activation at 125°C and 450°C (Figure 4.7), the formation of 3,4-DMH is much more pronounced after low-temperature activation, while 2,3- and 2,5-DMH show less abundancy. For isomer 2,4-DMH less effect of activation temperature was observed.

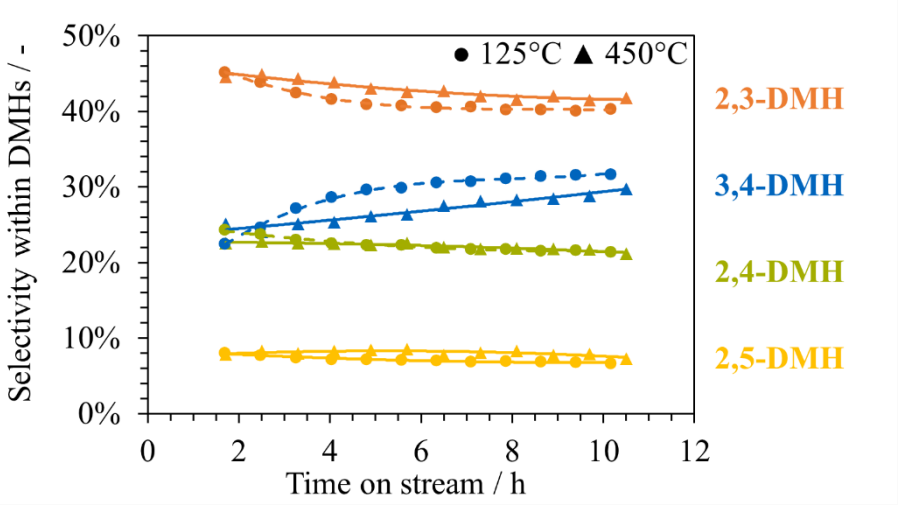

Figure 4.7. Distribution of individual DMH isomers within DMH fraction with time on stream for activation temperatures 125 and 450°C.

Less-branched octanes, dimethylhexanes and methylheptanes, can be generated by reaction of butene isomers with both, secondary as well as tertiary C_4^+ carbenium ions (Scheme 4.1, pathway III-VI). However, high activation temperature lead to an increased formation of 3,4-dimethylhexane (pathway V, Figure 4.7) as well as 2-methylheptane (pathway VI, Figure 4.5b), both formed by two linear butenes reacting without contribution of isobutane and therefore considered as dimerization products. The overall development within C_8 fraction accounting all isomers clearly underlines the fact that products generated by pathways I-VI, which include isobutyl or isobutene, are enhanced by activation temperature.

The shown consequences of activation temperature on overall selectivity as well as isomer distribution within C_8 fraction clearly indicate different nature and amount of acid sites leading to a so-called sweet spot of catalyst lifetime around 250°C under chosen activation and reaction conditions in a ¼" fixed-bed reactor. The comparison of reaction after activation at 125°C and 450°C indicates there are various inhibition factors, which reduce catalyst lifetime similarly, but affect selectivity differently. Applying low temperature, the dimerization pathway is enhanced compared to isobutane alkylation leading to the conclusion, that there are more acid sites able to catalyze butene dimerization instead of hydride transfer.

4.3.3. Characterization of sites during activation of LaX catalyst

The site exposure of LaX catalyst during activation was investigated by recording the desorption of molecular water under nitrogen flow at 150°C using IR spectroscopy. It has to be considered, that catalyst pellets are activated *in situ* in the fixed-bed reactor before starting the alkylation reaction, therefore, imitating the activation process in IR spectrometer may lead to slight abbreviations in time and temperature. Anyway, qualitative results can be used to understand the effect of activation conditions on isobutane/2-butene alkylation. As seen in Figure 4.8a IR bands in the region 3500-3650 cm-1 increased with time on stream, while OH bending vibration band of molecular water at 1630 cm-1 decreased (Figure 4.8b). The high-frequency band at 3600 cm-1 is assigned to OH vibrational mode of bridging Brønsted acid sites being exposed by ongoing water removal. Simultaneously, exposure of LaOH groups (OH band at 3520 cm^{-1}) was observed.

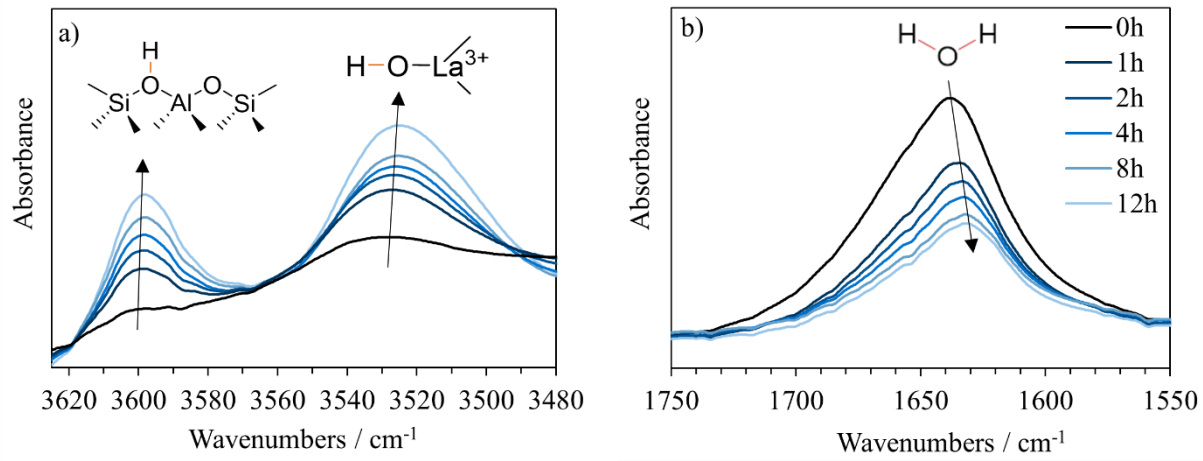

Figure 4.8. IR spectra of LaX catalyst under nitrogen flow at 150°C in the region a) 1550-1750 cm^{-1} and b) 3480-3620 cm^{-1}.

4.3.4. Determination of water content at different activation temperatures

The water content when applying different temperatures for 1 h was determined by TGA under flowing nitrogen simulating *in situ* activation conditions in the fixed-bed reactor. IR spectroscopy showed that required temperature for complete removal of adsorbed water is 450°C for 1 h. The amount of remaining water decreases with activation temperature from 11.0 wt% applying 100°C down to 0.5 wt% when heated to 400°C (see Figure 4.9). The corresponding number of water molecules per unit cell can be seen at the second y-axis, e.g. activating the catalyst at 250°C for 1 h leads to around 24 H_2O/UC. During activation process the rate of water removal shows two different stages in the measured range. From 100 to 300°C there is an exponential decrease of water content with increasing temperature, whereas removal rate is slowest in the range 200-300°C corresponding to 20-35 H_2O molecules per unit cell. Exceeding 300°C, the decrease of water content with temperature becomes linear until water removal is completed at 450°C. The change in water removal rate may explain the stronger impact of milder activation found for catalyst lifetime dependency on temperature. Slower desorption of water applying higher temperatures can be caused by different nature or strength of acid sites.

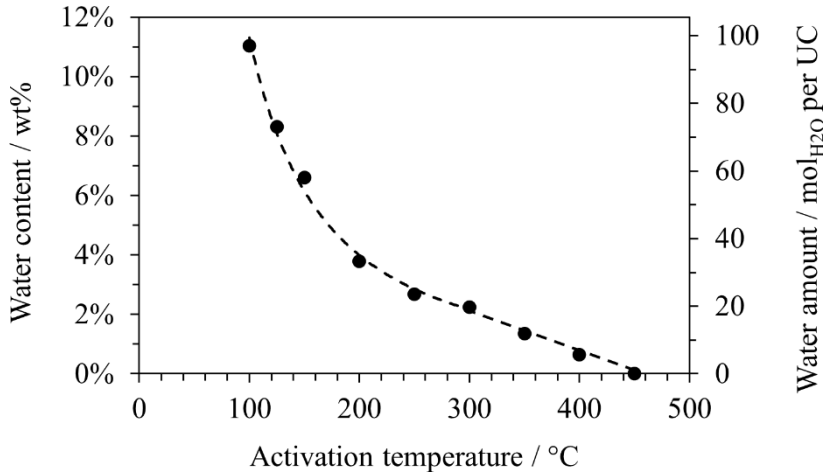

Figure 4.9. Effect of activation temperature on water content in wt% (based on dry zeolite mass) and water molecules per UC b) Dependence of heat of desorption on amount of water.

Figure 4.10 displays the heat of adsorption of water on activated LaX catalyst measured by thermogravimetric analysis under vacuum applying stepwise increase of water vapor pressure up to around 40 water/UC. Correlating with dependence of water content on temperature measured by Flow-TGA there is a threshold around 20 H_2O molecules per UC as heat of adsorption drastically increases below this limit. We attribute the higher relieve of energy for adsorbing water molecules at low water content to the adsorption on stronger acid sites.

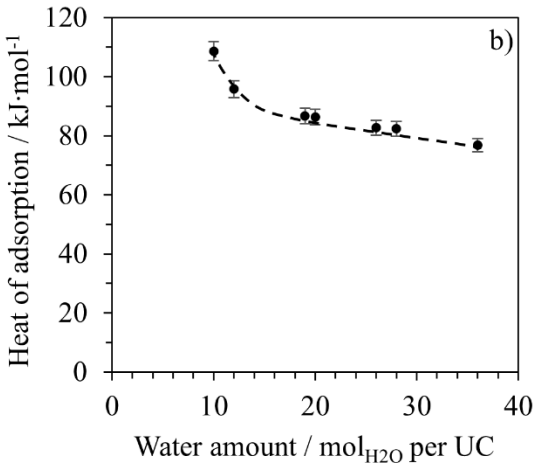

Figure 4.10. Dependence of the heat of adsorption on water amount of LaX zeolite.

4.3.5. Site quantification

The amount of different acid sites after activation was determined by using IR spectra of adsorbed pyridine at 150°C. Table 4.1 shows the results for measured concentrations of Brønsted (BAS) as well as Lewis acid sites generated by aluminum (Al-LAS) and lanthanum (La-LAS). Due to molar integral extinction coefficients being only available for 150°C, the site quantification was not carried out for temperatures below. The concentration of BAS is found to be highest after activation at 300 and 350°C and lowest for 150°C. Aluminum-generated Lewis sites also showed a minimum for lowest activation temperature and a maximum concentration for 350°C. Lewis sites originating from La^{3+} increase with increasing activation temperature up to their maximum concentration of 0.69 $mmol \cdot g^{-1}$, however, are not affected further when higher temperature is applied.

Table 4.1. Acid site concentration of LaX activated at different temperatures.

Site conc.	Activation temperature [°C]						
[$mmol \cdot g^{-1}$]	150	200	250	300	350	400	450
BAS	0.73	0.76	0.87	0.91	0.91	0.88	0.84
Al-LAS	0.29	0.35	0.42	0.40	0.44	0.41	0.39
La-LAS	0.63	0.65	0.62	0.63	0.69	0.69	0.69

*determined by IR spectra of adsorbed pyridine.

In addition to individual site concentrations, the ratio of BAS to different LAS is shown in Figure 4.11. The ratio of BAS/Al-LAS is decreasing with increasing temperature up to 250°C, however, does not change further for higher temperatures. In contrast to that, the ratio of BAS/La-LAS clearly shows a volcano-like dependency on activation temperature with a maximum around 250-300 °C. As a consequence, the ratio of Brønsted acid sites to overall Lewis sites only shows slight changes over temperature range, thus, there is a maximum around 300°C.

The conspicuous similarity between the development of BAS/La-LAS ratio and catalyst lifetime with increasing temperature encourages the assumption that these two sites are most crucial for catalytic performance of LaX. Consequently, several parallel influence factors of different sites have to be considered.

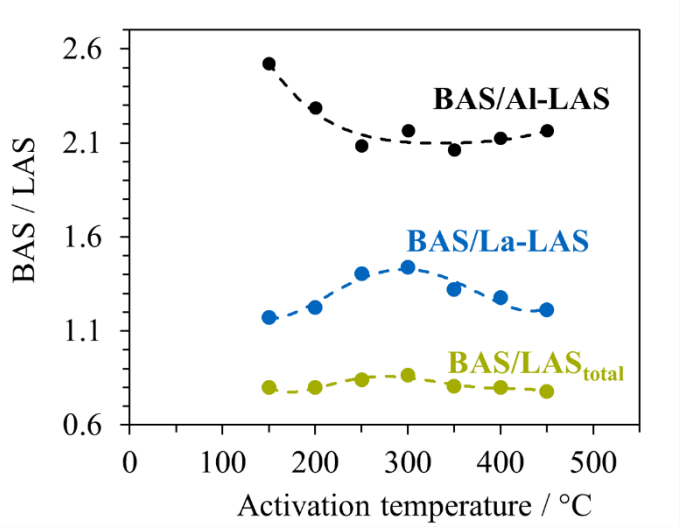

Figure 4.11. Dependence of BAS/Al-LAS, BAS/La-LAS and BAS/LAS$_{total}$ ratio on activation temperature of LaX in the range 150-450°C.

First, Brønsted acid sites are stated to be the active sites in proton-catalyzed isobutane/2-butene alkylation, therefore, the increasing exposure of these sites with ongoing water removal by heat treatment is correlated with lower butene concentration per active site, which suppresses the side-pathway dimerization. The increase of n-butane formation up to 250°C correlates with determination of BAS concentration.

Second, as already found by Sievers et al. La^{3+} cations enhance hydride transfer by polarization of hydrocarbons, [5] therefore, adsorbed water on lanthanum reduces their beneficial effect on alkylation by weaking the interaction of sites. Due to La-LAS concentration reaching a plateau, it is plausible to assume exposure of La^{3+} is completed when applying at least 350°C. Subsequently, increasing concentration of La-LAS by removing adsorbed water also contributes to prolongation of catalyst lifetime leading to the sharp increase in the range from 100 to 250°C.

All in all, the improve of catalytic performance for activation temperature raise up to 250°C is attributed to an increasing amount of available BAS as well as enhanced hydride transfer

assisted by increasing La^{3+} interaction with isobutane. Results of IR spectroscopy under flow conditions confirm that both sites are exposed initially when water removal is started. On the other hand, reduced catalyst lifetime paralleled with slight worsening of selectivity is supposed to be caused by stronger interaction of deactivating heavy hydrocarbons with catalytic surface. As seen at measured heat of adsorption the strength of sites is increased for water contents below 2 wt%, therefore, stronger sites are exposed when higher activation temperature is applied.

Considering less effect on overall selectivity in the range from 350° to 450°C, but a steady decrease of catalyst lifetime, it is plausible to assume interaction of side-products caused by multiple alkylation and dimerization is enhanced. Moreover, we detect a slight decrease of BAS concentration, which is attributed to the combination of bridging hydoyxl groups with each other or LaOH groups. The reduction of protonic sites comes along with higher local butene concentration per active site, thus, side-reactions increase again. To summarize the dependence of alkylate yield on water content is displayed in Figure 4.12. Based on selectivity results different nature of sites are supposed, each dominating at a certain amount of H_20 molecules per unit cell.

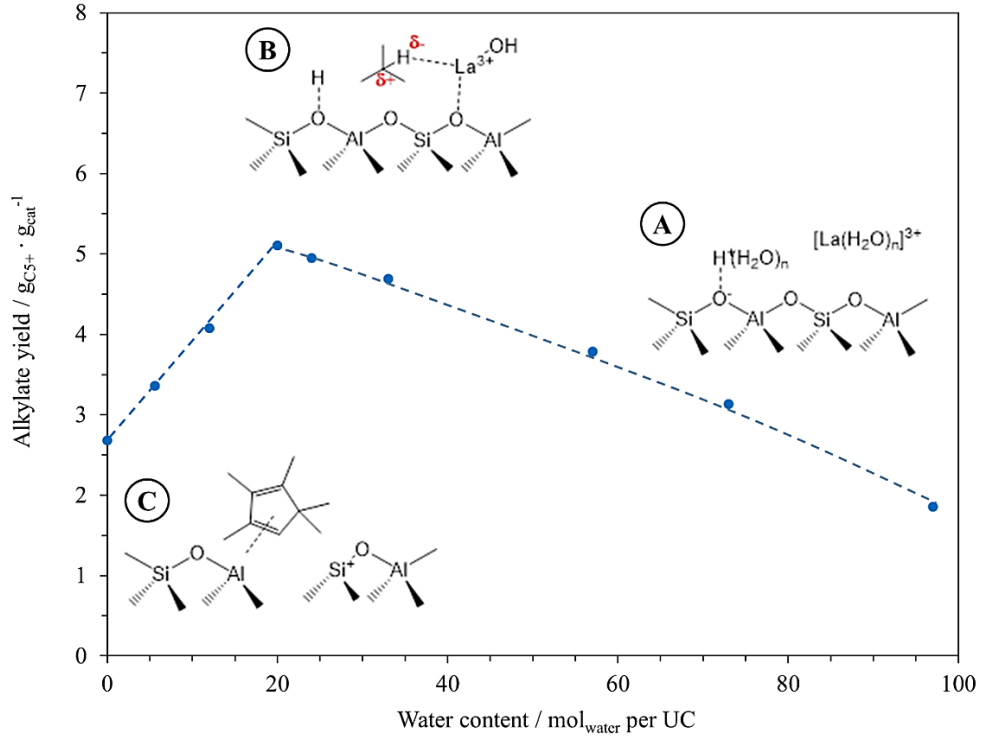

Figure 4.12. Dependence of alkylate yield on water content. A) High water content with H_2O adsorption on BAS and La^{3+}, B) optimum water content with $La(OH)_x^{n+}$ enhancing hydride transfer and C) dehydroxylated zeolite interacting with heavy hydrocarbons.

4.4. Conclusion

The huge impact of residual water of La^{3+} exchanged X zeolite on catalytic activity in isobutane/2-butene alkylation was investigated by varying the water content applying activation temperatures between 100°C and 450°C. Catalyst lifetime showed a volcano-like dependency with a maximum at 250°C correlating with inverse behavior of maximum deactivation rate determined when period of full butene conversion ended. In addition, selectivity towards desired high-octane products in C_8 range was highest for this temperature and lowest in case of mildest activation. Selectivity of by-products in C_5 to C_7 range as well as C_9 or lager compounds from side-reactions like multiple alkylation and cracking showed opposite trends having their minimum after activation at 250°C. Overall, catalyst lifetime and selectivity was stronger influenced if activation conditions were chosen too mild compared too very harsh treatment.

The direct comparison of two reactions with similar lifetime, but different selectivity was used to further investigate the role of residue water on LaX catalyst. While isomer distribution within C_8 range for catalyst activated at mild temperature (125°C) shows comparable high tendency to form dimerization products, severe heat treatment at 450°C does not enhance olefin addition in the same extent. Therefore, stronger interaction of deactivating heavy hydrocarbons with catalytic surface was supposed to be the reason for decline of catalyst lifetime when C activation temperature exceeds 250°.

Results of IR spectroscopy under flowing nitrogen prove bridging OH and LaOH are main sites to be exposed simultaneously during removal of molecular water when activating the catalyst. In addition, probing acid sites with pyridine after activation at different temperatures showed a volcano-like dependency of BAS/La-LAS ratio with a maximum around 300°C.

The water content was determined by TGA under flow conditions simulating in situ activation in the fixed-bed reactor. It was found to have two different stages with faster removal of water up to around 33 H_2O/UC and much slower decrease of water content for temperatures beyond this threshold. Therefore, we conclude water is adsorbed on different sites, which correlates with findings from measured heat of adsorption of water on LaX also showing a threshold around 20 H_2O molecules per UC.

4.5. References

1. A. Feller, A. Guzman, I. Zuazo, J. A. Lercher, *Journal of Catalysis* **2004**, *224*, 80-93.
2. A. Feller, I. Zuazo, A. Guzman, J. O. Barth, J. A. Lercher, *Journal of Catalysis* **2003**, *216*, 313-323.
3. R. Klingmann, R. Josl, Y. Traa, R. Gläser, J. Weitkamp, *Applied Catalysis A: General* **2005**, *281*, 215-223.
4. J. Huang, Y. Jiang, V. R. Reddy Marthala, Y. S. Ooi, J. Weitkamp, M. Hunger, *Microporous and Mesoporous Materials* **2007**, *104*, 129-136.
5. C. Sievers, A. Onda, R. Olindo, J. A. Lercher, *The Journal of Physical Chemistry C* **2007**, *111*, 5454-5464.
6. J. Pater, F. Cardona, C. Canaff, N. S. Gnep, G. Szabo, M. Guisnet, *Industrial & Engineering Chemistry Research* **1999**, *38*, 3822-3829.
7. C. A. Querini, E. Roa, *Applied Catalysis A: General* **1997**, *163*, 199-215.
8. A. Feller, J.-O. Barth, A. Guzman, I. Zuazo, J. A. Lercher, *Journal of Catalysis* **2003**, *220*, 192-206.
9. K. P. de Jong, C. M. A. M. Mesters, D. G. R. Peferoen, P. T. M. van Brugge, C. de Groot, *Chemical Engineering Science* **1996**, *51*, 2053-2060.
10. R. J. Taylor, D. E. Sherwood, *Applied Catalysis A: General* **1997**, *155*, 195-215.
11. A. Sengar, R. A. van Santen, E. Steur, J. A. M. Kuipers, J. Padding, *ACS Catalysis* **2018**, *8*, 9016-9033.
12. A. K. Cheetham, M. M. Eddy, J. M. Thomas, *Journal of the Chemical Society, Chemical Communications* **1984**, 1337-1338.
13. A. Guzman, I. Zuazo, A. Feller, R. Olindo, C. Sievers, J. A. Lercher, *Microporous and Mesoporous Materials* **2005**, *83*, 309-318.
14. F. Schüßler, E. A. Pidko, R. Kolvenbach, C. Sievers, E. J. M. Hensen, R. A. van Santen, J. A. Lercher, *The Journal of Physical Chemistry C* **2011**, *115*, 21763-21776.
15. P. B. Venuto, L. A. Hamilton, P. S. Landis, *Journal of Catalysis* **1966**, *5*, 484-493.
16. J. W. Ward, *Journal of Catalysis* **1969**, *14*, 365-378.
17. J. W. Ward, *The Journal of Physical Chemistry* **1968**, *72*, 4211-4223.
18. A. Guzman, I. Zuazo, A. Feller, R. Olindo, C. Sievers, J. A. Lercher, *Microporous and Mesoporous Materials* **2006**, *97*, 49-57.

5. Summary

The alkylation of isobutane with light alkenes upgrades light low-value products to high-octane gasoline. Commercial alkylation technology based on liquid acid catalysts, HF and H_2SO_4, suffers from numerous drawbacks, especially safety and environmental issues. To replace established catalysts by environmentally friendly solid acids like LaX zeolites, catalytic performance of the solid catalyst in alkylation reaction has to be enhanced.

In 2-butene/isobutane alkylation there are two competing reaction pathways after initiation occurred by protonation of 2-butene. The formed carbenium ion can either undergo alkene addition and hydride transfer. If alkene addition is the dominant pathway, oligomers are built up leading to catalyst deactivation. As this route is predominantly dependent on local olefin concentration, it is crucial to reduce the available butene at active site to improve catalytic performance of zeolites. It was shown that adjusting pellet size of used LaX catalyst is a very useful tool for tuning catalyst stability and selectivity, however, the effect of pellet size is opposed in the two reactor types CSTR and PFR.

Due to backmixing-mode the paraffin to olefin ratio is already quite low in CSTR, making the impact of pore diffusion less relevant. However, we show that local butene concentration at active site could be drastically lowered by decreasing pellet size and therefore increasing the amount of accessible sites. As a result, butene conversion level is enhanced which suppresses side-reactions leading to prolonged catalyst lifetime, improved product selectivity and increased alkylate yield. The smaller the pellets, the better the catalytic performance in CSTR.

For technical reasons, alkylation in fixed-bed reactors is only feasible at much larger paraffin to olefin ratios than in CSTR. As a consequence, actives sites face a very high local butene concentration leading to fast deactivation. However, it was shown that intentionally induced mass transport limitation by increased pellet size can be used to regulate the transport of butene reducing the operating butene concentration locally at the active sites inside the pellet. The expected butene concentration gradient over catalyst pellet predicted by the Thiele modulus was confirmed by revealing the pellet deactivation in a shell-core mechanism from outside to inside. Catalytic experiments proved catalyst lifetime was increased by more than threefold, while the product yield increased by 6 times when the catalyst pellet size was increased from 0.15-0.25 mm to 1.6 mm. Additionally, selectivity towards high-octane paraffins was enhanced.

Independent on reactor type the number of accessible sites and thus the local butene concentration at active site was found to be highly dependent on remaining amount of water after pretreatment. At constant reaction conditions, alkylate yield showed a volcano-like dependency on activation temperature, which correlates to water content. Combining the results of thermogravimetric analysis and IR spectroscopy studies two inhibiting site conditions were found. Insufficient water removal when choosing low activation temperature results in low acid site concentration as well as decreased acid site strength, both favoring catalyst deactivation. On the other hand, too low water content also results in reduced alkylate yield due to partial dehydroxylation leading to decreased BAS concentration and strong interaction of heavy hydrocarbons with LAS. The optimum remaining amount of water was found to be around 20 H_2O/UC when 250°C for 1h were applied.

All in all, the findings reported in this thesis provide a deeper understanding of the pellet deactivation mechanism of LaX zeolites used in 2-butene/isobutane alkylation finally leading to the counterintuitive reveal of the beneficial effect of mass transport limitation. The drastically improved catalyst lifetime, selectivity and thus alkylate yield makes LaX catalysts much more competitive for industrial application.